Data-Driven Design for
Position/Force Control

February 2021

Toshiaki OKANO

A Thesis for the Degree of Ph.D. in Engineering

Data-Driven Design for Position/Force Control

February 2021

Graduate School of Science and Technology
Keio University

Toshiaki OKANO

Acknowledgements

I have completed this dissertation as a summary of my research from September 2014 through March 2021 as a member of Murakami and Ohnishi laboratories, the Faculty of Science and Technology, in Keio University. I would like to express my gratitude to the people who supported my doctoral research.

First and foremost my gratitude should goes to my supervisor Professor Dr. Toshiyuki Murakami in Keio University. Without his guidance and supervision, the completion of this dissertation would not be a success. The experience gathered during the stay of his laboratory is invaluable.

I would like to express my deep gratitude to my another supervisor Professor Dr. Kouhei Ohnishi in Keio University. His enormous support and insightful comments were invaluable and always to the point which helped me a lot.

I gratefully acknowledge to the all of current and past SUM members, who gave me discussion, assistance, and comments for my works.

My deepest appreciation goes to Professor Dr. Hiroaki Nishi, Associate Professor Dr. Takahiro Yakoh, Professor Dr. Seiichiro Katsura, Assistant Professor Dr. Takahiro Nozaki, and Associate Professor Dr. Roberto Oboe in Padova University.

I greatly appreciate to the members of my Ph. D. dissertation committee, Professor Dr. Hideo Saito in Keio University, Professor Dr. Hiromitsu Ohmori in Keio University, Associate Professor Dr. Takahiro Yakoh, Professor Dr. Kouhei Ohnishi in Keio University. Their comments and advices greatly helped to improve the thesis.

I would like to convey my sincere thanks to Dr. Kenji Ogawa, Dr. Takuya Matsunaga, Dr. Kasun Prasanga, Dr. Kazuki Tanida, Mr. Takahiro Ishikawa, Mr. Hidekatsu Uchida, Mr. Kensuke Oda, Mr. Hayata Sakai, Mr. Daisuke Tomizuka, and all other colleagues. Their advice highly improved the direction and quality of my research.

I would like to thank Keio Program for Leading Graduate School for giving me the financial assistance throughout the Master and doctoral courses.

I also have a special feeling for the partnership between Politecnico di Milano and Keio University. A double degree program provides valuable opportunities, and I strongly desire the further development of its program for building a high level and reliable academic exchange and country relationship.

Finally, I would like to express my gratitude to my father, mother, and brother. Your kind and warm-hearted assistance have enabled me to focus on research, and I would like to thank you from my heart.

I would like to express my sincere gratitude again to all people who have supported me.

February, 2021

Toshiaki Okano

Contents

List of Figures

List of Tables

List of Algorithms

Chapter 1

Introduction

1.1 Robots and Position/Force Control

Robots that interact with uncertain surrounding environments are expected to replace the labor force and enhance productivity. A few industrial robots are installed in closed environments, such as factories. In addition, the operation of communication robots that function in open environments where humans are also active is gradually increasing [1]. However, the number of robots that interact with uncertain surrounding environments remains limited. Thus, the development of the following three types of robotic technologies is required: sensing, judgment, and actuation [2]. All of these are essential and expected to be further developed; however, this dissertation expands the discussion regarding the actuation of motion control.

Position and velocity control have been mainly applied to industrial robots in closed environments; however, forces are also important physical variables to consider in the interactive tasks. If a robot does not sense the force information, it does not have tactile sensation. Similar to humans changing motions based on the surrounding rigidness of uncertain environments, robots should sense tactile information to flexibly actuate accordingly and achieve safe and flexible motion similar to humans. The tactile information or rigidness of the uncertain surrounding environments can be represented by the impedance or admittance, which indicate the ratio between the position/velocity and force. If not only the position/velocity but also force values can be precisely sensed, analyzed, and controlled, the movements of robots can be approximately the same or greater than those of humans.

The ratio between position control and force control is represented by the control stiffness as follows:

Table 1.1: Target of motion and control stiffness.

Target of motion	Control stiffness
Position	∞
Compliant	Finite value
Force	0

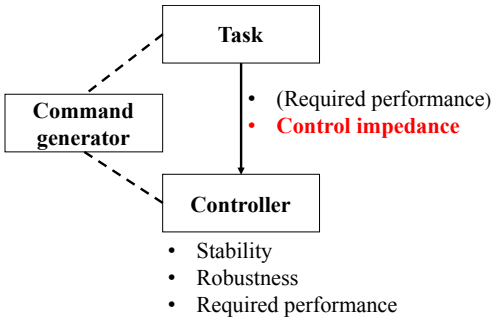

Fig. 1-1: Relationship between content of task and controller design.

[3–5]

$$\kappa = \frac{\text{position} \quad \text{control}}{\text{force} \quad \text{control}} \tag{1.1}$$

Table 1.1 presents the relationship between the target of motion and control stiffness. If only the position component is controlled, the control stiffness becomes infinite. By contrast, if only the force component is controlled, the control stiffness becomes 0. This dissertation considers not only the position but also the velocity for extending the control stiffness to the control impedance.

Various studies have been conducted regarding the position, velocity, and force control. Each object or controller should be independently designed as indicated by the class in object-oriented programming. Independency clarifies the role of each object and makes the system stronger to the amendment. The relationship between the content of a task and the controller design is shown in Fig. 1-1. The controller design is required to satisfy the stability or robustness, which are independent of the task content. Stability or robustness of systems must be secured regardless of the task assigned. Therefore, the controller can be systematically designed considering stability or robustness. The required performance is also necessary in addition to the stability or robustness when designing a controller; the required performance depends on the task content. However, the performance should be higher if the stability, robustness, and performance of the hardware/software permit it. For instance, the time constant or rise time should be

minimal. The criteria of stability, robustness, and required performance can be determined only by the model of the actuated device.

Unlike stability, robustness, and performance, the controller design cannot be independently determined from the task content considering control impedance. A few studies have addressed this issue with various tasks by making significant efforts for command generation. For instance, robots lift soft fragile material only by position/velocity control using a highly planned command; however, humans dynamically change the softness or hardness of their motions. The control impedance should be considered both passively and actively to increase the adaptability to the uncertain surrounding environments [6, 7].

The importance of control impedance has been discussed; however, the design of the balance of a position/velocity and force controller needs to be considered. Because the controller design depends on the task content, which is difficult to model, a prior understanding of the task is required, and it is thus difficult to expand the systematic discussion.

The system design generally starts from modeling and approximates the objects or phenomena. The analysis and synthesis are conducted based on the constructed model, which assist in the understanding and construction of systems. This modeling–analysis–synthesis approach is highly capable and versatile. In addition, this dissertation utilizes a data-driven approach for designing the position/force controller. The data-driven concept is widely known. For instance, the Japanese government often emphasizes the importance of a data-driven society as well as the concept of Society 5.0, and has stated that *"in the data-driven society of the 21st century, the most important currency of economic activity is high-quality, up-to-date, and abundant "real data."* [8].

A data-driven controller design would be based on data or behaviors of actuated devices [9]. The following three types of the data-driven approach relative to the topic of this dissertation are indicated below:

- Experimental data

  The controller is designed based on experimental data. Certain problems are formulated and solved based on experimental data to determine the parameter of the controller. For instance, the optimization problem is solved by tuning the control parameters based on experimental data using virtual reference feedback tuning or fictious reference iterative tuning [10, 11]. Certain parameters of the controller should be tuned by solving the formulated problem based on experimental data

using the design of the position/force control as well.

- Database

  The parameters of a controller are referenced from a database that is constructed by the data of actuated devices. Variables that represent the current state are input to the database, and the parameters are referenced from the database and applied to the actuated devices. This approach is similar to the method of learning from demonstration (LfD). The supervised data of various situations are collected and arranged in advance; the data having the most similar situations in the available history are referenced. Because the appropriate parameter is simply referenced from the database, this approach is suitable when the computation cost for deriving a parameter is comparatively high online. For instance, the reactions of a vehicle driver should be stored in a database.

- cerebellar calculation model

  The parameter of a controller is tuned based on the cerebellar calculation model. If the causality of a parameter and certain variables are clear, the database should be utilized owing to its simplicity and low computation cost. However, the weights of each variable for deriving the parameter of a controller are not clear at times, and thus, the concept of the cerebellar calculation model should be applied. The controller designed based on the cerebellar calculation model is utilized for the entire controller in a few studies; however, it should be partially combined with the controller designed based on the model if the model of the actuated device can be obtained.

In [12], a data-driven control design was applied for the gain tuning of a proportional-integral-derivative (PID) controller. The aforementioned data-driven approach should be applied or extended to the controller design regarding position/force control based on real data.

1.2 Motivation and Contribution

The motivation and contribution of this dissertation is to design and present cases of the position/force controller in a data-driven manner.

Various studies regarding the design of the position/velocity controller have been conducted. The controller design often ultimately results in the balance between the performance and the stability/robustness

in the case of position/velocity control, which is theoretically and systematically possible. On the other hand, the desired controller is changed according to the types of motion and uncertain surrounding environments, which makes it difficult to obtain the unique solution when force control is considered. In addition to having the design difficulty regarding force control, the design of the position/force controller needs to control multiple contradicted physical variables simultaneously, for which the theoretical or systematic design can be difficult to achieve. Therefore, this dissertation discusses a data-driven design based on simulations and real data from experiments, in addition to the model-based system design. Bilateral control is considered for the position/force controlled human support system, and the hybrid position and force control (HPFC) or impedance/admittance control is considered for the position/force controlled machine automation.

This dissertation considers three approaches of data-driven control design to set the parameters of position/force control. The first approach is based on the concept of the cerebellar calculation model. The performance enhancement of force control is particularly necessary for discussing the position/force control. The compensator is designed based on the concept of the cerebellar calculation model. The second approach is based on a database. The characteristics of an operator regarding the position/force information are collected and recorded in a database. Certain parameters of the control system are referenced from the database by substituting the variables of a current state. The third approach is based on experimental data. Experimental data regarding position/force are also collected and utilized for certain problems, such as the optimization problem, to determine the parameter of control.

This dissertation presents the following five data-driven designs for the position/force controller.

(1) Force controller design: cerebellar calculation model

(2) Operator's sensation-based design: Database

(3) Operator's motion-based design: Database

(4) Evaluation index-based design: Experimental data

(5) Task implementation-based design: Experimental data

The discussion in this section is summarized in Table 1.2.

Table 1.2: Data-driven control design and each chapter.

Chapter	Controller	Applied data-driven control design
3	Force control	Cerebellar calculation model
4	Bilateral control	Database
5	Hybrid position/force control	Database
6	Bilateral control	Experimental data
7	Hybrid position/force control	Experimental data

1.2.1 Data-driven Based Force Control Design

Force control is an essential concept in motion control or haptics, especially when the interactive motion is considered. Several studies have been conducted to enhance the performance of force control; however, the unique or theoretical control design can be difficult because it is affected by the contact to an environmental object or types of motion. Therefore, this dissertation proposes a data-driven-based force control design prior to discussing the human support and machine automation systems. Especially, the concept of the cerebellar calculation model in a data-driven control design is applied to the design of the force control.

Human support robots are in high demand in certain countries owing to the circumstances of the declining working population due to the lower birth rate and an aged society; moreover, these robots are expected to operate in open environments where they interact with other objects. The development of force control is expected in these environments, and the performance enhancement of force control has been extensively studied. This dissertation considers explicit force control with a disturbance observer (DOB) and reaction force observer (RFOB) [7, 13]. DOB and RFOB can enhance the robustness and estimate the external force without using force sensors.

A PID controller is often utilized for controlling certain physical variables; moreover, a PID controller can be applied for explicit force control. Certain studies estimated the derivative of force, which is referred to as jerk, and a proportional-derivative gain was applied by designing the state estimator [14]. The derivative gain improves the performance in the high-frequency range; however, the information in the dimension of the jerk is sometimes difficult to estimate and control owing to the noise effect. The DOB is designed in the dimension of force as a force-based DOB (FDOB) instead of a DOB in the acceleration dimension or based on the integral gain [15]. The transient response improved because the inertial force was also compensated in addition to other disturbances; however, the system easily becomes

unstable depending on the environmental impedance. Therefore, a damper or velocity feedback is often combined to stabilize the system in the FDOB; however, the transient response is degraded. A first- or high-order sliding mode control was combined with the force control to enhance the performance while guaranteeing stability [16]. However, chattering or a complicated parameter design can complicate the implementation of the sliding mode control into the force control. The explicit force control with DOB and RFOB has been extensively studied; however, the design of a controller and selection of appropriate gains are challenging because they are affected by the condition of motion. For instance, the appropriate gains can easily vary according to the environmental impedance. At the same time, certain disturbances such as model uncertainties or friction also affect the performance, and they easily vary according to the motion. Therefore, both feedback and feedforward components should be considered to enhance the performance of force control, which contrasts with the methods used in conventional studies.

The target of this dissertation is to combine a neural network (NN), which has both feedback and feedforward components, into the explicit force control composed of proportional–integral (PI) gain and DOB for enhancing the performance of force control. The implementation of an NN into motor control operations, such as position control, HPFC, and force control, has been extensively studied, and the parameters of the compensator are iteratively updated based on the error of the control variable [17–21]. For instance, a system of two feedforward neural networks was proposed to learn the nonlinearities of the position-controlled flexible arm associated with an inverse dynamics controller [22]. Moreover, an approach for a two-link flexible manipulator was also discussed [23]. HPFC was developed using feedback error learning (FEL) [24, 25]. Both the position and force controllers in the subspace were constructed using NNs and each controller learned based on the free and contact motions. The NN or FEL was also applied for the force control. Fuzzy logic and NN compensators were compared in a milling control operation, in which the cutting force was in the order of a hundred units [26]. Nonlinear viscoelastic environmental conditions were considered as a part of the system and approximated using an NN feedforward term and the interactive motion was considered based on its approximated model [27].

NNs were also developed to compensate for model uncertainties or to be added as an additional gain in these studies. The DOB is a critical tool for compensating model uncertainties of a system. To enhance the performance of force control, a combination method of DOB and NN must be discussed by avoiding the interference between the functions of these two methods.

This dissertation proposed a combination of NN and explicit force control with DOB by referring to the concept of the cerebellar calculation model in the data-driven control design. The structure of the

controller and composition of the NN were selected through simulation results, and the compensator based on NN was designed to operate in a frequency range higher than that of the cutoff frequency of the observer with a few hidden layers. Moreover, this dissertation discusses an online training method of weights. Simulations and experiments were performed to present the effectiveness of the proposal.

1.2.2 Operator's Sensation-based Data-driven Design

Certain parameters or characteristics of the human support system should be designed from the sensation of operators. Bilateral control is a human support system that enables the transmittance of haptic information from one location to another. Although this system is highly related to the tactile sensation, its design does not always consider the characteristics of operators. The sensation data of operators should be analyzed and utilized for the design of a system; therefore, this dissertation proposes a JNDs-based design policy of the haptics system. The concept of a database in a data-driven control design is applied by considering the operator's sensation. The database or look-up table is designed based on the actual data regarding the operator's sensation, and the control parameter is updated by referring to the database.

Teleoperation systems are gaining attention as a method for conducting activities in remote locations. Considering that phones and videos transmit auditory and visual information to remote locations, the transmission of a third sense, such as the haptic sense, may be highly useful for teleoperation.

Bilateral control is a teleoperation method of transmitting the position and/or force between an operator (master) and an environmental entity (slave) [28, 29].

The sampling time of a system is often designed to be significantly short for precise haptic transmission, which significantly increases the data traffic. A high-resolution sensor and a short sampling time are often used to improve the performance of impedance transmission in bilateral control. However, the design is occasionally over-specified for human perception or task implementation. Hence, an appropriate design strategy that considers the desired performance is required.

The human sensing ability may not be as precise as digital technology at times. This ambiguity can be used to design the auditory and visual presentation systems [30, 31]. "Just noticeable differences" (JNDs) indicate the detectable amount of difference between two stimuli, and have been studied not only for the auditory and visual senses, but also for the haptics sense. For instance, the time resolution of an operator is 10 ms to feel a strong stimulus and 50 ms to feel a weak stimulus [32]. In addition, the spatial resolution of an operator is 1–2 mm at the fingertip (one of the most sensitive parts). Regarding force,

previous studies have shown that JNDs are 5–10%, depending on the part of the human body, posture of measurement, range of measurement, etc. [33–35]. As indicated by the aforementioned studies, it may be possible to deliberately reduce the quality of haptic transmission if the operators scarcely feel any difference. Reducing the quality helps reduce data traffic.

Several studies have attempted to reduce the data size or data traffic for haptic systems. Data have been compressed by adaptive sampling or quantization [36–40]. These approaches can be implemented not only for a general haptic system, but also for bilateral control. For bilateral control, floating-point compression has reduced the amount of data transmission [41]. The concept of JNDs has also been considered in bilateral control [42, 43]. To reduce data traffic in bilateral control, haptic information has been transmitted when either the velocity or force was changed more than the ratio of JNDs [44, 45]. Perceptual deadband and the time-domain passivity approach have been combined to reduce data transmission while guaranteeing passivity. This approach has been expanded to the energy prediction-based approach [46]. The prediction-based approach has also been proposed [47]. The least-squares method and median filtering have been applied to predict the information of unreceived packets. This approach has been expanded to multiple degrees of freedom [48].

These studies have focused on 2ch bilateral control, in which velocity and force components were treated independently. The JNDs of velocity and force have been measured and used for data traffic reduction. In 4ch bilateral control, the position and force components are combined and mutually involved in communication between the master and slave because the transmitted information includes both position/velocity and force. JNDs should be measured and discussed by considering not only the JNDs of position/velocity and force, but also the performance of the bilateral control system. The data transmission must be designed based on the impedance transmission performance of the bilateral control system.

The purpose of this dissertation is to design the multirate sampling of the 4ch bilateral control by considering JNDs against the variation of multirate sampling to reduce data traffic. Because the multirate is an integer value and is therefore not suitable for representing the performance in bilateral control, the performance of impedance transmission under various multirates is simulated. This performance is indirectly or alternatively used as the variable of JNDs. A remarkable contribution of this dissertation is the idea to measure JNDs against the variation of multirate and to analyze the relationship between the multirate and performance of the impedance transmission, which is discussed in the frequency domain. The deterioration criteria of the impedance transmission can be freely set depending on the situation;

however, in this dissertation, it is determined based on the psychological tests. A look-up table is constructed by referring to an appropriate multirate based on the results of the JND tests, which is based on the concept of the database in the data-driven control design. Our proposal is highly versatile owing to the fact that our approach is directly designed for the desired performance of impedance transmission, which can be determined in several ways.

1.2.3 Operator's Motion-based Data-driven Design

A data-driven design for the position/force controlled human support system or bilateral control was discussed considering the operator's sensation in Section 1.2.2. The idea of a data-driven design for position/force control based on an operator is also applicable to machine automation systems. More specifically, the design of control impedance can be referenced from the operator. This dissertation proposes an approach to extract the control impedance from the actual motion of an operator as a data-driven design method for position/force control. Once the characteristics of the operator are extracted, the database can be built similar to the database in a data-driven controller design. This chapter discusses the method for estimating parameters, which will be a part of the database.

Owing to the decline of the laborious population due to the lower birth ratio and aged society, skill succession is gaining attention. In particular, the motion conducted by skilled workers should be visualized and preserved. Industrial robots are installed in factories to replace human labor force; however, most of their tasks are simple. On the other hand, human workers judge the current situation and adapt to the uncertain surrounding environments for achieving complicated motions. Further development of skill succession technology is highly expected for passing along the advanced motions. Therefore, the extraction of operator motions is highly expected as one of the countermeasures of the social issue.

Operator motion extraction based on visual information has been widely studied [49,50], in which the trajectories of cardinal points were extracted; however, the interactive motion is out of scope. Because the operators are constantly interacting with the uncertain surrounding environments, the motion extraction method should consider the interactive force information.

The position, force, and impedance are well-known physical variables in the field of motion control. Hybrid position/force control, compliance control, and impedance control have been widely applied in several studies to consider both the position and force information simultaneously. However, these control strategies indicate that not only the position and force information is required for achieving human-like advanced motions, but also the impedance information; these three physical variables should

be extracted for skill succession. The position and/or the force information is obtainable by using sensors, while the impedance information must be estimated based on the obtained information.

The estimation method for the operator impedance has been widely studied. The impedance of fingers, finger joints, hands, ankles, or arms have been estimated by considering postures or the direction of force [51–61]. Friedman *et al.* considered the grasp stiffness matrices and represented them in ellipsoids [51]. Yoshikawa *et al.* made the impedance model of the fingertip and estimated the parameters by the least-squares method. They have confirmed their proposals by a mechanical structure and concluded that varying perturbations should be added for estimating different parts of the operator [52]. Dong *et al.* considered the finger-hand-arm responses by adding a variety of sinusoidal excitations [55]. Theodore *et al.* measured the two-dimensional static stiffness of each finger and discussed their characteristics by involving posture and force direction [60]. Lee *et al.* estimated the ankle impedance by approximating the second-order model based on the environment while the subject was walking [61]. Most of these approaches have considered non-contact-point impedances such as those involved with joints, arms, and ankles, although interactive motions with the uncertain surrounding environments has been conducted. A few studies have considered the end-point impedance, but have not conducted any tasks. Because subjects must grasp the sticks due to the experimental constraints, the variation of end-point impedance while conducting the tasks cannot be obtained. Therefore, this dissertation aims to estimate the end-point impedance while conducting actual tasks, such as pushing environmental objects. Because the sensitive parameter setting of virtual impedance is expected in certain control strategies, including impedance or hybrid position/force controllers, the information of impedance variation at the end-point is highly valuable for achieving human-like motions [62, 64, 98]. The estimation of dynamics is not part of the scope of this dissertation because the end-point impedance information is sufficient for designing these control strategies.

The bilateral controller is suitable for considering both the operators and the environmental information simultaneously; its controller has been utilized for motion extraction and impedance estimation [65–68]. However, these approaches considered the position and force information independently or estimated the impedance of environmental objects instead of the operators. Because the position and force responses of the bilateral controller are determined by the equilibrium point and the impedance of the environmental objects, the impedance of the operators is unattainable.

The elemental separation method [4] was proposed in the study of the impedance estimation of operators by using the bilateral controller, Nozaki *et al.*. Sinusoidal force vibrations were added to the common

mode of the bilateral control system, and both the operator and environmental stiffness were estimated from the obtained haptic information, which contains both the position and force responses. However, this has neglected the effect of manipulation, thus the estimated stiffness has been highly dependent on the setting of the fingertip impedance. Moreover, the appropriateness of the proposed method has not been confirmed by the true value including the virtual impedance.

The proposal of this dissertation aims to extend the impedance estimation method by using the bilateral control system with an extra signal. The effect of manipulation is estimated and removed from the impedance estimation process. The proposed method was evaluated by simulations with certain conditions, and its effectiveness was confirmed through other simulations and an experiment.

1.2.4 Evaluation Index-based Data-driven Design

Data-driven designs for the position/force controlled system that refer to the operator's information from the database were presented in Sections 1.2.2 and 1.2.3. However, a system has a purpose or goal, and the operator is only a component of the system. Therefore, position/force controlled systems should also be designed considering its purpose or goal. This dissertation proposes a design of the position/force control based on the experimental data using the data-driven approach.

Regarding the gain setting for position/velocity control, in particular PID tuning, several studies have been conducted to reveal the open-loop step response, Ziegler-Nichols frequency response, Cohen-Coon, and the limit sensitivity method [69–71]. The ideal PID gains can be theoretically or experimentally obtained by using these approaches. Unlike the position control, the impedance of an operator and/or environment vary for interactive tasks, where the force controller is often implemented [72]. Moreover, describing the contact motion is insufficient at times because certain objects interfere each other. Therefore, the gain setting approaches for position control should not simply apply to interactive tasks. In addition, the balance between the position and force components must be considered for the HPFC [73].

The gain setting for bilateral control has also been studied, especially for stability theorems, such as the $H_{\inf}$ theorem or the passivity theorem, by building the system model [74–77]. Stability is necessary for every control strategy; however, the bilateral controlled system is stable if the communication delay between the master and slave is significantly short [78]. A few studies have solved the optimization problem by considering the stability constraint, tracking constraint, and fidelity measure, but they have considered the model-based 2ch bilateral control [79, 80]. However, describing the contact motion and precise identification of certain nonlinear terms such as noise, saturation, and friction can be difficult,

and the approach that models all the elements of a system is not necessarily suitable for bilateral control. Therefore, this dissertation considers the gain setting of bilateral control considering precise impedance transmission in the evaluation index-based approach by using the experimental data.

The gains of bilateral control tend to be designed in an empirical manner, and the gains of the master and slave have been set to be the same although their transfer functions are different. Therefore, in this dissertation, gain tuning relative to the relationship between the master and slave were considered by the different gain settings. In addition, this dissertation also aims to present the gain searching setup with a limited number of trials for practical use.

The evaluation index-based gain tuning for bilateral control is proposed in this dissertation by referring to the concept of experimental data in a data-driven control design. Moreover, this dissertation presents the design process of the gradient-descent algorithm for an actual gain setting by considering the obtained evaluation index-based gain tuning. This was conducted using a limited number of trials for practical use. Two algorithms were considered for two cases, having the same and different gains between the master and slave; the order and number of tuning was designed. The effectiveness of the proposed gain tuning methods was verified through experiments.

1.2.5 Task Implementation-based Data-driven Design

As indicated in Section 1.2.4, the position/force controlled system should also be designed considering its purpose or goal. The position/force controlled machine automation system can be designed by referring to the operator's motion; however, the purpose is not to reproduce the referred motion, rather to achieve the tasks. This dissertation proposes a selection method of position/force control considering task completion based on the utilization of experimental data in the data-driven control design.

LfD is used to design parameters based on skilled motion to make robots conduct tasks [81–84]. LfD saves the motion demonstrated by an operator and utilizes it as the skilled motion data. LfD is advantageous owing to its simplicity and intuitiveness. The obtained physical responses, such as position, velocity, and force can be utilized as the command values. This method can reproduce the saved motion and achieve the tasks. MCS is an LfD method, which is based on a bilateral controller that transmits and receives the tactile or haptic information, and is composed of the position, velocity, and force information between master and slave robots [85, 86]. MCS is composed of the motion saving and loading phases. The skilled motion is demonstrated by the operator and stored in a database in the saving phase, and its saved motion is performed in the loading phase. However, this system can only play back the saved

skilled motion accurately when the environmental conditions between the motion saving and loading phases are the same. Environmental variations, such as the position and impedance, degrade the motion reproduction performance. For instance, the slave robot cannot sufficiently touch the environmental object when it is farther in the motion loading phase. Moreover, the slave robot cannot add a sufficient force when the impedance of the environmental object is larger than that of the motion saving phase. The operators are constantly changing their impedance to adapt to the uncertain surrounding environments and achieve a flexible motion. Therefore, the human-like adaptable motion is expected to be developed in MCS.

The calligraphy motion method is considered for target tasks [87]. The original MCS, position-based MCS, and force-based MCS are applied for reproducing motion under conditions where certain environmental variations occur. These systems correspond with HPFC, position control, and force control. However, the appropriate control strategy used against the environmental variations should be changed from one time and axis to another. The environmental variation is treated as the disturbance of MCS in [88]. The position of an environmental object is varied between the saving and loading phases, which is considered as a disturbance and compensated by the observer. It mainly focuses on the position variation; however, the impedance variation is also a challenging issue because the compensation logic of impedance variation should be designed by considering the task. In addition, the purpose of these studies appears to load the original motion rather than the reproduction of a task, and the control architecture is basically fixed.

Studies regarding the appropriate modular or controller determination are also analyzed [89, 90]. The concept of MOSAIC architecture is useful for considering the switching of a module or control [91]. The weight of each module is updated based on the responsibility signal, and an appropriate module is iteratively studied to implement the adaptability. These studies targeted the position or trajectory control, such as a pendulum, while this dissertation considers not only the position but also force related tasks.

Implementing robot flexibility in LfD for either position or force-based tasks is widely studied. There are mainly two methods for obtaining the flexibility of motion in the frame of LfD: estimation and direct measurement. The estimation approach assumes certain models and estimates the variation of impedance from the obtained position and force by LfD. A few studies have estimated the stiffness by fitting the responses with a mass-spring-damper model [92–94]. For instance, the Gaussian Mixture Model is trained and utilized for generating continuous stiffness profiles. Li *et al.* also considers the probabilistic Gaussian process model and achieves variable impedance control. This estimation approach appears

intuitive; however, it is difficult to distinguish between the impedance of the environment and operator, as indicated in Chapter 5 [95]. Because the force information of the operator becomes the same as that of the reaction force from the environment due to the law of action and reaction, the estimated impedance is not necessarily the impedance of the operator. The direct measurement approach measures the force response. Kronander *et al.* measured the grasping force of an operator, which corresponds with the stiffness of the interactive joint [82]. Wu *et al.* measured the electromyogram of an arm, which corresponded with the stiffness of the robot for achieving the variable impedance control [96]. These approaches complicate distinguishing between the impedance of the environment and an operator; however, this occasionally highlights the difficulty of intuitive manipulation. Moreover, these approaches utilize the stiffness of one axis for another axis. These related studies consider impedance control [62, 64, 97, 98]; however, this dissertation utilizes HPFC by considering the concept of MCS [73]. HPFC unifies both position and force information into the same dimension and controls them simultaneously.

Considering the aforementioned studies, the purpose of this dissertation is to clarify the dominant element of motion in each axis and time for improving the adaptability of MCS. Unlike the command values, the balance between the position and force gains in HPFC is rarely emphasized for task achievement. The gain is maximized in the range where the stability of the system is guaranteed. Therefore, the stability of the system is only concerning for the proper selection of controller gains. Therefore, the amount of gain should be set considering the stability of the system, although they increase task performance. Therefore, the method that clarifies the dominant element of a specific motion determined by gain selection, that is, position dominant, force dominant, or impedance dominant, must be developed. The flexibility of motion, which corresponds with the required controller, is learned not only from the operator but also in the task implementation. Therefore, the required controller is experimentally learned by considering the task achievements.

This dissertation considers the selection method of a required controller in each phase and axis for MCS. The motion flexibility of MCS is conventionally fixed, and this dissertation aims to select the required controller by considering the task realization. The results of experiment 1 showed that the task was achieved by motions based only on the required controller, and it was confirmed that the required controller was properly extracted. The adaptability to the environmental variations and the effectiveness of the command design considering the conditions for the success and type of controller design were confirmed through experiments 2 and 3. For future studies, the determination method of an appropriate controller value or range has to be developed, and the abstraction of human skilled motion by the

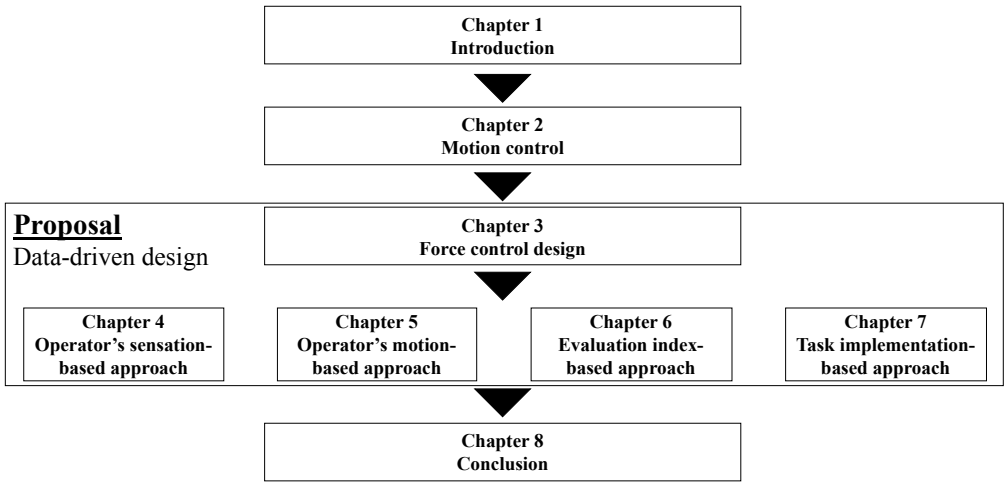

Fig. 1-2: Chapter organization.

proposed controller selection algorithm would be expected.

1.3 Organization of Dissertation

The rest of this dissertation is organized by seven chapters as shown in Fig. 1-2.

In Chapter 2, fundamental of motion control considered in this dissertation is introduced. In section 2.1, the modeling of a linear motor used in this dissertation is explained. In section 2.2, DOB and RFOB are introduced for enhancing the robustness and estimating the external force without using force sensors. In section 2.3, acceleration control is introduced for controlling certain physical variables in motion control.

Studies regarding the data-driven design for position/force control are discussed from Chapter 3 to Chapter 7.

In Chapter 3, a development method for force control with DOB and a NN is discussed based on the concept of the cerebellar calculation model in a data-driven control design. In Section 3.1, the explicit force control is explained. In Section 3.2, the proposed NN-based explicit force control is introduced. In Section 3.3, the contents of the simulation are introduced. In Section 3.4, the contents of the experiment are introduced. This chapter is summarized in Section 3.5.

In Chapter 4, a JNDs-based design policy of the haptics system is discussed as an approach for constructing a database regarding operator sensation. In Section 4.1, the outline of transparency is introduced. In Section 4.2, the proposed JNDs-based design policy is introduced. In Section 4.3, the estima-

tion method of time-delay and stiffness is introduced. In Section 4.4, the simulations are discussed. This chapter is summarized in Section 4.6.

In Chapter 5, an estimation method of the end-point impedance based on a bilateral control system is discussed as an approach for constructing a database regarding operator motion. In Section 5.1, a motion extraction method with bilateral control is explained. In Section 5.2, the outline of simulation is explained. In Section 5.2.1, the simulations with multiple amplitude, bandwidth, and impedance setups are discussed. In Section 5.2.2, the simulations with moving motors and changing impedances are discussed. In Section 5.3, the experiment is discussed. This chapter is summarized in Section 5.4.

In Chapter 6, an approach for evaluating index-based gain tuning for bilateral control is discussed as an index-based data-driven design using experimental data. In Section 6.1, the transfer function of a master or slave is explained. In Section 6.2, the analysis for gain setting is introduced. In Section 6.3, the gain tuning method is introduced. In Section 6.4, the experiments are introduced. This chapter is summarized in Section 6.5.

In Chapter 7, a selection of the required controller for a position and force-based task in the motion copying system is discussed as a task implementation-based data-driven design using experimental data. In Section 7.1, the task statement is introduced. In Section 7.2, the task and motion analyses for MCS is introduced. In Section 7.3, the experiments are introduced. This chapter is summarized in Section 7.4.

This dissertation is concluded in Chapter 8.

Nomenclature

Abbreviations

ABC	Acceleration-based bilateral control
DOB	Disturbance observer
DOF	Degree-of-freedom
FDOB	Force-based DOBD
FEL	Feedback error learning
HPFC	Hybrid position and force control
JNDs	Just noticeable differences
LfD	Learning from demonstration
MCS	Motion copying system
MOSAIC	Module selection and identification for control
NN	Neural network
PID	Proportional-integral-derivative
RFOB	Reaction force observer

Variables

b	Bias
c	Continuous number of trial successes
c'	Total number of situations
C	Controller
D	Viscosity
d	Damper
E	Error function
f	Force
g	Cutoff frequency
H	Number of units in the hidden layer
I	Number of units in the input layer
I	Current
J	Cost function
k	Stiffness
K	Gain
K_{t}	Torque constant
M	Mass
o	Node value
s	Laplace operator
ST	Sampling time

t	Current time
T	Total duration of motion
u	Input value
U	Unit
w	Weight
x	Position
y	Output value
z	Output from unit
Z	Impedance
α	Amount of improvement
η	Learning rate
κ	Control stiffness
θ	Angle
τ	Torque

Superscripts

cmd	Command value
comp	Compensation value
con	Contact value
dis	Disturbance value
dri	Driving value
eq	Equilibrium value
ext	External value
h1	Hidden layer 1
h2	Hidden layer 2
i	Input layer
load	Load value
o	Output layer
R	RNN layer
ref	Reference value
res	Response value
vir	Virtual value
$\hat{\circ}$	Estimated value

Subscript

a	Armature
all	Value in all frequency ranges
c	Virtual value
col	Corioli

conv	Conventional approach
d	Value of DOB
e	Environmental value
f	Value of force
g	Gravitational value
high	Value higher than the cutoff frequency
H	Number of units in hidden layer
i	Value of integral
int	Internal value
I	Number of units in input layer
k	Number of iterations
n	Nominal value
nn	Value of NN
O	Number of units in output layer
op	Operation's value
p	Value of proportional
prop	Proposed approach
r	Value of RFOB
t	Value of the current data
$t-1$	Value of previous data
v	Value of pseudo derivative

Chapter 2

Fundamental of Motion Control

In this chapter, fundamental of motion control used in this dissertation is described. In section 2.1, the modeling of a linear motor is explained. In section 2.2, DOB and RFOB are introduced. In section 2.2.1, DOB is briefly explained. In section 2.2.2, RFOB is briefly explained. In section 2.3, acceleration control is introduced. In section 2.3.1, position control is explained. In section 2.3.2, HPFC is explained. In section 2.3.3, admittance control is explained. In section 2.3.4, force control is explained. In section 2.3.5, bilateral control is explained.

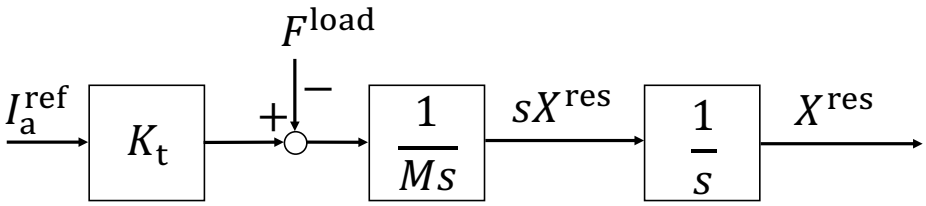

Fig. 2-1: The block diagram of motor dynamics.

2.1 Modeling of Linear Motor

This section considers one DOF linear motor for discussing the fundamental of motion control. Its equation of motion is given as follows:

$$Ms^2X^{\mathrm{res}} = F^{\mathrm{dri}} - F^{\mathrm{load}}. \tag{2.1}$$

Driving force is obtained by the multiplication of a thrust constant and an armature current and derived as follows by postulating a current minor loop with a high gain:

$$F^{\mathrm{dri}} = K_{\mathrm{t}}I_{\mathrm{a}}^{\mathrm{ref}}. \tag{2.2}$$

The block diagram of motor dynamics is shown in Fig. 2-1.

The load force can be broken down an external force, an internal interference force including Coriolis and centrifugal forces, Coulomb and viscous friction forces, and a gravity. The internal interference force and Coulomb and viscous friction forces are able to be neglected due to characteristics of 1 DOF linear motor, which this dissertation mainly considers. In addition, 1 DOF linear motor is not affected by the gravity because its motor is attached horizontal manner with the ground. Therefore, the load force F^{load} is derived as follows:

$$F^{\mathrm{load}} = F^{\mathrm{ext}}. \tag{2.3}$$

By combining Eqs. (2.1), (2.2), and (2.3), the following equation is obtained:

$$Ms^2X = K_{\mathrm{t}}I_{\mathrm{a}}^{\mathrm{ref}} - F^{\mathrm{ext}}. \tag{2.4}$$

Although nominal values of mass and thrust constant can be identified in advanced, they can be fluctuated

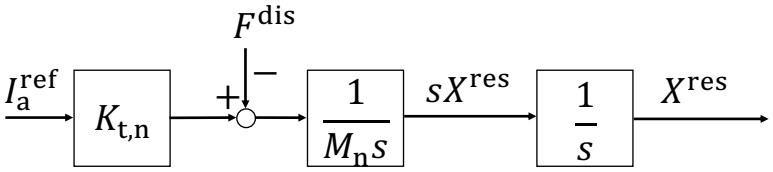

Fig. 2-2: The block diagram of motor dynamics taking into account the parameter variations.

and formulated as follows:

$$M = M_{\mathrm{n}} + \Delta M, \tag{2.5}$$

$$K_{\mathrm{t}} = K_{\mathrm{t,n}} + \Delta K_{\mathrm{t}}. \tag{2.6}$$

The equation of motion with parameter variations is formulated as follows:

$$(M_{\mathrm{n}} + \Delta M)\, s^2 X = (K_{\mathrm{tn}} + \Delta K_{\mathrm{t}})\, I_{\mathrm{a}}^{\mathrm{ref}} - F^{\mathrm{load}}. \tag{2.7}$$

This dissertation defines disturbances as the summation of load force and parameter variations as follows:

$$F^{\mathrm{dis}} = F^{\mathrm{load}} + \Delta M s^2 X - \Delta K_t I_{\mathrm{a}}^{\mathrm{ref}}. \tag{2.8}$$

The equation of motion considering the parameter variations is derived as follows:

$$M_{\mathrm{n}} s^2 X^{\mathrm{res}} = K_{\mathrm{t,n}} I_{\mathrm{a}}^{\mathrm{ref}} - F^{\mathrm{dis}}. \tag{2.9}$$

Its block diagram is shown in Fig. 2-2.

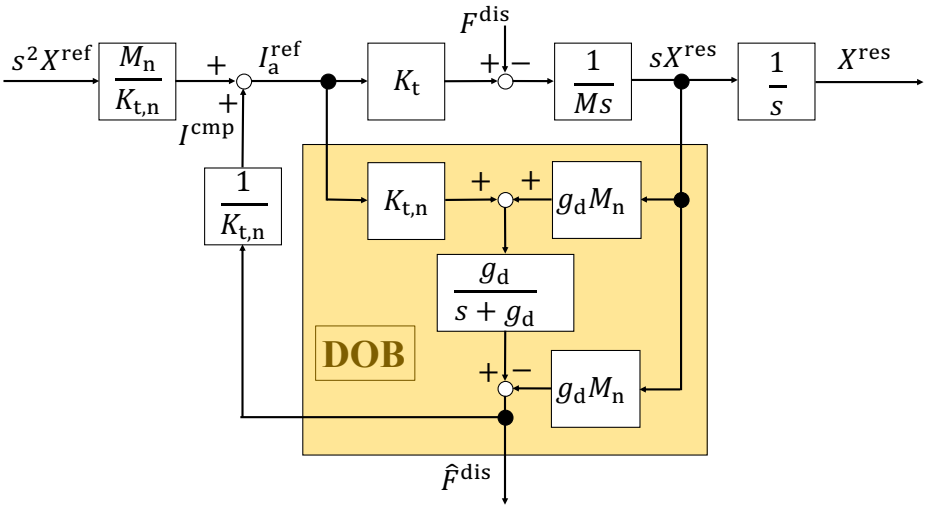

Fig. 2-3: The block diagram of DOB.

2.2 Disturbance OBserver and Reaction Force OBserver

2.2.1 Disturbance OBserver

An enhancement of robustness is essential for realizing the desired motion control. This section considers DOB as an approach for realizing the robust motion control [7]. DOB estimates the disturbance from the current reference value and the velocity response. The estimated disturbance is fed forward for suppressing the disturbance, and the robust acceleration control is achieved.

Disturbance can be computed as follows from Eq. (2.9):

$$F^{\mathrm{dis}} = K_{\mathrm{t,n}} I_\mathrm{a}^{\mathrm{ref}} - M_\mathrm{n} s^2 X^{\mathrm{res}}. \tag{2.10}$$

The acceleration response is computed from the derivative of position response that is obtained from an encoder, and it sometimes contains a high-frequency noise such as quantization errors and sensor noise. Therefore, a first-order low pass filter is utilized for suppressing the high-frequency noise in DOB. In addition, a pseudo-differential is applied instead of the simple differential for the purpose of suppressing the effect of high frequency noise. The block diagram of DOB and its equivalent form are shown in Figs. 2-3 and 2-4.

Due to the feedforward of the estimated disturbance, the acceleration response is obtained as follows:

$$s^2 X^{\mathrm{res}} = s^2 X^{\mathrm{ref}} - \frac{1}{M_\mathrm{n}} \frac{s}{s+g_\mathrm{d}} F^{\mathrm{dis}}. \tag{2.11}$$

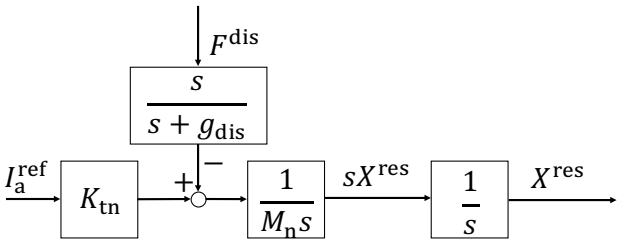

Fig. 2-4: The block diagram of equivalent form of DOB.

As the second term of right-hand side in Eq. (2.11) shows, the disturbance lower than DOB's cut-off frequency is suppressed due to the high-pass filter. Higher cut-off frequency ideally removes the effect of disturbance although the effect of noise is enhanced.

If the nominal values are set larger or smaller than actual values, DOB works as the phase lead/lag compensators [99]. The nominal values are set the same with the actual value of experimental set-up or the value in the specification sheet in this dissertation, and DOB enables to compensate the disturbance lower than its cut-off frequency. The external force estimated by RFOB is composed of stiffness and viscous components because its observer is designed in the acceleration dimension.

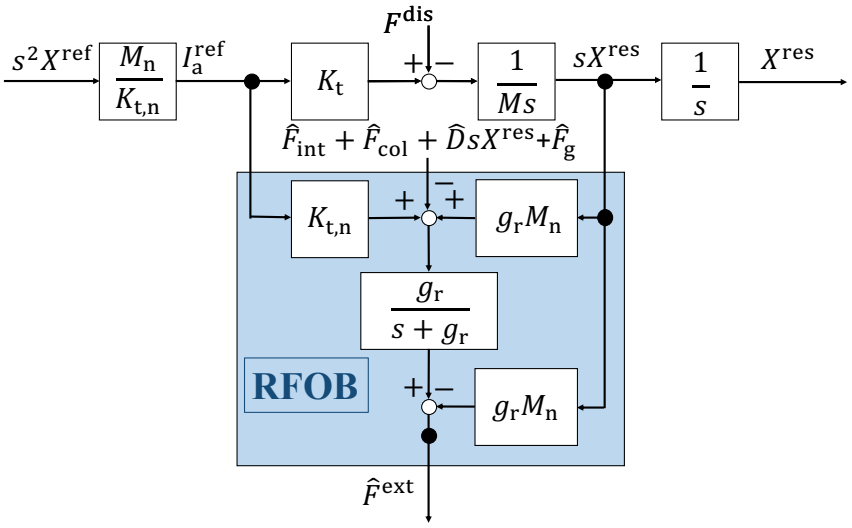

Fig. 2-5: The block diagram of RFOB.

2.2.2 Reaction Force OBserver

Information of external force is useful for considering the interactive motion with the surrounded environment. Force sensors are often utilized for its estimation although some disadvantages: the sensitiveness to the ambient environment and the severeness of allocations are known. As an alternative approach of force sensors, RFOB is introduced [13]. RFOB enables to estimate the external force from an identified dynamical model and the principle of DOB.

The disturbance is represented as Eq. (2.10), but it includes the variation of mass ΔM and thrust constant ΔK_{t}. Moreover, the internal interference force and Coulomb and viscous friction force have to be considered for general use. All these variables are needed to be identified in advance in the use of RFOB although they can be suppressed by DOB. The disturbance coincides with the external force is represented as follows if the variables are perfectly identified and compensated:

$$F^{\mathrm{dis}} = F^{\mathrm{ext}}. \tag{2.12}$$

The block diagram of RFOB is shown in Fig. 2-5. RFOB also uses the low-pass filter as similar as DOB although the former is a model-based approach while the latter is not. The estimated external force is computed as follows by inserting the low-pass filter.

$$\hat{F}^{\mathrm{ext}} = \frac{g_{\mathrm{r}}}{s+g_{\mathrm{r}}} F^{\mathrm{ext}}. \tag{2.13}$$

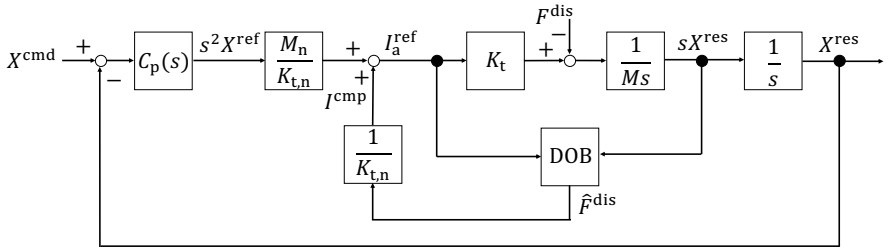

Fig. 2-6: The block diagram of position control system.

2.3 Acceleration Control

Position, velocity, and force are three well-known physical variables in motion control. The differentiation of position becomes the velocity, and the differentiation of velocity becomes the acceleration. In addition, the force divided by the mass becomes acceleration. These facts specify that the precise control of acceleration enables the precise control of both position and force simultaneously. This chapter considers acceleration based position, admittance, force, and bilateral controllers.

2.3.1 Position Control

A position response coincides with a position command in the case of the ideal position controller is realized [100]. The block diagram of position control is shown in Fig. 2-6. A Proportional-Derivative controller is used in position controller as follows:

$$C_{\mathrm{p}}(s) = K_{\mathrm{p}} + K_{\mathrm{v}}s. \tag{2.14}$$

The velocity gain is designed for making position controller critical damping as follows:

$$K_{\mathrm{v}} = 2\sqrt{K_{\mathrm{p}}}. \tag{2.15}$$

The acceleration reference is obtained as follows:

$$\begin{aligned} s^2X^{\mathrm{ref}} &= C_{\mathrm{p}}(s)(X^{\mathrm{cmd}} - X^{\mathrm{res}}) \\ &= K_{\mathrm{p}}(X^{\mathrm{cmd}} - X^{\mathrm{res}}) + K_{\mathrm{v}}(sX^{\mathrm{cmd}} - sX^{\mathrm{res}}) \end{aligned} \tag{2.16}$$

2.3.2 Hybrid Position/Force Control

Regarding control methods of both position and force at the same axis, two approaches: HPFC and impedance/admittance control, are often discussed [101]. This section introduces a hybrid position and force control. Task space is divided into two subspaces for controlling position and force. The acceleration reference is computed as follows:

$$s^2 X^{\mathrm{ref}} = K_{\mathrm{p}}(X^{\mathrm{cmd}} - X^{\mathrm{res}}) + K_{\mathrm{v}}(sX^{\mathrm{cmd}} - sX^{\mathrm{res}}) - K_{\mathrm{f}}(F^{\mathrm{cmd}} - F^{\mathrm{ext}}). \quad (2.17)$$

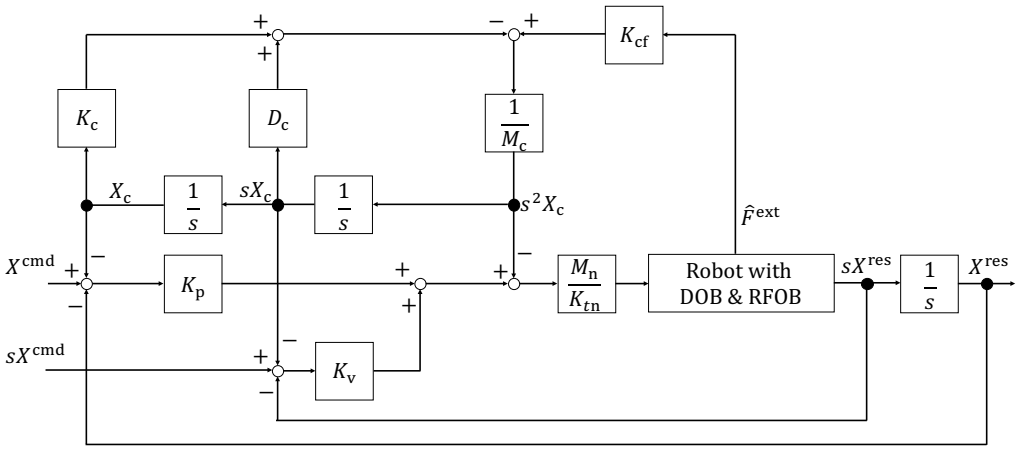

Fig. 2-7: The block diagram of admittance control.

2.3.3 Admittance Control

Another approach that combines both position and force at the same axis is admittance control [64]. This regulates mechanical impedance by objects and realizes the dynamical relationship between position and force of end-effector. The input and output of manipulator are position and force.

The acceleration reference of admittance control is computed as follows:

$$s^2X^{\mathrm{ref}} = K_{\mathrm{p}}(X^{\mathrm{cmd}} - X^{\mathrm{res}} - X_{\mathrm{c}}) + K_{\mathrm{v}}(sX^{\mathrm{cmd}} - sX^{\mathrm{res}} - sX_{\mathrm{c}}) - s^2X_{\mathrm{c}}, \tag{2.18}$$

$$s^2X_{\mathrm{c}} = \frac{\hat{F}^{\mathrm{ext}} - K_{\mathrm{c}}X_{\mathrm{c}} - D^{\mathrm{c}}sX_{\mathrm{c}}}{M^{\mathrm{c}}}. \tag{2.19}$$

The block diagram of admittance control is shown in Fig. 2-7.

2.3.4 Force Control

A force response coincides with a force command in the case of the ideal force controller is realized [102]. The block diagram of force control is shown in Fig. 2-8. The force controller is represented as follows:

$$C_{\mathrm{f}} = K_{\mathrm{f}}. \tag{2.20}$$

PD gains are sometimes applied into its controller, but the derivative of force is in the dimension of jerk and heavily affected by noises. Therefore, this dissertation simply applies Proportional (P) gain into the

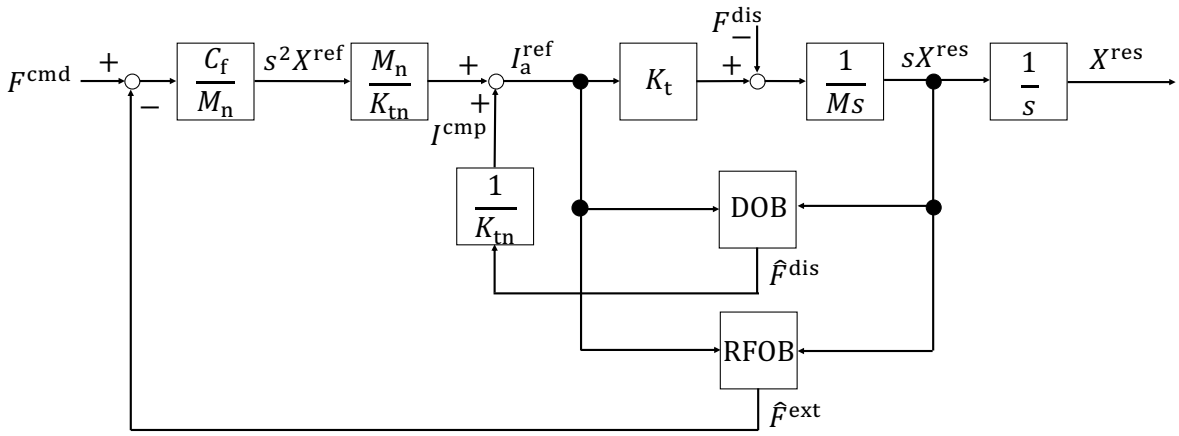

Fig. 2-8: The block diagram of force control system.

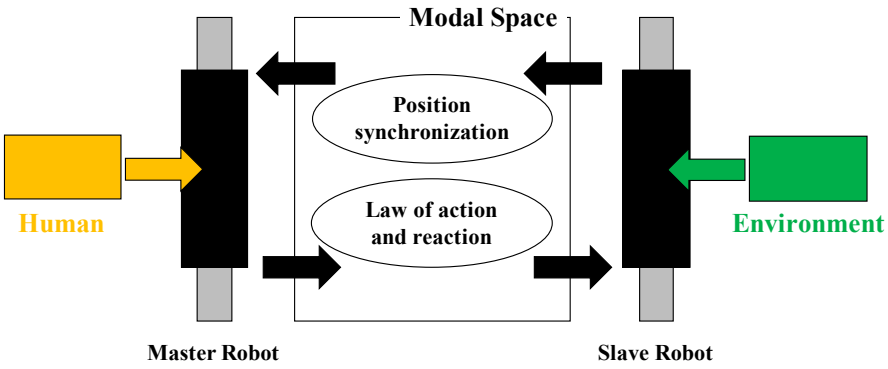

Fig. 2-9: Concept of bilateral control.

force controller. The acceleration reference is obtained as follows:

$$\begin{aligned} s^2X^{\mathrm{ref}} &= C_{\mathrm{f}}(F^{\mathrm{cmd}} - \hat{F}^{\mathrm{ext}}) \\ &= K_{\mathrm{f}}(F^{\mathrm{cmd}} - \hat{F}^{\mathrm{ext}}). \end{aligned} \tag{2.21}$$

2.3.5 Bilateral Control

Bilateral control system aims at transmitting haptic information to remote places as shown in Fig. 2-9 [86, 103].

Four-ch (4ch) bilateral control system, which this dissertation simply calls the bilateral control system from later on, is composed of master and slave robots, and the control goals are the position synchro-

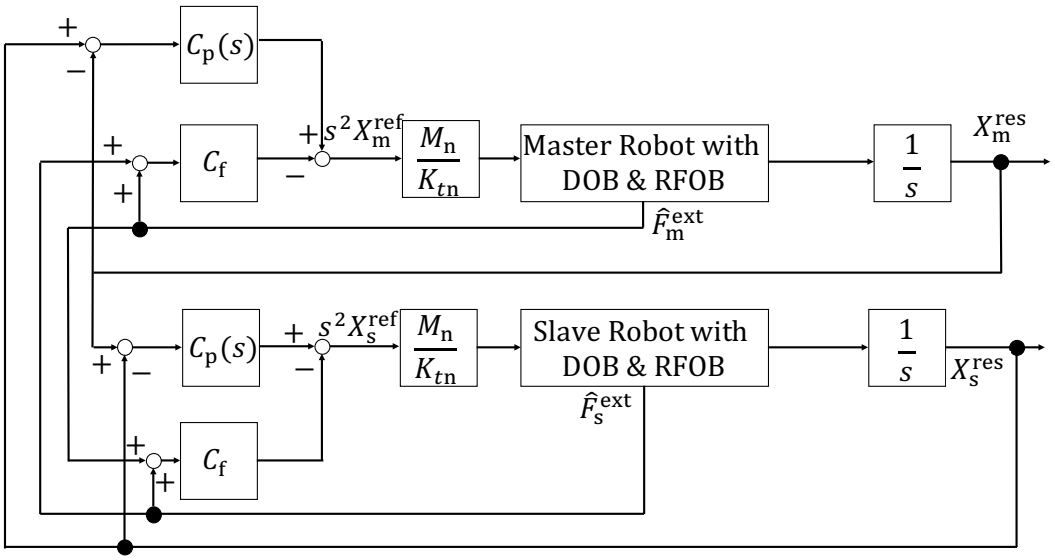

Fig. 2-10: The block diagram of bilateral control system.

nization and the realization of the law of action and reaction as follows:

$$X_{\mathrm{m}} - X_{\mathrm{s}} = 0, \tag{2.22}$$

$$F_{\mathrm{m}} + F_{\mathrm{s}} = 0. \tag{2.23}$$

The entire block diagram of the bilateral controller is shown in Fig. 2-10.

Chapter 3

Data-driven Design of Force Control

This chapter discusses a development method of force control with DOB and neural network. In Section 3.1, the explicit force control is explained. In Section 3.2, the proposed NN-based explicit force control is introduced. In Section 3.2.1, the idea of combining NN and DOB is explained as an outline of proposal. In Section 3.2.2, the structure of NN is explained. In Section 3.2.3, the learning method of NN is explained. In Section 3.2.4, the learning result of NN is discussed. In Section 3.2.5, the idea of fault tolerance is explained. In Section 3.3, the contents of simulation are introduced. In Section 3.3.1, the outline of simulation is explained. In Section 3.3.2, the proposal and conventional methods are compared. In Section 3.3.3, the performance of NN is investigated. In Section 3.4, the contents of experiment are introduced. In Section 3.4.1, the outline of experiment is explained. In Section 3.4.2, the setups of experiment is explained. In Section 3.4.3, the results of experiment are discussed. This chapter is summarized in Section 3.5.

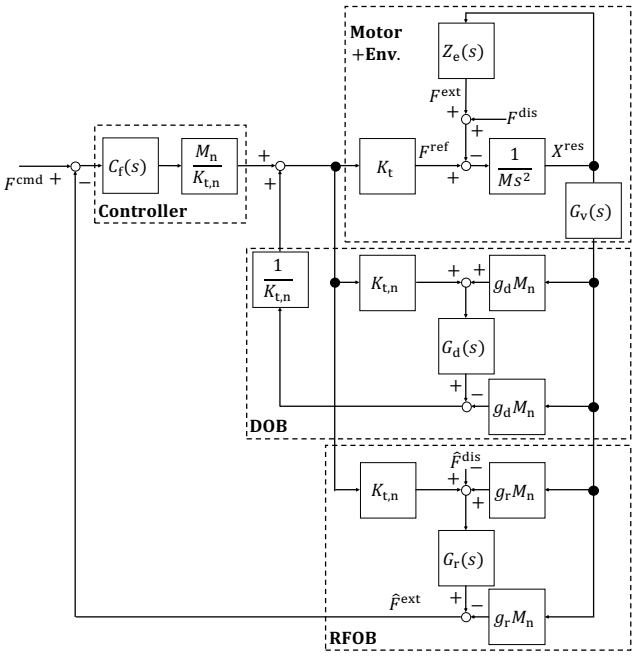

Fig. 3-1: Block diagram of explicit force control with DOB and RFOB (conventional)

3.1 Explicit Force Control

This dissertation considers explicit force control with DOB and RFOB, and its block diagram is shown in Fig. 3-1. The first-order environmental impedance is considered as follows:

$$F^{\mathrm{ext}} \quad = \quad Z_{\mathrm{e}}(s)X^{\mathrm{res}} = (sd_{\mathrm{e}} + k_{\mathrm{e}})X^{\mathrm{res}}. \tag{3.1}$$

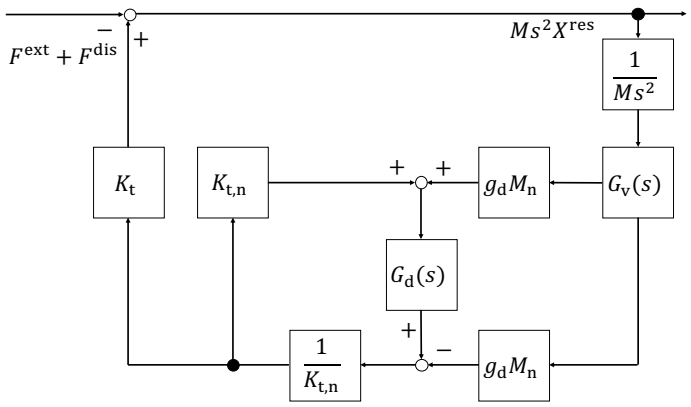

Fig. 3-2: Block diagram of the operations from the occurrence of external and disturbance forces to the force response

The transfer function of its control is computed as follows:

$$
\begin{aligned}
\frac{\hat{F}^{\mathrm{ext}}}{F^{\mathrm{cmd}}} &= \frac{L(s)}{1+L(s)}, \\
L(s) &= C_{\mathrm{f}}(s)\frac{M_{\mathrm{n}}}{K_{\mathrm{t,n}}}\frac{G_1(s)}{G_2(s)}, \\
G_1(s) &= K_{\mathrm{t,n}}G_{\mathrm{r}}(s)Z(s) - \{1-G_{\mathrm{r}}(s)\}g_{\mathrm{r}}K_{\mathrm{t}}M_{\mathrm{n}}G_{\mathrm{v}}(s), \\
G_2(s) &= \{1-G_{\mathrm{d}}(s)\}\{Z(s) + \frac{K_{\mathrm{t}}}{K_{\mathrm{t,n}}}g_{\mathrm{d}}M_{\mathrm{n}}G_{\mathrm{v}}(s)\}, \\
C_{\mathrm{f}}(s) &= K_{\mathrm{p}} + \frac{K_{\mathrm{i}}}{s}, \\
G_{\mathrm{d}}(s) &= \frac{g_{\mathrm{d}}}{s+g_{\mathrm{d}}}, \\
G_{\mathrm{r}}(s) &= \frac{g_{\mathrm{r}}}{s+g_{\mathrm{r}}}, \\
G_{\mathrm{v}}(s) &= \frac{sg_{\mathrm{v}}}{s+g_{\mathrm{v}}}, \\
Z(s) &= Ms^2 + Z_{\mathrm{e}}(s).
\end{aligned}
\tag{3.2}
$$

The position response is measured using an encoder, and the velocity response is estimated through the pseudo derivative of position response by $G_{\mathrm{v}}(s)$. The external force is estimated by RFOB. Derivative control is sometimes implemented in the force controller with DOB and RFOB, but its dimension becomes a jerk in force control and is affected by noise. Therefore, PI controller was considered instead of the PID controller in $C_{\mathrm{f}}(s)$ in this chapter. The first-order low-pass filter is implemented as $G_{\mathrm{d}}(s)$ and $G_{\mathrm{r}}(s)$ in the DOB and RFOB, respectively.

The block from external and disturbance forces to the force response is shown in Fig. 3-2 and com-

Table 3.1: Parameter setup for Bode diagram

Description	Value
Nominal mass of motor	$2.1\ \mathrm{kg}$
Torque constant	$33\ \mathrm{N/A}$
Cutoff frequencies of DOB, RFOB, pseudo derivative	$500\ \mathrm{rad/s}$
Proportional gain	$0.9\ \mathrm{kg}^{-1}$
Integral gain	$156\ s\mathrm{kg}^{-1}$
Environmental stiffness	5000 N/m
Environmental viscosity	20 sN/m

puted as follows:

$$\frac{Ms^2X^{\mathrm{res}}}{F^{\mathrm{ext}}+F^{\mathrm{dis}}} = -\frac{s^2}{s^2+g_{\mathrm{d}}G_{\mathrm{v}}(s)\dfrac{K_{\mathrm{t}}M_{\mathrm{n}}}{K_{\mathrm{t,n}}M}}. \tag{3.3}$$

If the pseudo derivative can be treated as a simple derivative and the nominal parameters are properly identified, Eq. (3.3) can be recomputed as follows:

$$\frac{Ms^2X^{\mathrm{res}}}{F^{\mathrm{ext}}+F^{\mathrm{dis}}} = -\frac{s}{s+g_{\mathrm{d}}}. \tag{3.4}$$

Eqs. (3.3) and (3.4) show the filtering effect by DOB.

The motion equation of explicit force control with DOB is computed as follows:

$$Ms^2X^{\mathrm{res}} = C_{\mathrm{f}}(s)\frac{M_{\mathrm{n}}}{K_{\mathrm{t,n}}}(F^{\mathrm{cmd}}-\hat{F}^{\mathrm{ext}}) - \{1-G_{\mathrm{d}}(s)\}(F^{\mathrm{ext}}+F^{\mathrm{dis}}). \tag{3.5}$$

Here, $G_{\mathrm{d}}(s)$ is equivalent to Eq. (3.3) or (3.4). The estimated external force is computed as follows:

$$\hat{F}^{\mathrm{ext}} = F^{\mathrm{cmd}} - \{1-G_{\mathrm{d}}(s)\}\frac{K_{\mathrm{t,n}}}{C_{\mathrm{f}}(s)M_{\mathrm{n}}}(F^{\mathrm{ext}}+F^{\mathrm{dis}}) - \frac{K_{\mathrm{t,n}}}{C_{\mathrm{f}}(s)M_{\mathrm{n}}}Ms^2X^{\mathrm{res}}. \tag{3.6}$$

The second and third terms on the right-hand side of Eq. (3.6) become smaller as the gain of the force controller becomes larger. Therefore, the setting of appropriate control gain or a combination of another controller is able to improve the performance of its control.

The Bode diagram of explicit force control and the filtering effect by DOB with the parameters listed in Table 3.1 are shown in Fig. 3-3. DOB ideally compensates for disturbances that are lower than its cutoff frequency; however, the parameter setup of the nominal values or nonlinear terms affects the performance. Moreover, the inertial force is not compensated because the DOB is designed in the dimension

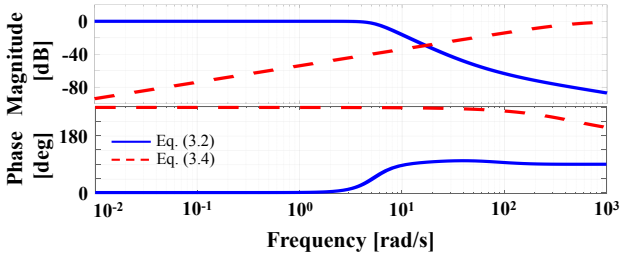

Fig. 3-3: Bode diagram of explicit force control

of acceleration, and the transient response of explicit force control with DOB must be improved. This dissertation aimed to improve the performance of force control from the perspective of both feedback and feedforward components without significantly limiting the condition of motion.

Table 3.2: Candidate structures

	DOB	NN (all frequencies)	NN (high frequency)
Conventional	✓	–	–
Structure 1	–	✓	–
Structure 2	✓	✓	–
Structure 3	✓	–	✓

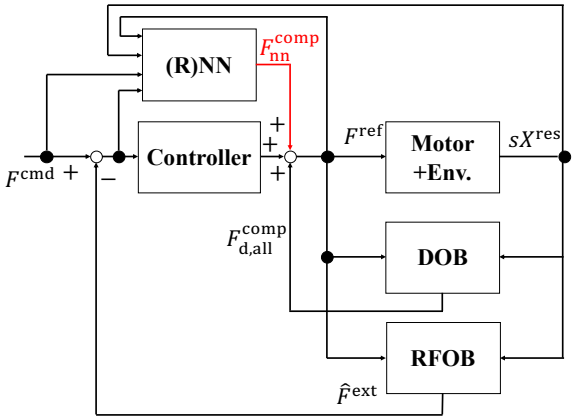

Fig. 3-4: Block diagram of explicit force control with neural network (NN) (all frequency)

3.2 Proposed Neural Network (NN)-based Explicit Force Control with Disturbance Observer

3.2.1 Outline

The NN is implemented into the explicit force control with DOB and RFOB. This dissertation considers three candidate structures, as listed in Table 3.2, in order to select the method for combining DOB and NN. The tick mark (✓) represents that the compensator of the structure is implemented, while the dashed mark (–) represents that the compensator is not implemented. NN (all frequencies) shows that the compensator works in all frequency ranges, while NN (high frequency) shows that the compensator works in frequency ranges higher than the cutoff frequency of the DOB. The block diagrams of Structures 2 and 3 are shown in Figs. 3-4 and 3-5, where $\bigcirc_{\mathrm{d,all}}$ and $\bigcirc_{\mathrm{d,high}}$ denote the values generated by DOB in the case of NN (all frequencies) and NN (high frequency), respectively. The force references of

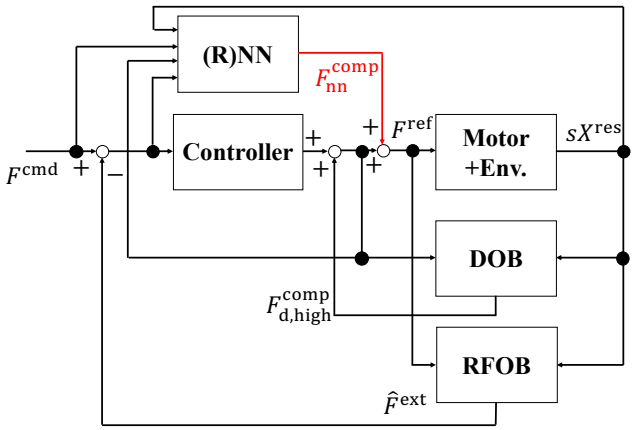

Fig. 3-5: Block diagram of explicit force control with NN (high frequency)

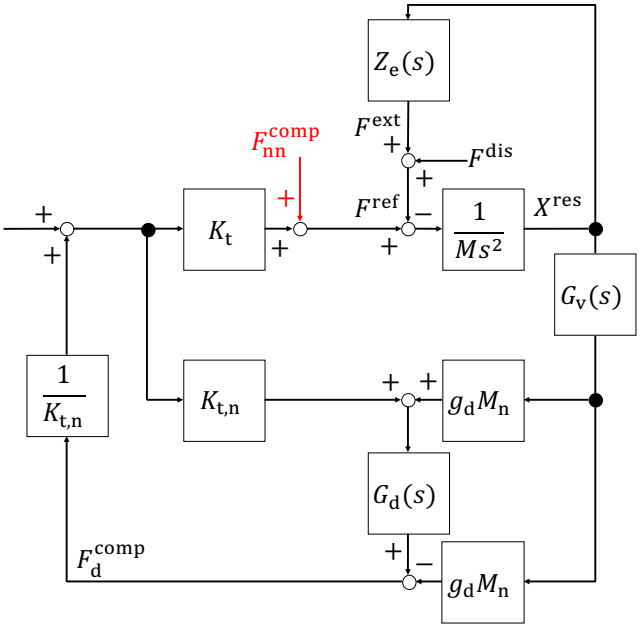

Fig. 3-6: Composition of DOB with NN (high frequency)

Structures 2 and 3 are computed based on Eqs. (3.7) and (3.8), respectively:

$$F^{\mathrm{ref}} = C_{\mathrm{f}}(s)\frac{M_{\mathrm{n}}}{K_{\mathrm{t,n}}}(F^{\mathrm{cmd}} - \hat{F}^{\mathrm{ext}}) + F_{\mathrm{d,all}}^{\mathrm{comp}} + F_{\mathrm{nn}}^{\mathrm{comp}}, \tag{3.7}$$

$$F^{\mathrm{ref}} = C_{\mathrm{f}}(s)\frac{M_{\mathrm{n}}}{K_{\mathrm{t,n}}}(F^{\mathrm{cmd}} - \hat{F}^{\mathrm{ext}}) + F_{\mathrm{d,high}}^{\mathrm{comp}} + F_{\mathrm{nn}}^{\mathrm{comp}}. \tag{3.8}$$

The block parts labeled Motor+Env. and DOB in Fig. 3-5 are equivalently transformed as illustrated in Fig. 3-6. The compensation value generated by the NN (high frequency) is substituted from a similar point to the external and disturbance forces, as illustrated in Fig. 3-6.

The motion equations of Structures 2 and 3 are computed using Eqs. (3.9) and (3.10), respectively:

$$\begin{aligned} M^2 X^{\mathrm{res}} &= C_{\mathrm{f}}(s)\frac{M_{\mathrm{n}}}{K_{\mathrm{t,n}}}(F^{\mathrm{cmd}} - \hat{F}^{\mathrm{ext}}) \\ &- \{1 - G_{\mathrm{d}}(s)\}(F^{\mathrm{ext}} + F^{\mathrm{dis}}) + F_{\mathrm{nn}}^{\mathrm{comp}}, \end{aligned} \tag{3.9}$$

$$\begin{aligned} M^2 X^{\mathrm{res}} &= C_{\mathrm{f}}(s)\frac{M_{\mathrm{n}}}{K_{\mathrm{t,n}}}(F^{\mathrm{cmd}} - \hat{F}^{\mathrm{ext}}) \\ &- \{1 - G_{\mathrm{d}}(s)\}(F^{\mathrm{ext}} + F^{\mathrm{dis}} - F_{\mathrm{nn}}^{\mathrm{comp}}). \end{aligned} \tag{3.10}$$

In Structure 3 or Eq. (3.10), the compensation value generated by NN (high frequency) also becomes the input of the transfer function as well as $F^{\mathrm{ext}} + F^{\mathrm{dis}}$ in Fig. 3-2. Therefore, it works for compensating the external and disturbance forces higher than the cutoff frequency of the DOB.

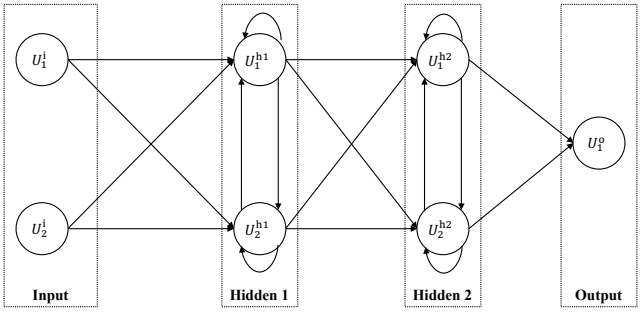

Fig. 3-7: Example of a network structure

3.2.2 Structure of NN

The structure of recurrent NNs (RNNs) is useful when the time-sequence data is considered [104]. NN nodes are connected not only feedforward direction but also the recurrent direction in the RNN. An example of network structure is illustrated in Fig. 3-7. Two units in the input layer, two units in the hidden 1 layer with recurrent network, two units in the hidden 2 layer with recurrent network, and one unit in the output layer are shown in this example. Each layer has certain units, which are represented by circles. A leaky rectified linear unit (LReLU) is utilized as the activation function of all units. The number of units in each hidden layer is set the same, and the outputs from the hidden 1, hidden 2, and output layers are computed as Eqs. (3.11), (3.12), and (3.13), respectively:

$$
\begin{aligned}
o_{\mathrm{h1}}^t &= \sum_{\mathrm{I}} w_{\mathrm{h1,i}} z_{\mathrm{i}}^t + \sum_{\mathrm{H}} w_{\mathrm{h1,h1}} z_{\mathrm{h1}}^{t-1} + b_{\mathrm{h1}}, \\
z_{\mathrm{h1}}^t &= \mathrm{LReLU}(o_{\mathrm{h1}}^t). \qquad (3.11) \\
o_{\mathrm{h2}}^t &= \sum_{\mathrm{H}} w_{\mathrm{h2,h1}} z_{\mathrm{h1}}^t + \sum_{\mathrm{H}} w_{\mathrm{h2,h2}} z_{\mathrm{h2}}^{t-1} + b_{\mathrm{h2}}, \\
z_{\mathrm{h2}}^t &= \mathrm{LReLU}(o_{\mathrm{h2}}^t). \qquad (3.12) \\
o_{\mathrm{o}}^t &= \sum_{\mathrm{H}} w_{\mathrm{o,h2}} z_{\mathrm{h2}}^t + b_{\mathrm{o}}, \\
z_{\mathrm{o}}^t &= \mathrm{LReLU}(o_{\mathrm{o}}^t). \qquad (3.13)
\end{aligned}
$$

The subscript of weight represents the connected layers. For instance, $w_{\mathrm{h1,i}}$ specifies the weight from the input layer to the hidden 1 layer, and $w_{\mathrm{h2,h1}}$ specifies the weight from the hidden 1 layer to the hidden 2 layer. $w_{\mathrm{h1,h1}}$ indicates the recurrent network and specifies the weight from the hidden 1 layer in the previous data to the hidden 1 layer in the current data.

The error between the command and response becomes an input in the FEL scheme. If the error is

Table 3.3: Available compositions of neural networks

Candidate	H	L	RNN
1	26	1	w/o
2	6	1	w/
3	9	2	w/o
4	4	2	w/
5	7	3	w/o

considered as one of the inputs, the NN works similar to the controller gains or feedback component. Thus, the NN adjusts the controller gains to the appropriate values. In addition to the error, the force command, input value to the DOB from the left side, and input value to DOB from the right side (velocity response) are considered as the input variables of the NN. The force command is expected to operate the NN as the feedforward component. The input values to the DOB from the left and right sides are also set as inputs to ensure that the NN owns the element of the DOB or feedforward component. The selection of input variables to the NN compensates the disturbance from the perspective of both feedback and feedforward components. The input variables are selected based on the knowledge of actual controller design.

The number of layers or units is generally expected to be as large as possible to enhance the representation ability of various situations; however, the composition of NN should be designed by considering not only the performance but also the processing ability of the computer. The specifications of the computer used in the experiment are Intel Core 2 Duo CPU E8400 at 3.00 GHz with 1.8 GB memory, using Linux operating system. The NN was experimentally investigated based on the available compositions in this experimental setup; the available compositions are listed in Table 3.3. Here, w/ and w/o denote the compositions with and without the RNN layers, respectively. If the number of variables is increased, the computer stops working. This dissertation selects an appropriate system from the three candidate structures listed in Table 3.2 and available compositions listed in Table 3.3.

3.2.3 Learning Method of NN

The network is trained by backpropagation and backpropagation through time for the NN and RNN [104], respectively, and the weights are updated in each sample by the gradient descent algorithm as follows:

$$w_{k+1} = w_k - \eta \frac{\partial J_k}{\partial w_k}. \tag{3.14}$$

The cost function is designed based on the square error and is set as follows:

$$J = \frac{1}{2}(F^{\mathrm{cmd}} - \hat{F}^{\mathrm{ext}})^2. \tag{3.15}$$

The objective of training is to minimize the cost function, and the estimated external force is expected to follow the command by iterating the process of gradient descent. The objective is satisfied even if the motor is accelerated in the negative direction owing to the inertial force, and the position response is added as a constraint ($X^{\mathrm{res}} \geq 0$). If the cost function continuously increases 1000 times, all parameters are initialized and the training is carried out again.

The network is trained on a simulation, and the trained network is directly utilized in the actual experimental setup. The environmental stiffness, environmental viscosity, and coefficient of command amplitude were changed to enhance the versatility of the system.

The learning algorithm is as presented subsequently. Here, the amount of improvement α takes a value smaller than one. The learning was performed until the NN-based approach achieved better performance than the conventional approach in all situations, where PI gain with DOB was considered as the conventional approach. The weights were updated at each sampling time if the error function of the NN-based approach was larger than the conventional approach in Lines 9 – 10. Once the error function of the NN-based approach became smaller than that of the conventional approach, the continuous number of trial successes was increased and the situation was updated in Lines 15 – 16. The error function was computed after one training was completed as follows:

$$E = \sum_{t=0}^{t=T} |F^{\mathrm{cmd}} - \hat{F}^{\mathrm{ext}}|. \tag{3.16}$$

The error function shows the absolute mean square error of one training.

The learning code was written in C language; moreover, the learning process was performed 10 times for each candidate structure and available composition of the NN. The learning was terminated after one

Algorithm 1 The process of learning NN

while $c < c'$ **do**
  if Violate constraints **then**
    Initialization
  else
    Initialization except weights
  end if
  while $t \leq$T **do**
    Motor Control
    if c==0 **then**
      Update weights based on Eq. (3.14)
    end if
    t+=ST
  end while
  Compute E_{nn} and E_{conv}
  if $E_{\mathrm{nn}} < (\alpha E_{\mathrm{conv}})$ **then**
    c+= 1
    Update situation
  else
    c=0
  end if
end while

hundred thousand iterations if the learning was not completed by the algorithm within its number of iterations. The learning was performed again in the actual experimental setup because certain elements of the experiment, such as contact, could not be described perfectly in the simulation. Therefore, a structure of the NN that requires fewer learning iterations is expected to be revealed and selected through the learning process.

The parameters that were setup for the learning process are listed in Table 3.4. The remaining parameters are similar to those listed in Table 3.1. While considering the controller gain setting, the proportional gain was initially tuned in the order of 0.1 by minimizing the error function similar to the limit sensitivity method. Then, the integral gain was tuned in the order of 1 by minimizing the error function. The tuned proportional and integral gains, which were designed for the conventional method, were applied to all candidates structures for a fair comparison. The learning rate was randomly chosen at the initialization step. The faster convergence tends to be achieved by the larger learning rate, but the smaller learning rate should be selected from the perspective of small steady-state error and stability of learning [105, 106].

Table 3.4: Parameter setup for learning

Description	Value
Sampling time	1 ms
Amount of improvement	0.9
Learning rate	0.0001 – 0.01
Assumed range of force command	-10 – 10
Assumed range of input value to DOB from the right side	-1 – 1
Assumed range of input value to DOB from the left side	-0.05 – 0.05
Assumed range of error	-10 – 10

Table 3.5: Parameter setup for different situations

Description	Range	Amount of change
Environmental stiffness	2000 N/m – 40000 N/m	2000 N/m
Environmental viscosity	$10s$ N/m – $100s$ N/m	$10s$ N/m
Coefficient of command amplitude	1 – 3	0.5

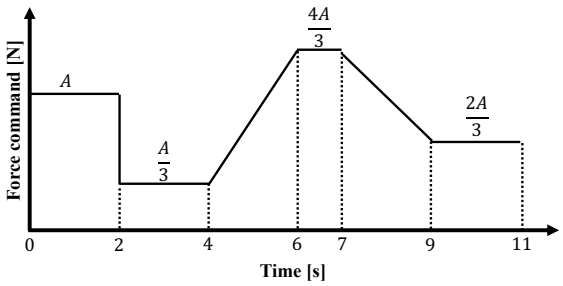

Fig. 3-8: Command of motion

The input of the NN was normalized by assuming the range of each variable. For instance, the assumed range of force command was ± 10 and the input to NN was 0, 0.5, or 1 if the force command was -10N, 0N, or 10N, respectively.

The parameters were set in different situations are listed in Table 3.5. One thousand different types of situations (twenty types of environmental stiffness values, ten types of environmental viscosity values, and five types of amplitudes) were considered. The command of motion was designed as shown in Fig. 3-8, where A represents the coefficient of the command amplitude. The motion includes both the step and ramp motions, and these amplitudes and inclinations are varied based on the coefficient of the command amplitude.

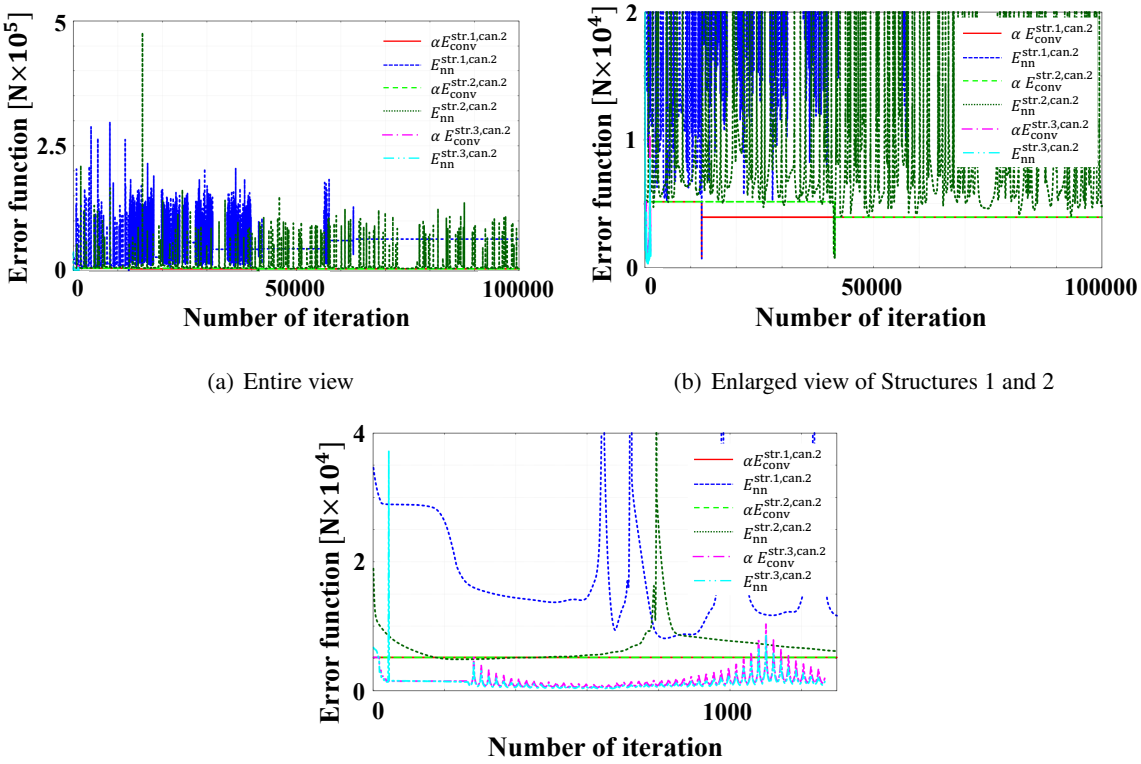

(a) Entire view

(b) Enlarged view of Structures 1 and 2

(c) Enlarged view of Structure 3

Fig. 3-9: Learning result based on the different candidate structures

3.2.4 Learning Results

The learning results based on the different candidate structures with composition candidate 2, as listed in Table 3.3, are shown in Fig. 3-9, where $\bigcirc^{\mathrm{str}.1}$, $\bigcirc^{\mathrm{str}.2}$, $\bigcirc^{\mathrm{str}.3}$, and $\bigcirc^{\mathrm{can}.2}$ denote the values of Structures 1, 2, and 3, and composition candidate 2 of the NN, respectively. The learning was not terminated within one hundred thousand iterations in the case of Structures 1 and 2, as shown in Fig. 9 (b). The error functions gradually became smaller, and the situation was updated at approximately 12000 and 40000 iterations in Structures 1 and 2. However, once the situation was updated, where the error functions of conventional approaches were updated, the learned weight was not useful for the updated situation. DOB is a significantly powerful method for compensating the disturbance, and it is considerably difficult to achieve the work of DOB only by (R)NN with a limited number of layers. The enlarged view of Structure 3 is shown in Fig. 9 (c). It can be observed that the amount of error functions of the proposed method became smaller than that of the conventional method even if the situation was updated. Structure

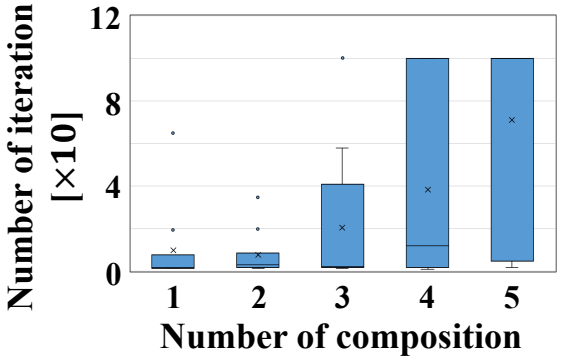

Fig. 3-10: Learning results of Structure 3

3 enables the avoidance of the interference between DOB and NN, and the learning of the NN could be appropriately performed. The compensation by NN improves the performance. Therefore, the implementation of the NN for explicit force control with DOB improves the performance; however, it should be designed without interrupting the work of DOB.

The learning results of Structure 3 with five available compositions of NN are shown in Fig. 3-10. Compositions 3, 4, and 5 could not complete the learning within one hundred thousand iterations in certain trials. Conversely, compositions 1 and 2 terminated the learning within the limited number of iterations in all 10 trials. In particular, composition 2 required fewer iterations from the average of 10 trials in each composition. In summary, this dissertation implemented Structure 3 with composition 2.

3.2.5 Fault Tolerance

Fault tolerance is also designed for the case when the learning of the NN is not performed appropriately. Because NN may not operate properly if it is utilized in a situation that it has not encountered previously, this dissertation cannot guarantee that the command designed in Fig. 3-8 includes all types of motions. The force references of the conventional method ($F^{\mathrm{ref}}_{\mathrm{conv}} = C_{\mathrm{f}}(s)\frac{M_{\mathrm{n}}}{K_{\mathrm{t,n}}}(F^{\mathrm{cmd}} - \hat{F}^{\mathrm{ext}}) + F^{\mathrm{comp}}_{\mathrm{dob}}$) and proposed methods $F^{\mathrm{ref}}_{\mathrm{prop}}$ are computed.

The following four cases are the desired generation of force references when the force command takes a value larger than zero:

1. $(F^{\mathrm{cmd}} = F^{\mathrm{cmd}}_{t-1}) \wedge (\hat{F}^{\mathrm{ext}} > F^{\mathrm{cmd}}) \wedge (F^{\mathrm{ref}}_{\mathrm{prop}} \leq F^{\mathrm{ref}}_{\mathrm{prop},t-1})$,
2. $(F^{\mathrm{cmd}} = F^{\mathrm{cmd}}_{t-1}) \wedge (\hat{F}^{\mathrm{ext}} \leq F^{\mathrm{cmd}}) \wedge (F^{\mathrm{ref}}_{\mathrm{prop}} > F^{\mathrm{ref}}_{\mathrm{prop},t-1})$,
3. $(F^{\mathrm{cmd}} > F^{\mathrm{cmd}}_{t-1}) \wedge (F^{\mathrm{ref}}_{\mathrm{prop}} > F^{\mathrm{ref}}_{\mathrm{prop},t-1})$,
4. $(F^{\mathrm{cmd}} < F^{\mathrm{cmd}}_{t-1}) \wedge (F^{\mathrm{ref}}_{\mathrm{prop}} \leq F^{\mathrm{ref}}_{\mathrm{prop},t-1})$.

The force reference of the proposed method is utilized if the above-mentioned four cases are satisfied, while the force reference of the conventional method is utilized if these cases are violated.

The switching algorithm also contributes to the safety of the experiment. The stability of the control system cannot be assured because the transfer function of the NN cannot be precisely described. The NN works as the feedforward component; moreover, the setting constraints to the NN compensation value or cutting off NN enables the avoidance of unacceptable motion.

Table 3.6: Parameters for environmental impedance in simulation

Description	Amount
Environmental stiffness of hard object	25000 N/m
Environmental viscosity of hard object	100 sN/m
Environmental stiffness of soft object	2000 N/m
Environmental viscosity of soft object	15 sN/m

3.3 Simulation

3.3.1 Outline

Simulations were conducted to observe the performance of the proposed NN-based explicit force control. The objectives of the simulations are as follows: 1. to compare the proposed method with the conventional method; 2. to show the performance for a wide frequency range of disturbances. In the first simulation, the leaning of NN was performed and the proposed method was compared with the conventional method (PI + DOB). In the second simulation, the sweep sine disturbance was intentionally added to check the compensation performance of the NN. The motor was assumed to contact both hard and soft objects, and the environmental impedances were set as listed in Table 3.6. The rest of the parameters were set to the values listed in Table 3.1.

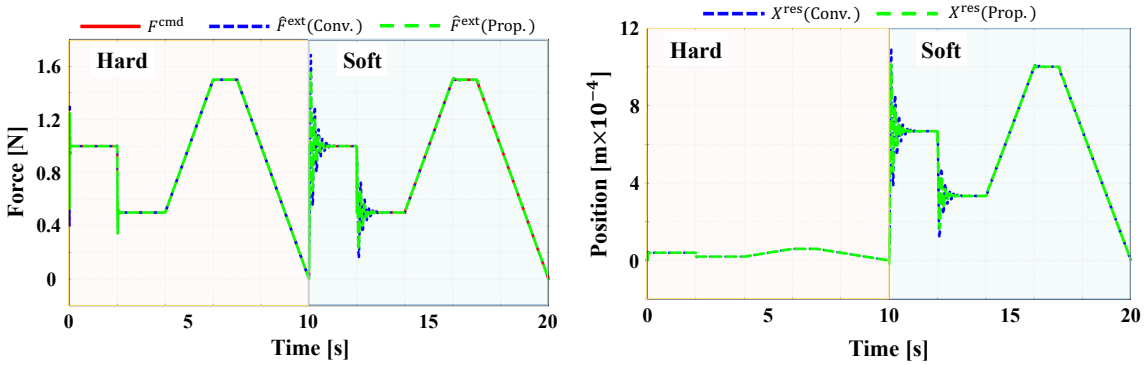

(a) Force (b) Position

Fig. 3-11: Result of simulation 1

Table 3.7: Root mean square errors (RMSEs) of force response in the simulation

Method	RMSE [N×10^{-2}]
Conventional	5.58
Proposed	4.41

3.3.2 Comparison between Proposed and Conventional Methods

The motor was simulated to contact hard and soft objects for a time ranging from 0 to 5 s and 5 to 10 s. The force and position responses and root mean square error (RMSE) of the force responses are shown in Fig. 3-11 and listed in Table 3.7. The proposed method achieved faster command tracking and a smaller RMSE. In particular, the force response oscillated faster in the proposed method when the step commands were provided.

3.3.3 Performance against Wide Frequency Range of Disturbance

The motor was simulated to contact the hard and soft objects from 0 to 5 s and 5 to 10 s with a wide frequency range of disturbances. A sweep was intentionally added as the disturbance, and the amplitude of disturbance was $\pm$0.1 N. The frequency was gradually increased and decreased from 10 to 1000 rad/s in steps of 0.1 s. The command of force control was constantly set as 1 N to evaluate the performance against the disturbance. The input variables of the NN were the same as those illustrated in Fig. 5; further, the learning was performed as discussed in Section 3. However, the constant value of 1 N was set as the command of motion, and the coefficient of command amplitude was not changed in this simulation. The proposed method was compared not only with the conventional approach but also with the conventional approach with high control gains. The proportional and integral gains in the case of high control gains were set as $1.6\ \mathrm{kg}^{-1}$ and $190\ s\mathrm{kg}^{-1}$, respectively. These gains were designed based on the error function. The force result, position result, and added disturbance and estimated result are shown in Fig. 3-12. The simulation results show that the enhancement of control gains marginally improved the response although its amount of improvement was limited. Conversely, the output of NN z_{o}^{t} almost estimated the added disturbance F^{dist}, and the NN compensated the added disturbance. NN has the capability to compensate for a wide frequency range of disturbances by the feedforward method if the learning is properly performed.

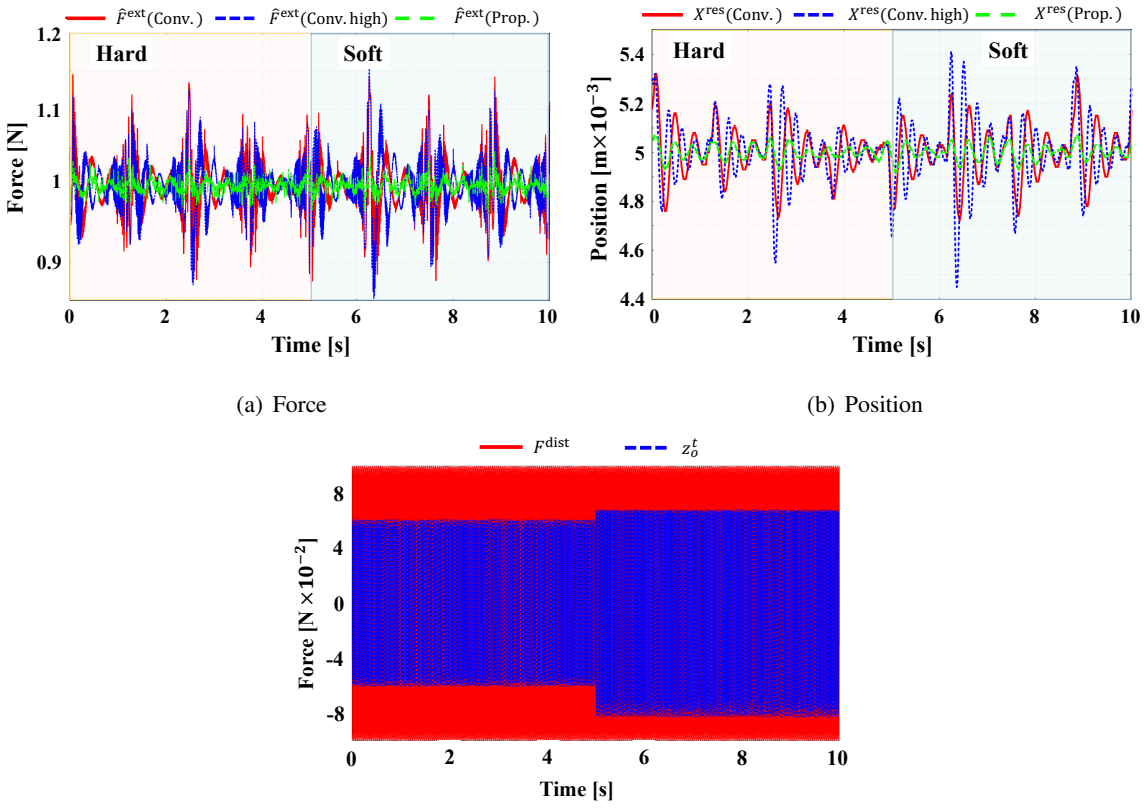

(a) Force

(b) Position

(c) Actual disturbance F^{dist} and estimated value z_{o}^{t}

Fig. 3-12: Result of simulation 2

3.4 Experiments

3.4.1 Outline of Experiments

Experiments were conducted to confirm the effectiveness of the proposed method. Four types of experiments were performed: frequency, contact, disturbance, and fault tolerance experiments. The conventional method was composed of PI gain + DOB, while the proposed method was composed of PI gain + DOB + NN (high frequency) with composition 2.

Frequency experiment

In the frequency experiment, the sweep sine was utilized as the input, and the frequency response of the conventional and proposed methods were measured by a contact with a screw box. The magnitude and phase of the conventional and proposed methods were experimentally measured and compared to determine the performance of the controller in the frequency domain.

Contact experiment

In the contact experiment, the motor contacted the screw box (hard object) and sponge (soft object) using the conventional and proposed controllers to compare the performance of the controllers. In addition to these two controllers, the feedback-based NN (NN:FB) and the feedforward-based NN (NN:FF) were also considered to observe the effects of the feedback and feedforward components.

Disturbance experiment

In the disturbance experiment, unexpected disturbances were deliberately added to the system to verify whether the proposed system could handle the disturbances. The motor contacted the screw box, similar to the contact experiment, and the step- and lamp-shaped disturbances were added in the negative direction from 2.5 to 2.8 s and from 4.5 to 4.8 s, respectively.

Fault tolerance experiment

In the fault tolerance experiment, the amounts of certain weights were deliberately changed from the arbitrary value to zero at 4.5 s to check whether the undesirable control motion could be avoided by the four cases defined in Section 3.7. The force reference of the conventional method was utilized subsequently.

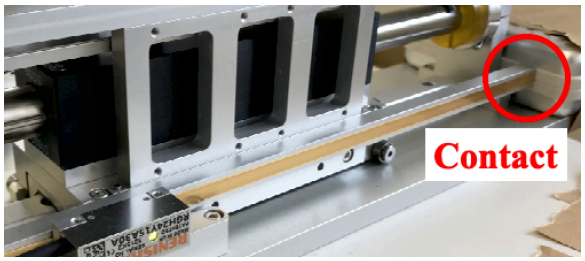

Fig. 3-13: Picture of experimental setup

Fig. 3-14: Picture of contact objects

3.4.2 Experimental Setup

The linear motor shown in Fig. 3-13 was utilized. The weights were learned in the simulation and applied in the experimental setup. Learning was also performed in the experimental setup again to adapt to the real environment, which could not be modeled in the simulation environment. Because the gain setup, which minimized the error function, was different from that listed in Table 3.1, the proportional and integral gains were tuned again for minimizing the error function in the experimental setup. The proportional and integral gains were set as 2.0 kg^{-1} and 18.0 $s\mathrm{kg}^{-1}$, respectively. The learning of weights was conducted with the tuned gains again in the simulation and directly applied to the experimental setup. The remaining parameters were the same as those listed in Tables 3.1 and 3.4.

The training of the NN was performed using six items and the testing or experiment was conducted using two items, as shown in Fig. 3-14, and listed in Table 3.8. The learning result of the experimental setup is shown in Fig. 3-15. Because the error function of the proposed method became smaller when compared to the product of the error function of the conventional method and the amount of improvement

Table 3.8: Stiffness of each contact object

Item	Use	Stiffness [N/m]
Box	Training	6077
Towel	Training	1056
Alminum	Training	37581
Rope	Training	2911
Eraser	Training	14827
Bottle	Training	4060
Screw box	Testing	28596
Sponge	Testing	1369

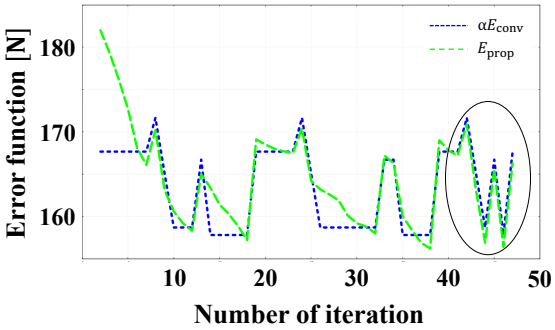

Fig. 3-15: Learning result of the experiment

from the 42^{nd} to 47^{th} iterations, the proposed method that was composed of the same weights could contact six training objects with a smaller error functions. In the contact experiment, NN:FB and NN:FF were also considered. These NNs were also initially trained by the simulation; then, the training was performed in the actual experimental setup. The structures of each NN were the same as that in the proposed method; however, the number of input variables was different. Only the error was considered as the input variable in NN:FB, while the remaining three variables were considered as the input in NN:FF.

The unstable behavior was not observed at the learning process by experimental setup, but the algorithm of forced learning termination was necessary in order to secure the safety of experiments if the model used in simulation was not trustworthy.

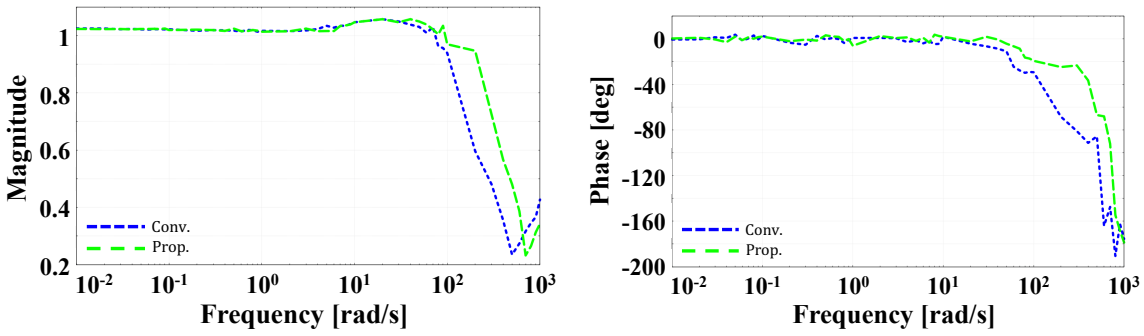

(a) Magnitude (b) Phase

Fig. 3-16: Bode diagram

3.4.3 Experimental Results

Frequency experiment

The results of magnitude and phase are shown in Fig. 3-16. The magnitude and phase in the low-frequency range (approximately 0.01 rad/s to 100 rad/s) were almost the same between the conventional and proposed methods. The decay of the magnitude or the lag in the phase began at a higher frequency in the proposed method. The proportional and integral gains were tuned based on the error function; however, a combination of NNs can be considered to further improve the control performance.

Contact experiment

The force and position responses of the contact with the screw box and sponge are shown in Figs. 3-17 and 3-18, respectively. The result of the proposed methods followed the force step command among other methods pertaining to the contact to the screw box and sponge. NN:FB and NN:FF also achieved better performance than the conventional approach. In particular, the force response of NN:FF was better than that of NN:FB in the contact experiment with the sponge. All methods appropriately tracked the lamp command from 5 to 9.5 s. The RMSEs of the force response are listed in Table 3.9. The proposed method achieved the smallest RMSEs in the contact with both the screw box and sponge. Both the feedback and feedforward components contributed to the performance improvement of force control with the DOB.

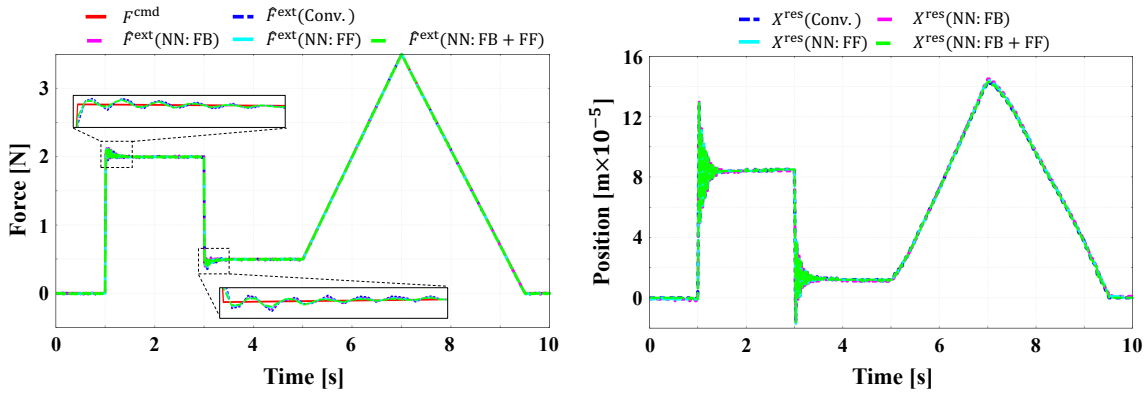

(a) Force (b) Position

Fig. 3-17: Contact results with screw box

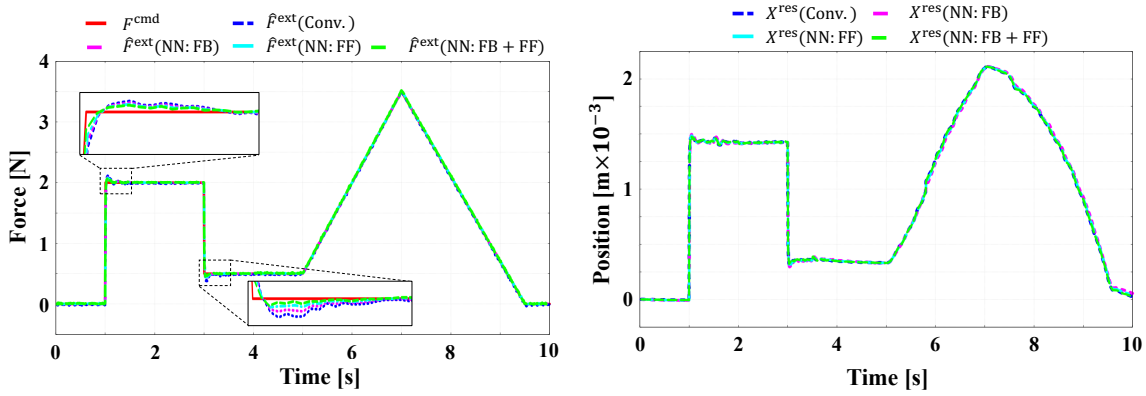

(a) Force (b) Position

Fig. 3-18: Contact results with sponge

Disturbance experiment

The force and position responses are shown in Fig. 3-19 and the RMSEs of the force response are listed in Table 3.10. The proposed method could tackle unexpected disturbances as well as the conventional method.

Fault tolerance experiment

The force and position responses are shown in Fig. 3-20 and the RMSEs of the force response are listed in Table 3.11. Even if the method of reference generation was suddenly changed, the force controller continued to follow the force command.

Table 3.9: RMSEs of the contact experiment

Contact object	Method	RMSE [N $\times$ 10^{-2}]
Screw box	Conventional	1.85
Screw box	Proposed (NN:FB)	1.74
Screw box	Proposed (NN:FF)	1.68
Screw box	Proposed (NN:FB+FF)	1.59
Sponge	Conventional	2.63
Sponge	Proposed (NN:FB)	2.45
Sponge	Proposed (NN:FF)	2.32
Sponge	Proposed (NN:FB+FF)	2.23

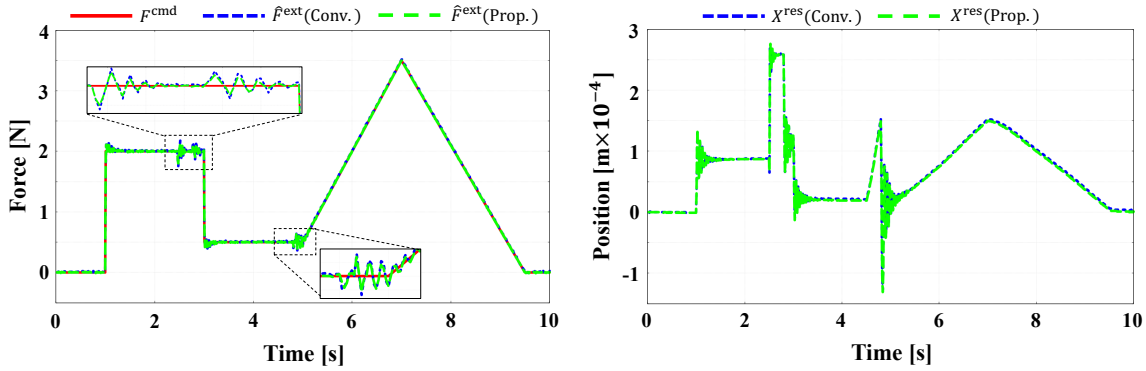

(a) Force (b) Position

Fig. 3-19: Results against disturbance

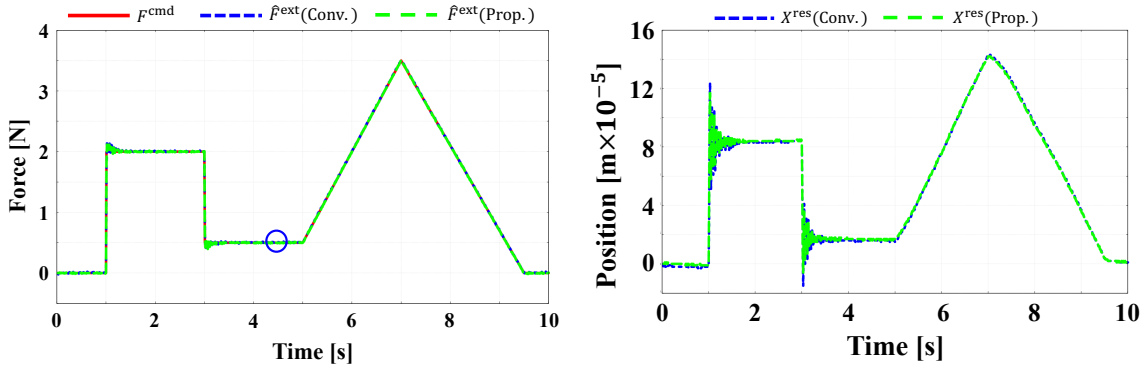

(a) Force (b) Position

Fig. 3-20: Results of fault tolerance

Table 3.10: RMSEs of disturbance experiment

Method	RMSE [$\mathrm{N} \times 10^{-2}$]
Conventional	2.73
Proposed	2.31

Table 3.11: RMSEs of fault tolerance experiment

Method	RMSE [$\mathrm{N} \times 10^{-2}$]
Conventional	1.86
Proposed	1.63

3.5 Summary

This dissertation proposed an NN-based explicit force control with DOB and RFOB. The compensator of the NN was designed by comparing certain candidate structures and available compositions. Because the DOB is already a strong method, the NN was designed in a frequency range higher than the cutoff frequency of the DOB (Structure 3). The weights of the NN were updated at each sampling time based on the cost or error function in both the simulation and actual setups. The simulation and four experiments, i.e., frequency, contact, disturbance, and fault tolerance experiments, were performed to demonstrate the effectiveness of the proposed method.

This chapter collects real motion data of force control and train the NN based on cerebellar calculation model of data-driven control design. The design of force control is sometimes much more tough than the one of position/velocity control, and the utilization of real data contributes to improve the performance of force control.

Chapter 4

Operator's Sensation-based Data-driven Design

This chapter discusses a JNDs-based design policy of haptics system. In Section 4.1, the outline of transparency is introduced. In Section 4.1.1, the bilateral control is explained. In Section 4.1.2, the bilateral control with multirate sampling is explained. In Section 4.2, the proposed JNDs-based design policy is introduced. In Section 4.2.1, the outline of proposal is explained. In Section 4.2.2, the test of JNDs is discussed. In Section 4.2.3, the constructed look-up table is discussed. In Section 4.3, the estimation method of time-delay and stiffness is introduced. In Section 4.4, the simulations are discussed. In Section 4.5, the experiments are introduced. In Section 4.5.1, the experimental setup is explained. In Section 4.5.2, the experimental results are discussed. This chapter is concluded in Section 4.6.

4.1 Transparency

The relationship between the external force and the position response of the master and slave is computed by using a hybrid matrix as follows:

$$\begin{bmatrix} F_{\mathrm{m}}^{\mathrm{ext}} \\ X_{\mathrm{m}}^{\mathrm{res}} \end{bmatrix} = \begin{bmatrix} H_{11} & H_{12} \\ H_{21} & H_{22} \end{bmatrix} \begin{bmatrix} X_{\mathrm{s}}^{\mathrm{res}} \\ -F_{\mathrm{s}}^{\mathrm{ext}} \end{bmatrix}. \tag{4.1}$$

The external force on the master and slave sides is computed as follows:

$$F_{\mathrm{m}}^{\mathrm{ext}} = Z_{\mathrm{h}}(X_{\mathrm{h}}^{\mathrm{ref}} - X_{\mathrm{m}}^{\mathrm{res}}), \tag{4.2}$$

$$F_{\mathrm{s}}^{\mathrm{ext}} = Z_{\mathrm{e}}(X_{\mathrm{e}}^{\mathrm{ini}} - X_{\mathrm{s}}^{\mathrm{res}}), \tag{4.3}$$

By combining Eqs. (4.1) - (4.3), the followings are obtained:

$$F_{\mathrm{m}}^{\mathrm{ext}} = H_{11}X_{\mathrm{s}}^{\mathrm{res}} + H_{12}Z_{\mathrm{e}}(X_{\mathrm{s}}^{\mathrm{res}} - X_{\mathrm{e}}^{\mathrm{ini}}), \tag{4.4}$$

$$X_{\mathrm{m}}^{\mathrm{res}} = H_{21}X_{\mathrm{s}}^{\mathrm{res}} + H_{22}Z_{\mathrm{e}}(X_{\mathrm{s}}^{\mathrm{res}} - X_{\mathrm{e}}^{\mathrm{ini}}). \tag{4.5}$$

Eqs. (4.4) and (4.5) are recomputed as follows by assuming that the initial contact position of the environment is constant:

$$F_{\mathrm{m}}^{\mathrm{ext}} = H_{11}X_{\mathrm{s}}^{\mathrm{res}} + H_{12}Z_{\mathrm{e}}X_{\mathrm{s}}^{\mathrm{res}}, \tag{4.6}$$

$$X_{\mathrm{m}}^{\mathrm{res}} = H_{21}X_{\mathrm{s}}^{\mathrm{res}} + H_{22}Z_{\mathrm{e}}X_{\mathrm{s}}^{\mathrm{res}}. \tag{4.7}$$

The following equation is obtained from Eq. (4.1) by assuming $F^{\mathrm{ext}} = ZX^{\mathrm{dis}}$ where Z and $\bigcirc^{\mathrm{dis}}$ denote the impedance and the amount of displacement, respectively [86]:

$$\begin{aligned} F_{\mathrm{m}}^{\mathrm{ext}} &= \frac{H_{12}Z_{\mathrm{e}} + H_{11}}{H_{21} + H_{22}Z_{\mathrm{e}}} X_{\mathrm{m}}^{\mathrm{res}} \\ &= \left\{ \frac{H_{12}}{H_{21} + H_{22}Z_{\mathrm{e}}} Z_{\mathrm{e}} + \frac{H_{11}}{H_{21} + H_{22}Z_{\mathrm{e}}} \right\} X_{\mathrm{m}}^{\mathrm{res}} \\ &= \left\{ P_{\mathrm{r}}Z_{\mathrm{e}} + P_{\mathrm{o}} \right\} X_{\mathrm{m}}^{\mathrm{res}} \\ &= P_{\mathrm{imp}}X_{\mathrm{m}}^{\mathrm{res}}. \end{aligned} \tag{4.8}$$

The performance of bilateral control is often evaluated by the transparency [29]. A transparent system transmits the impedance to the operator as close as the environmental impedance. The impedance transmitted to the operator becomes $P_{\mathrm{imp}} = P_{\mathrm{r}}Z_{\mathrm{e}} + P_{\mathrm{o}}$ by transforming the left-hand side of Eq. (4.8) as $\frac{F_{\mathrm{m}}^{\mathrm{ext}}}{X_{\mathrm{m}}^{\mathrm{res}}}$. The reproducibility shows the transmission ratio of environmental impedance, while the operationality

shows the excessive mechanical impedance. When the reproducibility and operationality are 1 and 0, respectively, the environmental impedance is perfectly transmitted to the master side, and a transparent system is achieved.

The reproducibility and operationality are obtained from the hybrid parameters, which are independent from the environmental impedance. Each hybrid parameter is computed as follows.

$$\begin{bmatrix} H_{11} & H_{12} \\ H_{21} & H_{22} \end{bmatrix} = \begin{bmatrix} \frac{F_{\mathrm{m}}^{\mathrm{ext}}}{X_{\mathrm{s}}^{\mathrm{res}}}|_{-F_{\mathrm{s}}^{\mathrm{ext}}=0} & \frac{F_{\mathrm{m}}^{\mathrm{ext}}}{-F_{\mathrm{s}}^{\mathrm{ext}}}|_{X_{\mathrm{s}}^{\mathrm{res}}=0} \\ \frac{X_{\mathrm{m}}^{\mathrm{res}}}{X_{\mathrm{s}}^{\mathrm{res}}}|_{-F_{\mathrm{s}}^{\mathrm{ext}}=0} & \frac{X_{\mathrm{m}}^{\mathrm{res}}}{-F_{\mathrm{s}}^{\mathrm{ext}}}|_{X_{\mathrm{s}}^{\mathrm{res}}=0}. \end{bmatrix} \tag{4.9}$$

Here, H_{11} and H_{22} terms are expected to become 0, while H_{12} and H_{21} terms are expected to become 1 to achieve an ideal performance of the impedance transmission. Because the hybrid parameter can be obtained for computing the position and force of the master and slave by simulations, the performance of impedance transmission $P_{\mathrm{r}}Z_{\mathrm{e}} + P_{\mathrm{o}}$ can be obtained by considering the sampling time.

A time delay occurred between the master and slave, and term e^{-ts} is substituted in the block diagram.

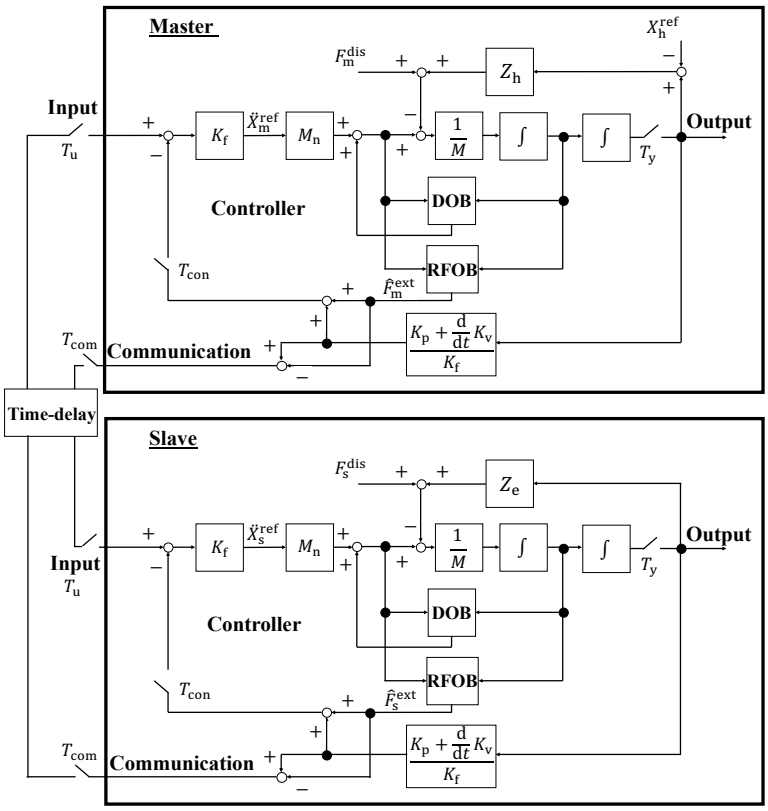

Fig. 4-1: Block diagram of the impedance field expressed 4ch bilateral control.

4.1.1 Bilateral Control

The block diagram of this system is shown in Fig. 4-1. This dissertation considers stiffness as a main component of impedance. This block diagram includes some switching.

4.1.2 Bilateral Control Based on Multirate Sampling

The sampling time value of bilateral control should be as short as possible to achieve a higher impedance transmission, although the shorter sampling time increases the data traffic. The basic idea is to apply the concept of multirate sampling to bilateral control. To obtain output information is significantly more important than to provide input information in case of acceleration control, because the sampling period of the feedback loop should be small to enhance the stability [108, 109]. The sampling time of input, output, controller, and communication can be designed as follows:

$$T_{\mathrm{u}} = T_{\mathrm{com}} = nT_{\mathrm{y}} = nT_{\mathrm{con}}. \tag{4.10}$$

The input, output, controller, and communication show the receiving cycle from another side, measuring cycle of sensor, cycle of observer or feedback, and transmission cycle to another side, as shown in Fig. 4-1. The data traffic can be reduced while suppressing the stability deterioration by considering multirate.

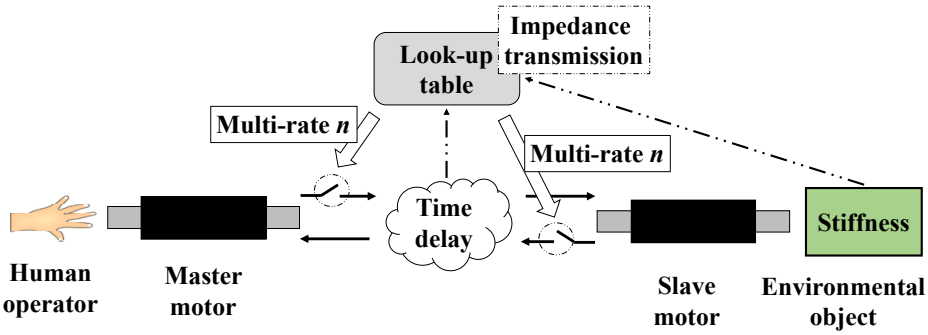

Fig. 4-2: Outline of the proposal.

4.2 Proposed Multirate Design Method

4.2.1 Outline

This section explains the multirate design method. An outline of the proposal is shown in Fig. 4-2. The time delay and environmental stiffness are input to a look-up table that is constructed offline, and the multirate is referred from the look-up table online. Because the relationship between the value of multirate and deterioration of the impedance transmission cannot be calculated, the look-up table is constructed based on a simulation. The performance of the impedance transmission is used as an evaluation index, and the human perception is also considered to determine a deterioration criteria of the impedance transmission or the desired performance of the impedance transmission.

4.2.2 JND Tests and Simulation

This dissertation considers to obtain JNDs of operators in order to JND tests aims at obtaining JND values of operators against the variation of multirate n, while the simulation aims at computing JNDs of the impedance transmission. Because the multirate is an integer value that cannot be directly used to design a data traffic reduction method, the performance of impedance transmission under each investigated multirate was simulated. The hybrid parameters in Eq. (4.9) were simulated, and these parameters were substituted into Eq. (4.8) to obtain the impedance transmission.

Just Noticeable Differences of Impedance Transmission

Just noticeable differences show the detectable amount of difference between two stimuli. JNDs have been combined with the transparency as the perceived transparency [110]. Because the operators are limited in noticing the differences, JND of impedance transmission should be used to design a data traffic reduction method. JNDs against the variation of multirate n was investigated in JND tests, but multirate n is an integer that is not suitable for representing the performance of a bilateral control system. Therefore, the performance of impedance transmission under different multirates was computed by obtaining the hybrid parameters Eq. (4.9) in the simulation. In this way, JNDs against the variation of multirate n correspond to JND of impedance transmission. The variation ratio of impedance transmission between the single-rate and multirate is considered and defined as follows:

$$\omega_{\mathrm{imp}} = \frac{|\int P_{\mathrm{imp|n=1}}\mathrm{d}fre - \int P_{\mathrm{imp|n=n_{ntc}}}\mathrm{d}fre|}{\int P_{\mathrm{imp|n=1}}\mathrm{d}fre}, \tag{4.11}$$

where ω_{imp}, $\bigcirc_{|n=1}$, $\bigcirc_{|n=n_{\mathrm{ntc}}}$, and $\int \mathrm{d}fre$ denote the variation ratio of impedance transmission, value under single-rate, value under multirate when the operator notices the difference, and the integration of frequency, respectively. This dissertation calls ω_{imp} as JND of impedance transmission.

Protocols of JND Tests

JND tests were conducted based on up-down methods with a fixed step size [111, 112]. The multirate was ascended by the fixed amount until the participants stopped noticing the difference between the single-rate ($n = 1$) and multirate ($n > 1$), and vice versa. Seven right-handed participants (five males and two females, average age: 23 years) took part in JND tests. All of them have been engaged in research on motion control. This study was approved by the ethics committee of our university.

Table 4.1: Parameters for JND Tests and Simulation

Description	Value
Nominal mass of master and slave robots	0.5 kg
Position gain	1600 s^2
Velocity gain	80 s
Force gain	1
Cut-off frequency of DOB and RFOB	500 rad/s
Sampling time	0.1 ms

Two single DOF linear motors were used to conduct the tests as the master and slave. Only position information was measured by encoders, and the velocity and external force were estimated by pseudo derivative and RFOB.

There were 3 motions (free motion, contact motion with sponge, and contact motion with plastic box), and each motion was tested for 9 test conditions: 3 frequencies times 3 time delays. Therefore, each participant participated in 27 test conditions. The frequencies of motion were 0.5 Hz, 1 Hz, and 2 Hz, and the time delays were 10 ms, 20 ms, and 30 ms. The stiffness of sponge and plastic box were 1158 N/m and 5164 N/m, respectively. The parameters for JND tests and simulation are shown in Table 7.3.

In each test, the participants were asked to grasp the master motor by the thumb and index fingers of the dominant hand and to manipulate the master motor in the sinusoidal manner while perceiving the dynamics of manipulator. The slave motor, which was connected to the master motor by a bilateral control, did not contact any environmental object in the free motion. The participants were feeling the operational force mainly due to the time delay. Because the multirate can be considered as the time delay from the perspective of performance of bilateral control, the multirate can be set larger as the time delay becomes longer for keeping $\frac{\text{Multirate}}{\text{Time-delay+Multirate}}$ constant. This ratio shows the effect of multirate on the total time delay (Time-delay + Multirate). The participants manipulated the master motor, and the slave motor was always in contact with the environmental objects in the contact motion. The participants were mainly feeling not only operational force but also the force generated by the transmission of the environmental impedance. A metronome was used to adjust the manipulated frequency of participants, and the amplitude was shown by the line marker in the master side when the free motion was conducted. The master and slave motors were physically separated, and the participants were only looking at the master side. Therefore, the participants did not receive any visual information about the slave side.

Table 4.2: Results of JND Tests: Free Motion

Frequency (Hz)	Time delay (ms)	Smallest multirate n	Standard deviation of multirate n	JND of impedance transmission (%)
0.5	10	13	3.50	3.4
	20	16	3.11	3.5
	30	23	3.16	3.6
1.0	10	13	3.33	2.8
	20	18	3.64	3.5
	30	25	3.36	2.0
2.0	10	16	3.49	3.3
	20	19	3.21	2.8
	30	23	1.76	2.9

The participants were asked to compare the feelings in two trials (one a single-rate and another multirate) and to respond whether they felt any differences or not. At the beginning of each test, the multirate started from 1. The multirate was increased by 1, if they did not feel the difference in the ascending procedure. The multirate was doubled if they felt the difference, and the procedure was shifted to descending. The multirate was decreased by 1, if they continued to feel the difference in the descending procedure. The multirate was reduced by half, if they stopped feeling the difference, and the procedure was shifted to ascending. Each participant was asked to perform one test for every test condition, and each test was composed of the three ascending/descending procedures. The average values of all procedures were adopted as the final JND of multirate. It typically took 90 to 120 minutes per participant to complete the test, including one break. Before starting the experiment, the corresponding instructions were provided to the participants, and they were given time to familiarize themselves with the experimental hardware.

Results

The results of JND tests are summarized in Tables 4.2 and 4.3. JND of multirate n tended to become smaller as the time delay was shorter, especially in the free motion. Because multirate n can be considered as a time delay from the perspective of performance of bilateral control, the larger time delay may be able to mitigate the difference in feeling. In a pilot study, the authors noticed the difference between the single-rate ($n = 1$) and multirate of $n = 2$ if the time delay was 0.1 ms. Therefore, the larger time delay makes it possible to set a higher multirate. In other words, the multirate can be set higher as

Table 4.3: Results of JND Tests: Contact Motion

Contact object	Frequency (Hz)	Time delay (ms)	Smallest multirate n	Standard deviation of multirate n	JND of impedance transmission [%]
Sponge	0.5	10	10	2.31	2.2
		20	17	1.85	2.8
		30	16	3.23	2.1
	1.0	10	12	2.44	2.6
		20	13	3.25	2.3
		30	18	2.96	2.8
	2.0	10	14	2.70	3.0
		20	20	2.75	2.2
		30	28	3.33	2.0
Plastic box	0.5	10	13	2.77	2.7
		20	13	2.91	2.3
		30	15	3.33	3.1
	1.0	10	10	3.20	3.0
		20	20	2.96	2.4
		30	24	3.29	2.0
	2.0	10	22	2.75	2.8
		20	24	3.04	2.5
		30	21	2.77	2.7

the original performance of impedance transmission becomes poorer. The enhancement of multirate increases the position/velocity difference between the master and slave, and it causes the larger operational force. The operational force or operationality caused by the time delay was the dominant component in the impedance transmission in the free motion, while both the reproducibility and operationality due to the time delay and environmental stiffness were mutually affected to JND of multirate in the contact motion.

The smallest JND of impedance transmission among seven participants were listed in these tables, because the most severe condition was used to construct a look-up table. The smallest or the most critical JND values among all conditions was 2.0% change of impedance transmission, and this value was used as a performance deterioration criterion. The adoption of the smallest JND values to all conditions was highly conservative and not able to dramatically reduce data traffic, but the operators did not notice the

significant difference from the single-rate system.

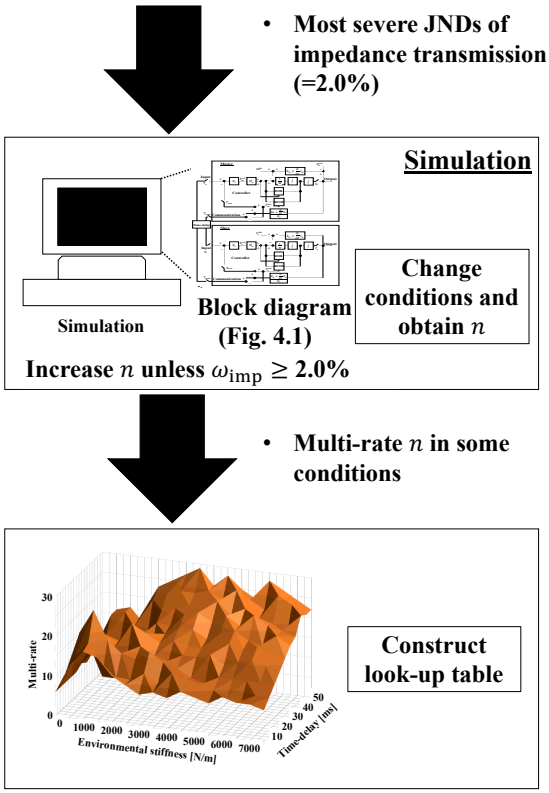

Fig. 4-3: Outline of Section 4.2.3.

4.2.3 Constructing a Look-Up Table

Outline of Constructing a Look-Up Table

The look-up table was constructed to determine the multirate based on the conditions. An outline of constructing a look-up table is shown in Fig. 4-3. The simulation was conducted by considering the obtained deterioration criteria of impedance transmission. The multirate was increased until the change of impedance transmission Eq. (4.11) became larger than its JND values obtained in JND tests (2.0%), and the obtained multirate was recorded in the look-up table. This process was repeatedly conducted with a varied time delay and environmental stiffness. This look-up table was constructed based on the simulation.

The target frequency range should be determined to calculate the variation ratio of the impedance transmission Eq. (4.11). This range is often designed by respecting the human motion or perception, but this dissertation is focused on the performance of reproducibility. This dissertation assumes that there is almost no value in reproducing a particular frequency range that is far from the ideal reproducibility

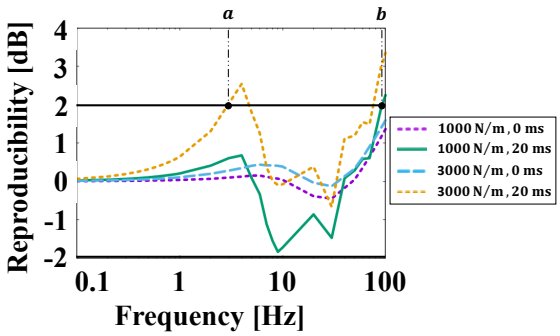

Fig. 4-4: Reproducibility of single-rate 4ch bilateral control (example).

value. The reproducibility of single-rate 4ch bilateral control in some example conditions is shown in Fig. 4-4. The frequency analysis of four conditions (purple, green, light blue, and orange lines) is shown by varying the environmental stiffness and time delay. In case of no time delay (purple and light blue lines), the reproducibility was almost 0 dB from 0 to 100 Hz, which means that the environmental stiffness on the slave side was almost properly transmitted to the operators on the master side. However, the reproducibility was fluctuating and was not close to 0 dB when a time delay was present (green and yellow lines). Because this dissertation assumes that there is no value in considering the frequency range where the reproducibility is not close to 0 dB, the target frequency was determined as plus/minus 2 dB, which was arbitrarily chosen. For instance, 0 to a Hz was the target frequency range of the variation ratio of impedance transmission in the condition of orange line in Fig. 4-4, while 0 to b Hz was the target frequency in the condition of green line.

Results

The constructed look-up table is shown in Fig. 5. The multirate tended to become higher when the environmental stiffness was larger and the time delay was longer.

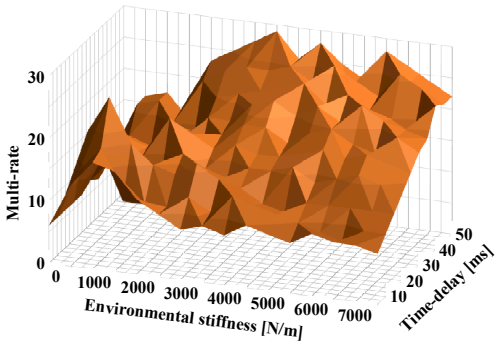

Fig. 4-5: Constructed look-up table.

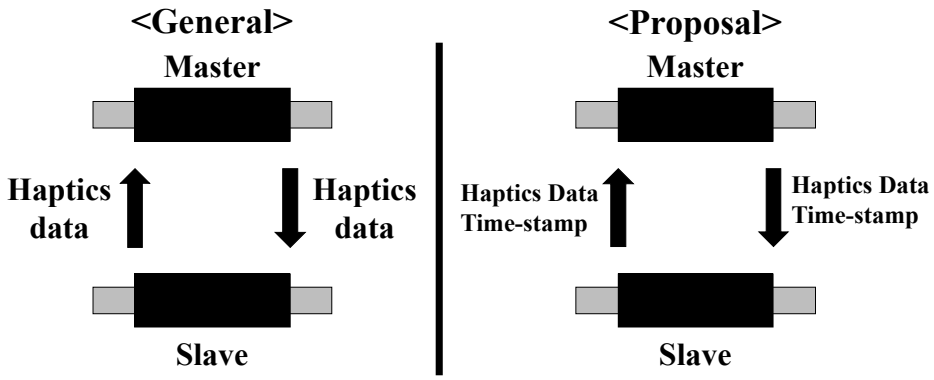

Fig. 4-6: Transmitted data between the master and slave in the general and proposed system.

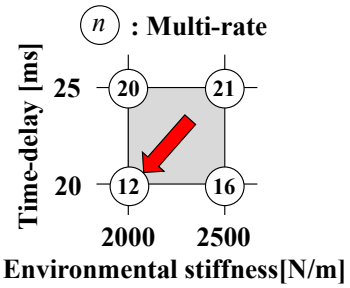

Fig. 4-7: Example of multirate selection.

4.3 Estimation of Time Delay and Environmental Stiffness

The time delay and environmental stiffness have to be estimated to determine the multirate online. The time delay was estimated by the round trip of a timestamp. The elapsed time at the master side was transmitted to the slave, and its data was directly transmitted back to the master. The time delay was computed by comparing the previous and current values of the timestamp. The environmental stiffness was estimated by the least squares method in both the master and slave, where the force threshold that determined whether the estimation was started was set as plus/minus 0.5 N. This threshold was used to determine an initial contacting point. The transmitted information in the general and proposed approaches are shown in Fig. 6. The proposed method needs two times larger data traffic, but it can reduce the data traffic in total when the multirate can be set larger than two.

An example of multirate selection is shown in Fig. 7. The vertical and horizontal axes show the time delay and environmental stiffness, respectively. The numbers surrounded by circles show the multirate referred from the constructed look-up table. Because the environmental stiffness is hard to estimate, the

most severe multirate should be selected. The multirate becomes 12, which is the smallest value in this example. The range of time delay and environmental stiffness should be adjusted based on the estimation performance of the time delay and environmental stiffness.

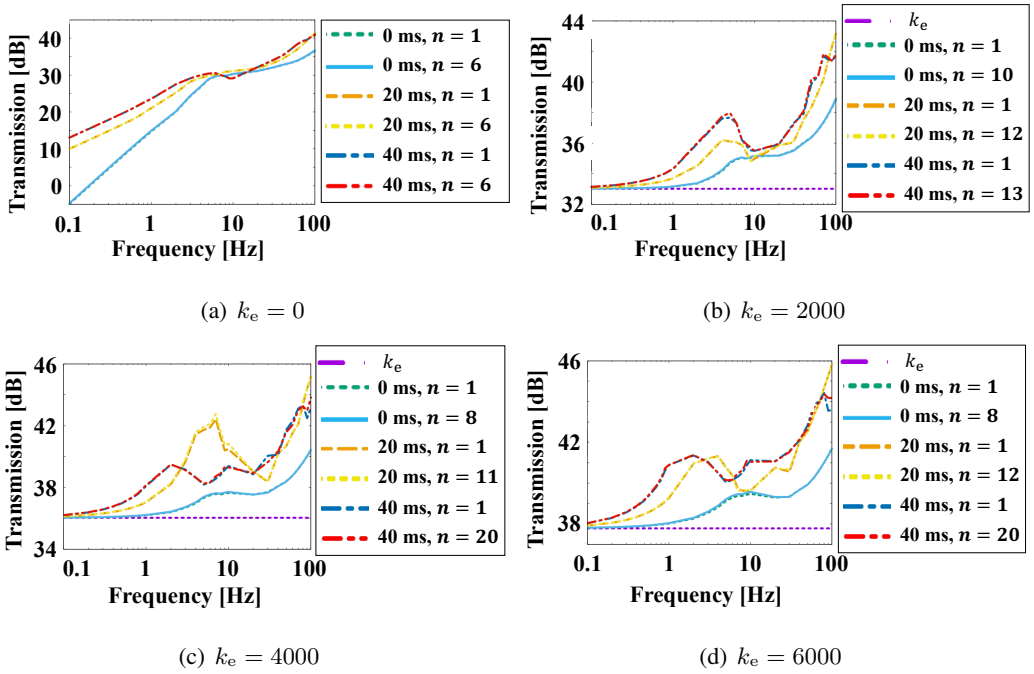

(a) $k_e = 0$ (b) $k_e = 2000$

(c) $k_e = 4000$ (d) $k_e = 6000$

Fig. 4-8: Impedance transmission for each condition.

4.4 Performance Confirmation

This section discusses the performance of multirate sampling and the constructed profile. The purpose of this section is to show that the impedance transmission deterioration of the constructed profile is less than 2%.

The performance of the constructed look-up table was confirmed by setting some conditions in the frequency domain. Both the environmental stiffness and time delay were changed to 0 N/m, 2000 N/m, 4000 N/m, and 6000 N/m and 0 ms, 20 ms, and 40 ms, respectively. The multirate sampling was referred from the constructed look-up table by assuming that the conditions were known in advance. The performance based on the constructed look-up table was compared with the case when the multirate is equal to 1 (single-rate). The transmission shows $P_r k_e + P_o$, which is the transfer function from the position on the master side to the estimated external force on the master side. The simulation results are shown in Fig. 8. The purple line shows the environmental stiffness k_e, and other lines are better to follow the purple line from the perspective of impedance transmission. The green and light blue lines, the orange and yellow lines, and the blue and red lines almost overlap: therefore, the deterioration of impedance transmission is limited. The error percentage between $n = 1$ and $n \neq 1$ of the target frequency in each condition is

Table 4.4: Error Percentage Between $n = 1$ and $n \neq 1$ of the Target Frequency in Each Condition

Environmental stiffness [N/m]	Time delay (ms)	Error percentage [%]
0	0	3.5
	20	1.9
	40	1.0
2000	0	0.5
	20	0.5
	40	0.5
4000	0	0.4
	20	0.5
	40	0.8
6000	0	0.7
	20	0.6
	40	0.9

summarized in Table 4.4. The criteria percentage obtained from JND tests was 2.0%, and all conditions except the condition when both the time delay and environmental stiffness were 0 satisfied these criteria. Because this dissertation did not consider the condition when the time delay was 0 for constructing the look-up table, this unsatisfactory situation may occur. Note that the true multirate for the condition when both time delay and environmental stiffness are 0 becomes 3, and the error percentage becomes 1.4% if $n = 3$ is applied. Most error percentages were lower than 1% due to the selection logic of multirate, which caused the conservative data-traffic reduction. In summary, the constructed look-up table properly worked for suppressing the deterioration of impedance transmission less than 2.0%, except for the condition when both time delay and environmental stiffness were 0.

4.5 Experiments

This section examines the effectiveness of the constructed look-up table and exemplifies the performance of data traffic reduction. The position and force responses of single-rate and multirate sampling are compared and discussed in the time domain under some conditions regarding the time delay and contact object.

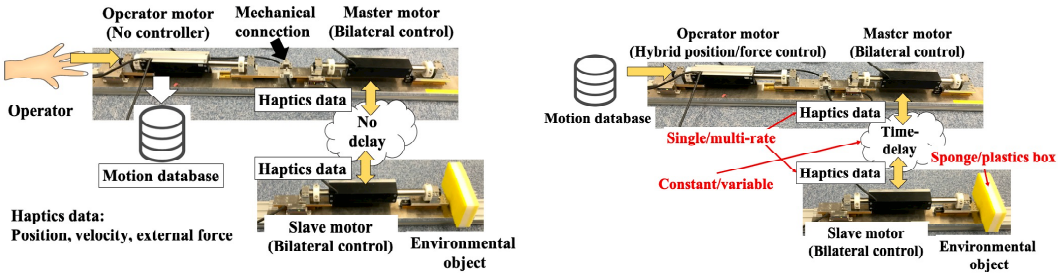

(a) Saving phase (b) Loading phase

Fig. 4-9: Illustration of the experimental setup.

4.5.1 Experimental Setup

The experiments were carried out to confirm the performance of data traffic reduction. The command motion was performed by the operator and obtained through 4ch bilateral control in advance by using the concept of the motion-copying system [85]. An illustration of the experimental setup is shown in Fig. 9. There were three motors: operator, master, and slave. The experiment included saving and loading. In the motion saving, the operator manipulated the operator motor, which was not controlled. This operator motor was mechanically connected with the master motor, and the manipulation was transmitted to the master motor. The master motor was electrically connected with the slave motor by 4ch bilateral control. The motions were conducted by the operator once for every condition, and the position, velocity, and external force of the master motor were saved in the motion database. The single-rate sampling was applied to the bilateral control, because the purpose was to obtain the command value of the operator motor. In the motion loading, the saved motion was used as a command value of the operator motor, which was controlled by hybrid position and force control. Thanks to this experimental setup, the same disturbance or motion can be added to the master motor from the operator motor in both the single-rate and multirate cases, and the performance between two cases can be fairly compared.

Four types of experiments were carried out by changing the environmental objects (sponge and plastic box) and time delay (constant and variable). The experiments were conducted once per each condition. In case of a variable time delay, it linearly varied between 10 ms and 40 ms. The constant time delay was set as 25 ms. The experimental setup was the same as one summarized in Table 7.3.

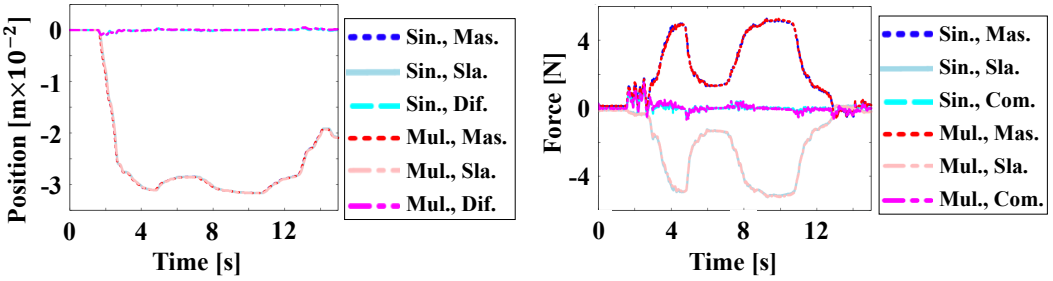

(a) Position responses (b) Force responses

Fig. 4-10: Responses to a contact with the sponge with the constant time delay.

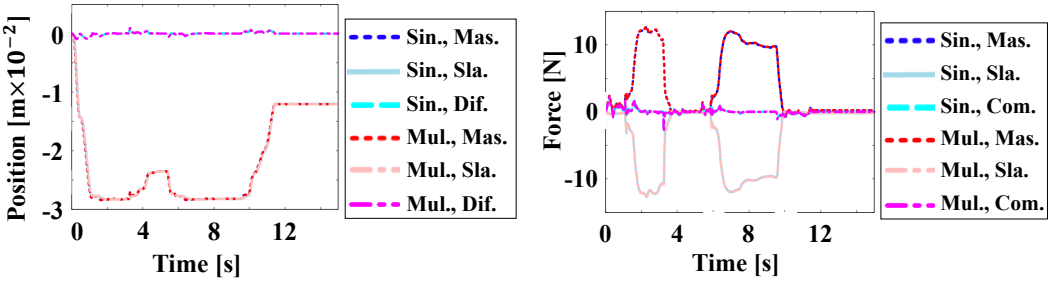

(a) Position responses (b) Force responses

Fig. 4-11: Responses to a contact with the plastic box with the constant time delay.

4.5.2 Experimental Results

The position and force results of the single-rate (n was always 1) and the proposed multirate (n was referred from the profiles) sampling are shown in Figs. 10 – 13 where "Sin.," "Mul.," "Mas.," "Sla.," "Dif.," and "Com." denote the conventional single-rate, multirate, master, slave, differential mode ($X_{\mathrm{m}}^{\mathrm{res}} - X_{\mathrm{s}}^{\mathrm{res}}$), and common mode ($\hat{F}_{\mathrm{m}}^{\mathrm{ext}} + \hat{F}_{\mathrm{s}}^{\mathrm{ext}}$), respectively. Both the differential and common modes should be 0 to satisfy two control goals: position tracking and realization of law of action and reaction. The position and force results of the proposed multirate sampling were expected to follow the one of single-rate to achieve a similar impedance transmission between the single-rate and the proposed multirate sampling. The amount of differential and common modes is almost similar, except for the transient states between the single-rate and proposed multirate sampling, although the position and force performances deteriorated due to the time delay. Because the look-up table was not constructed by considering these high-frequency ranges, the reproducibility of high-frequency range tended not to be close to 0 dB

Root mean square error (RMSE) of the stiffness estimation between the single-rate and multirate

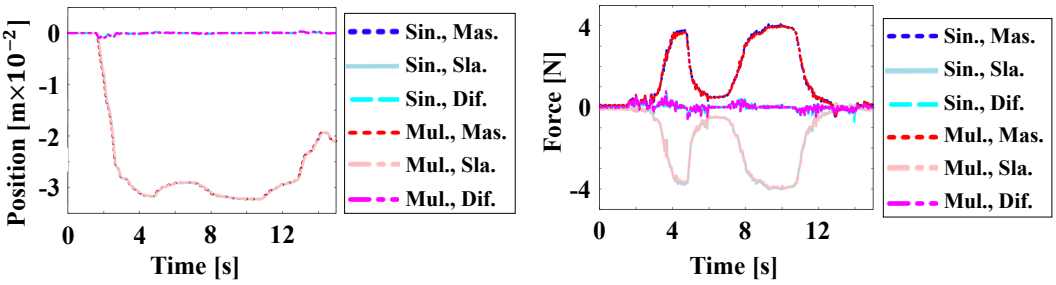

(a) Position responses (b) Force responses

Fig. 4-12: Responses to a contact with the sponge with a variable time delay.

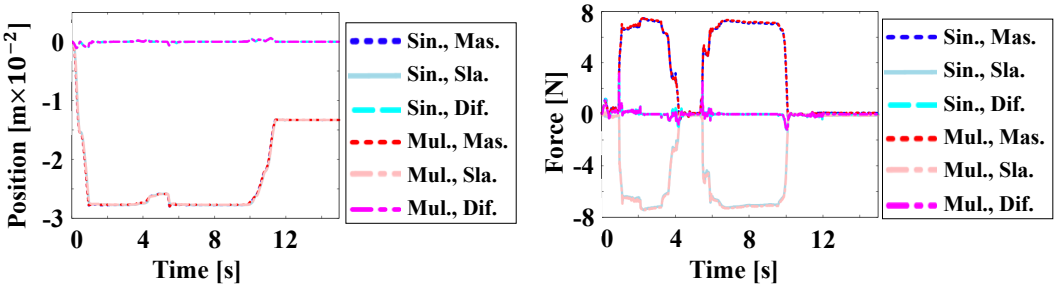

(a) Position responses (b) Force responses

Fig. 4-13: Responses to a contact with the plastic box with a variable time delay.

Table 4.5: RMSE of Stiffness Estimation Between the Single-Rate and Multirate Sampling

	Constant delay	Variable delay
Sponge	1.26%	1.67%
Plastic box	1.08%	0.72%

sampling is shown in Table 4.5. The stiffness estimation error for a plastic box was smaller than the one for a sponge, but all RMSEs of the stiffness estimation were smaller than 2%. The tuning of force threshold or selection of the estimation method would remain for future work.

The transitions of multirate n are shown in Fig. 14. Multirate n heavily transited when the slave contacted environmental objects. Multirate n of the plastic box tended to become larger than the one of the sponge in the contact state. Meanwhile, the time delay produced a varied multirate n, compared with the results of the constant time delay.

The amount of data traffic reduction was also confirmed, as shown in Table 4.6. The proposed multirate sampling significantly, by more than 75%, reduced the data traffic compared with the single-rate

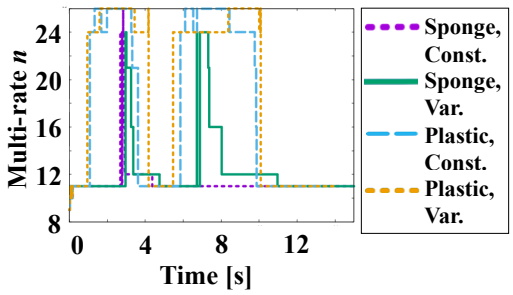

Fig. 4-14: Transitions of multirate n.

Table 4.6: Amount of Data Traffic Reduction

	Environmental object	Time delay	Data traffic [MB]
Single-rate	Sponge	-	1.83
Multirate	Sponge	Constant	0.41
Multirate	Sponge	Variable	0.38
Single-rate	Plastic box	-	1.46
Multirate	Plastic box	Constant	0.26
Multirate	Plastic box	Variable	0.25

sampling.

In summary, the proposed multirate system reduced the data traffic while suppressing the performance deterioration of impedance transmission. The experimental results validated the effectiveness of the proposal.

4.6 Summary

This dissertation proposed a JNDs-based design policy of haptics system by considering the deterioration criteria of impedance transmission. As a remarkable achievement of the proposed approach, the look-up table that transforms time delay and environmental stiffness to multirate n was constructed by considering the impedance transmission and human perception. In the experiments, more than 75% of data traffic reduction was achieved while suppressing the deterioration of impedance transmission less than the result shown in JND tests (2.0%).

This chapter collects real data regarding the sensation of operators and construct the look-up table based on the database of data-driven control design. Human support robots have been widely researched and developed, and some parameters, specifications, and standards should be considered based on the characteristics of operators. Because the characteristics of operator is hard to be modeled, the concept of data-driven design is necessarily.

Chapter 5

Operator's Motion-based Data-driven Design

This chapter discusses an estimation method of end-point impedance based on bilateral control system. In Section 5.1, a motion extraction method with bilateral control is explained. In Section 5.1.1, the contact model is explained. In Section 5.1.2, the conventional impedance estimation by bilateral control is explained. In Section 5.1.3, the bilateral control with extra signal is explained. In Section 5.1.4, the estimation method of original responses is explained. In Section 5.2, the outline of simulation is explained. In Section 5.2.1, the simulations with multiple amplitude, bandwidth, and impedance setups are discussed. In Section 5.2.2, the simulations with moving motors and changing impedances are discussed. In Section 5.3, the experiment is discussed. This chapter is summarized in Section 5.4.

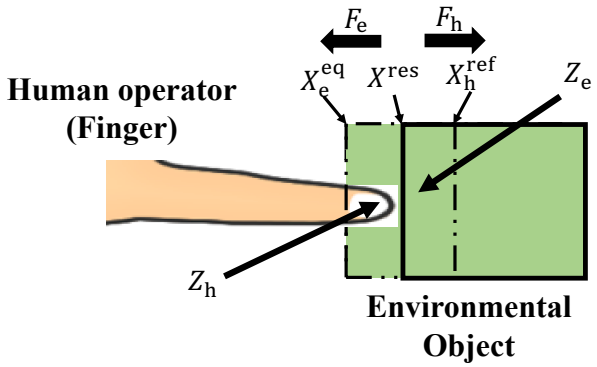

Fig. 5-1: The contact model.

5.1 Motion Extraction

5.1.1 Contact Model

The contact model is considered as shown in Fig. 5-1. The operators are pushing the environmental objects, while the environmental objects are pushing back the operators by the equivalent force due to the law of action and reaction. Since the end-point impedance of the operators and the environmental objects are different, the displacements from the contact position: $X_{\mathrm{h}}^{\mathrm{ref}} - X^{\mathrm{res}}$ and $X^{\mathrm{res}} - X_{\mathrm{e}}^{\mathrm{eq}}$ are also different. Its relationship is represented as follows:

$$F_{\mathrm{h}} = Z_{\mathrm{h}}(s)\{X_{\mathrm{h}}^{\mathrm{ref}} - X^{\mathrm{con}}\} = Z_{\mathrm{e}}(s)\{X^{\mathrm{con}} - X_{\mathrm{e}}^{\mathrm{eq}}\} = -F_{\mathrm{e}}. \tag{5.1}$$

The first-order spring-damper model is considered as a model of impedance as follows:

$$Z(s) \quad = \quad k + sd. \tag{5.2}$$

This dissertation assumes that the operators are realizing some tasks based on the position command and constantly changing their impedance for adapting the surrounded environment, which means both the end-point impedance of the operators and the position command are constantly changing. On the other hand, both the impedance of environmental objects and the equilibrium position of environmental objects are constant for assuming the static environmental objects. The operator's force and the environmental force become the same in the steady state.

5.1.2 Impedance Estimation by Bilateral Control

The bilateral controller is applied because this controller enables to consider both the operator and the environmental sides simultaneously. The structure of bilateral control is the same as one in Section 2.

The relationship regarding position and force are obtained by combining the contact model of Eq. (5.1) and the bilateral controller as follows:

$$X_{\mathrm{m}}^{\mathrm{res}} = X_{\mathrm{s}}^{\mathrm{res}} = X^{\mathrm{con}}, \tag{5.3}$$

$$F_{\mathrm{m}}^{\mathrm{ext}} = -F_{\mathrm{s}}^{\mathrm{ext}} = -F_{\mathrm{e}}. \tag{5.4}$$

The impedances of both the master and slave sides are computed by considering the cost function as follows:

$$\min_{\hat{\boldsymbol{I}}_{\boldsymbol{i}} \geq \mathbf{0}} J = \sum_{i=1}^{N} \left\{ -\hat{\boldsymbol{I}}_{\boldsymbol{i}} \boldsymbol{x}_{\boldsymbol{i}} + F_i \right\}, \tag{5.5}$$

$$\hat{\boldsymbol{I}} = \begin{bmatrix} \hat{M}_i & \hat{d}_i & \hat{k}_i & \hat{o}_i \end{bmatrix}, \tag{5.6}$$

$$\boldsymbol{x}_{\boldsymbol{i}} = \begin{bmatrix} s^2 X_i^{\mathrm{res}} & s X_i^{\mathrm{res}} & X_i^{\mathrm{res}} & 1 \end{bmatrix}^{\mathrm{T}}, \tag{5.7}$$

where $\bigcirc_i$ denotes the $i-\mathrm{th}$ value. The mass and offset are utilized for improving the convergence performance. Since the position and force responses of the master and slave are matched with the contact position and the environmental force as shown in Eqs. (5.3) and (5.4), the impedance estimation of both the master and the slave sides means to estimate the impedance of environmental objects because the position response and the external force from environmental objects are utilized for the impedance estimation. The purpose is to develop the method for estimating the end-point impedance of operators, and some modifications are necessary.

5.1.3 Bilateral Control with the Extra Signal

Since the position and force responses of the master and slave are matched with the contact position and the external force from environmental objects, the separation of master and slave has to be made deliberately. This dissertation adds the extra signal to the force controller of both the master and slave. A maximum length sequence and a sweep sine signal, which include the wide range of frequency information as similar as the white noise, are often utilized for the system identification for satisfying with the persistently exciting. In the case of maximum length sequence, however, the minimum and the maximum frequencies and the cycle of sequences are determined based on the order of its characteristic polynomial. It is hard to consider the appropriate sequence design from the perspective of both frequency and time due to the constraint of uncertainty principle between them. Therefore, this dissertation applies the sweep sine signal due to its simple design. The control goals of bilateral control are updated as follows:

$$X_{\mathrm{m}}^{\mathrm{res}} - X_{\mathrm{s}}^{\mathrm{res}} = 0, \tag{5.8}$$

$$F_{\mathrm{m}}^{\mathrm{ext}} + F_{\mathrm{s}}^{\mathrm{ext}} - F^{\mathrm{extra}} = 0. \tag{5.9}$$

The acceleration references of the master and slave are also updated as follows:

$$s^2 X_{\mathrm{m}}^{\mathrm{ref}} = K_{\mathrm{p}}(X_{\mathrm{s}}^{\mathrm{res}} - X_{\mathrm{m}}^{\mathrm{res}}) + K_{\mathrm{v}}(sX_{\mathrm{s}}^{\mathrm{res}} - sX_{\mathrm{m}}^{\mathrm{res}}) - K_{\mathrm{f}}(F_{\mathrm{m}}^{\mathrm{ext}} + F_{\mathrm{s}}^{\mathrm{ext}} - F^{\mathrm{extra}}), \tag{5.10}$$

$$s^2 X_{\mathrm{s}}^{\mathrm{ref}} = K_{\mathrm{p}}(X_{\mathrm{m}}^{\mathrm{res}} - X_{\mathrm{s}}^{\mathrm{res}}) + K_{\mathrm{v}}(sX_{\mathrm{m}}^{\mathrm{res}} - sX_{\mathrm{s}}^{\mathrm{res}}) - K_{\mathrm{f}}(F_{\mathrm{m}}^{\mathrm{ext}} + F_{\mathrm{s}}^{\mathrm{ext}} - F^{\mathrm{extra}}). \tag{5.11}$$

The stability of controller is equivalent with the original bilateral controller because the extra signal is added as the independent input, but the transparency is degraded based on the amplitude or frequency of the extra signal.

The entire block diagram and its concept are shown in Figs. 5-2 and 5-3.

Both the position and force responses are updated as the combination of two effects: bilateral control and extra signals. The position responses of the bilateral controller with the extra signal are computed as follows:

$$X_{\mathrm{m}}^{\mathrm{up}} = X_{\mathrm{m}}^{\mathrm{ori}} + \frac{F^{\mathrm{extra}}}{Z_{\mathrm{h}} + Z_{\mathrm{e}}}, \tag{5.12}$$

$$X_{\mathrm{s}}^{\mathrm{up}} = X_{\mathrm{s}}^{\mathrm{ori}} + \frac{F^{\mathrm{extra}}}{Z_{\mathrm{h}} + Z_{\mathrm{e}}}. \tag{5.13}$$

The updated value shows the summation of the response of original bilateral controller and the term concerning the extra signal. Since the extra force is added to both the master and slave, the second terms

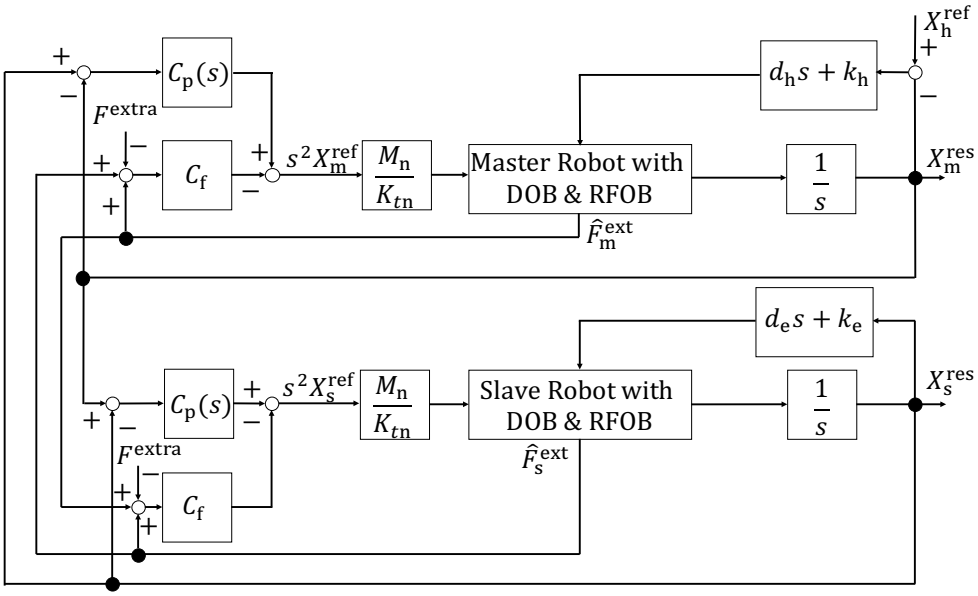

Fig. 5-2: The block diagram of bilateral control with the extra signal.

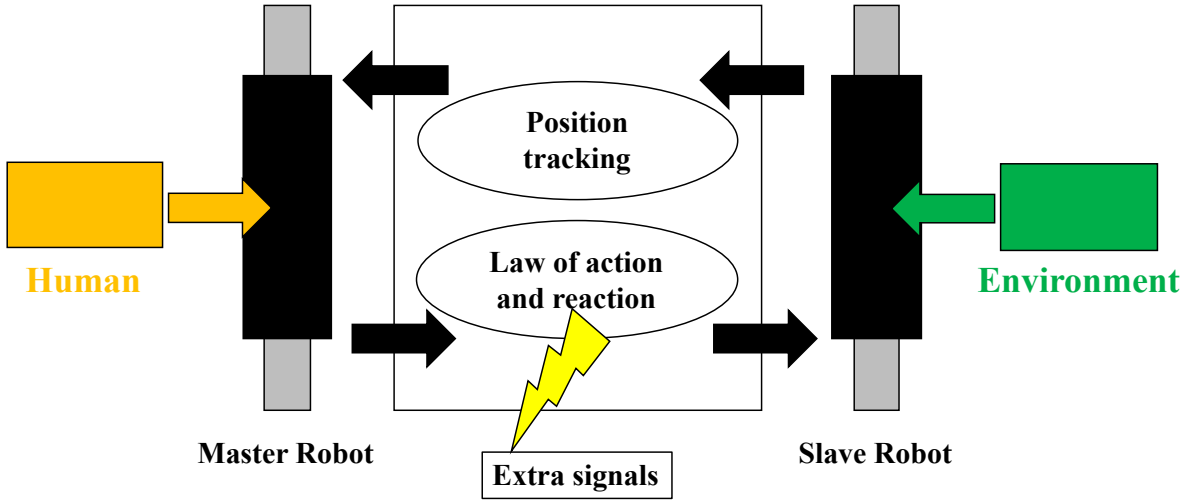

Fig. 5-3: The concept of approach.

of right-hand sides of Eqs. (5.12) and (5.13) are added. The position responses of the master and slave are matched as the updated position control goal Eq. (5.8) shows.

The force responses of the bilateral controller with the extra signal can derived from Eqs. (5.10) and (5.11) and computed as follows:

$$F_m^{up} = -F_s^{up} + F^{extra}, \tag{5.14}$$

$$F_s^{up} = -F_m^{up} + F^{extra}. \tag{5.15}$$

$F_{\mathrm{m}}^{\mathrm{up}}$ and $F_{\mathrm{s}}^{\mathrm{up}}$ are computed as follows:

$$F_{\mathrm{m}}^{\mathrm{up}} = F_{\mathrm{m}}^{\mathrm{ori}} + \frac{Z_{\mathrm{h}}}{Z_{\mathrm{h}} + Z_{\mathrm{e}}} F^{\mathrm{extra}}, \tag{5.16}$$

$$F_{\mathrm{s}}^{\mathrm{up}} = F_{\mathrm{s}}^{\mathrm{ori}} + \frac{Z_{\mathrm{e}}}{Z_{\mathrm{h}} + Z_{\mathrm{e}}} F^{\mathrm{extra}}. \tag{5.17}$$

The second terms of right-hand side show the effect of extra signal. The denominators become the summation of operator's and environmental objects' impedance because the extra signal is added to the system, on the other hand, the numerators become the operator's or environmental objects' impedance because the master/slave robot only contact operators/environmental objects. The updated position and force responses are recomputed as follows by combining Eqs. (5.14)–(5.17):

$$F_{\mathrm{m}}^{\mathrm{up}} = -F_{\mathrm{s}}^{\mathrm{up}} + F^{\mathrm{extra}} = -F_{\mathrm{s}}^{\mathrm{ori}} + \frac{Z_{\mathrm{h}}}{Z_{\mathrm{h}} + Z_{\mathrm{e}}} F^{\mathrm{extra}}, \tag{5.18}$$

$$F_{\mathrm{s}}^{\mathrm{up}} = -F_{\mathrm{m}}^{\mathrm{up}} + F^{\mathrm{extra}} = -F_{\mathrm{m}}^{\mathrm{ori}} + \frac{Z_{\mathrm{e}}}{Z_{\mathrm{h}} + Z_{\mathrm{e}}} F^{\mathrm{extra}}. \tag{5.19}$$

The force responses of the master and slave are not matched in the case the impedance of the operators and the environmental objects are not the same. Since the position and force responses are determined based on the effect of bilateral controller and extra signal, they should be separated for estimating the end-point impedance of operators.

5.1.4 Estimation of the Original Motion

The effect of bilateral controller, which is called the original motion in Section 5.1.4, should be removed for estimating the impedances of master and slave sides simultaneously and independently. Therefore, the original motion is estimated as follows:

$$\bigcirc_i^{\mathrm{ave}} = \sum_{j=0}^{n-1} \bigcirc_j \qquad (n \text{ is updated when } F^{\mathrm{extra}} = 0), \tag{5.20}$$

$$\bigcirc_i^{\mathrm{calc}} = \frac{\text{Elapsed time}}{\text{Length of this step}} (\bigcirc_i^{\mathrm{ave}} - \bigcirc_{i-1}^{\mathrm{ave}}) + \bigcirc_{i-1}^{\mathrm{ave}}. \tag{5.21}$$

The calculation value is computed by the linear interpolation between the average of each step, and it is updated when $F^{\mathrm{extra}} = 0$.

The cost function for estimating the impedance is updated from Eqs. (5.5) and (5.7) to as follows:

$$\min_{\hat{\boldsymbol{I}}_{\boldsymbol{i}} \geq \boldsymbol{0}} J = \sum_{i=1}^{N} \{ -\hat{\boldsymbol{I}}_{\boldsymbol{i}} \boldsymbol{x}_i^{\mathrm{up}} + (\hat{F}_i^{\mathrm{ext,up}} - F_i^{\mathrm{calc}}) \}, \tag{5.22}$$

$$\boldsymbol{x}_i^{\mathrm{up}} = \begin{bmatrix} s^2 X_i^{\mathrm{res,up}} - s^2 X_i^{\mathrm{calc}} & s X_i^{\mathrm{res,up}} - s X_i^{\mathrm{est}} & X_i^{\mathrm{res,up}} - X_i^{\mathrm{est}} & 1 \end{bmatrix}^{\mathrm{T}}. \tag{5.23}$$

This dissertation calls its subtraction the compensation. The impedance in master and slave sides are computed as follows in the case the compensation, which is based on the calculation value $\bigcirc^{\mathrm{calc}}$, is well designed:

$$\frac{F_{\mathrm{m}}^{\mathrm{up}}}{X_{\mathrm{m}}^{\mathrm{up}}} = \frac{F_{\mathrm{m}}^{\mathrm{ori}} + \dfrac{Z_{\mathrm{h}}}{Z_{\mathrm{h}} + Z_{\mathrm{e}}} F^{\mathrm{extra}} - F_{\mathrm{m}}^{\mathrm{calc}}}{X_{\mathrm{m}}^{\mathrm{ori}} + \dfrac{1}{Z_{\mathrm{h}} + Z_{\mathrm{e}}} F^{\mathrm{extra}} - X_{\mathrm{m}}^{\mathrm{calc}}} = \frac{\dfrac{Z_{\mathrm{h}}}{Z_{\mathrm{h}} + Z_{\mathrm{e}}} F^{\mathrm{extra}}}{\dfrac{1}{Z_{\mathrm{h}} + Z_{\mathrm{e}}} F^{\mathrm{extra}}} = Z_{\mathrm{h}}, \tag{5.24}$$

$$\frac{F_{\mathrm{s}}^{\mathrm{up}}}{X_{\mathrm{s}}^{\mathrm{up}}} = \frac{F_{\mathrm{s}}^{\mathrm{ori}} + \dfrac{Z_{\mathrm{e}}}{Z_{\mathrm{h}} + Z_{\mathrm{e}}} F^{\mathrm{extra}} - F_{\mathrm{s}}^{\mathrm{calc}}}{X_{\mathrm{s}}^{\mathrm{ori}} + \dfrac{1}{Z_{\mathrm{h}} + Z_{\mathrm{e}}} F^{\mathrm{extra}} - X_{\mathrm{s}}^{\mathrm{calc}}} = \frac{\dfrac{Z_{\mathrm{e}}}{Z_{\mathrm{h}} + Z_{\mathrm{e}}} F^{\mathrm{extra}}}{\dfrac{1}{Z_{\mathrm{h}} + Z_{\mathrm{e}}} F^{\mathrm{extra}}} = Z_{\mathrm{e}}. \tag{5.25}$$

Recursive Least-Squares (RLS) [107] is applied, and its solution is iteratively computed as follows:

$$\boldsymbol{g_i} = \frac{\boldsymbol{P_{i-1}} \boldsymbol{x_i}}{1 + \boldsymbol{x_i}^{\mathrm{T}} \boldsymbol{P_{i-1}} \boldsymbol{x_i}}, \tag{5.26}$$

$$\hat{\boldsymbol{I}}_{\boldsymbol{i}} = \hat{\boldsymbol{I}}_{i-1} + \boldsymbol{g_i} \{ (\hat{F}_i^{\mathrm{ext,up}} - F_i^{\mathrm{est}}) - \hat{\boldsymbol{I}}_{i-1} \boldsymbol{x_i} \}, \tag{5.27}$$

$$\boldsymbol{P_i} = \boldsymbol{P_{i-1}} - \boldsymbol{g_i} \boldsymbol{x_i}^{\mathrm{T}} \boldsymbol{P_{i-1}}. \tag{5.28}$$

The responses of the master are substituted in the case the end-point impedance of operators is estimated, while on the other hand, the responses of the slave are substituted in the case the impedance of environmental objects is estimated.

5.2 Simulations

The operator robot was designed in order to confirm the effectiveness of proposal. The virtual impedance is freely designed as the true value in the operator robot, and the validity of estimation value can be confirmed.

The first part of this section evaluated the characteristics of the proposed estimation method. The second part of this section applied the proposed estimation method into the moving and variable impedance operator robot.

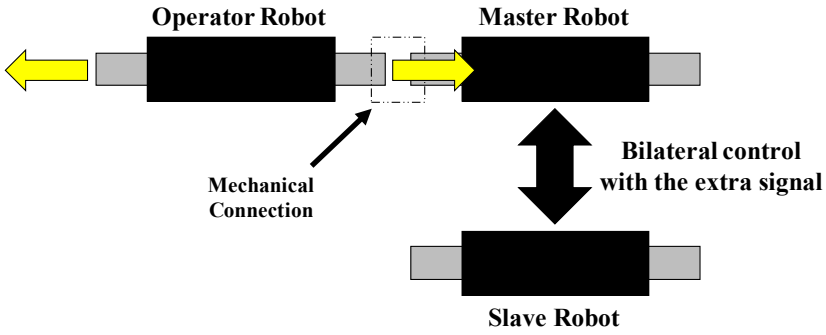

Fig. 5-4: The concept of simulation.

5.2.1 Evaluation of the Proposed Method

This section modified four parameters: the amplitude of the extra signal, the bandwidth of the extra signal, the end-point impedance of operator robot, and the environmental impedance, and evaluated the estimation performance by three indexes: the settling time, the absolute value of steady state error, and the error ratio. It is noted that the final value was obtained after 100 s elapsed.

The concept of this simulation is shown in Fig. 5-4. The master and slave robots were connected by the bilateral controller with the extra signal, and the operator robot was mechanically connected with the master robot. The acceleration reference of the operator robot was designed as follows:

$$s^2 X_{\rm op}^{\rm ref} = K_{\rm p}(X_{\rm op}^{\rm cmd} - X_{\rm op}^{\rm res} - X_{\rm op}^{\rm vir}) + K_{\rm v}(sX_{\rm op}^{\rm cmd} - sX_{\rm op}^{\rm res} - sX_{\rm op}^{\rm vir}) - s^2 X_{\rm op}^{\rm vir}, \quad (5.29)$$

$$s^2 X_{\rm op}^{\rm vir} = \frac{\hat{F}_{\rm op}^{\rm ext} - k^{\rm vir} X_{\rm op}^{\rm vir} - d^{\rm vir} s X_{\rm op}^{\rm vir}}{m^{\rm vir}}. \quad (5.30)$$

The simulation parameters are shown in Table 5.1.

Table 5.1: Simulation parameters.

Description	Value
Position gain	$900\ \mathrm{s}^{-2}$
Velocity gain	$60\ \mathrm{s}^{-1}$
Force gain	$1.0\ \mathrm{kg}^{-1}$
Cut-off frequency of DOB	$400.0\ \mathrm{rad/s}$
Cut-off frequency of RFOB	$400.0\ \mathrm{rad/s}$
Nominal mass of robots	$0.5\ \mathrm{kg}$
Torque coefficient	$33.0\ \mathrm{N/A}$
Interval of the extra signal	$1\ \mathrm{s}$
Sampling time	$0.1\ \mathrm{ms}$
Virtual mass	$0.5\ \mathrm{kg}$

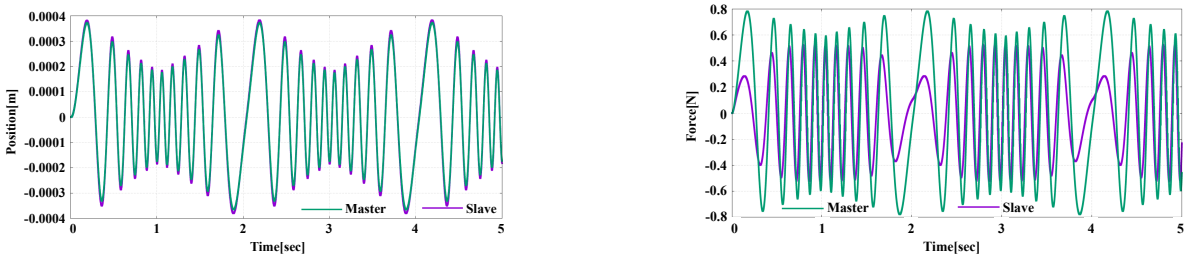

(a) Position response (b) Force response

Fig. 5-5: The responses when the amplitude is set as 1.

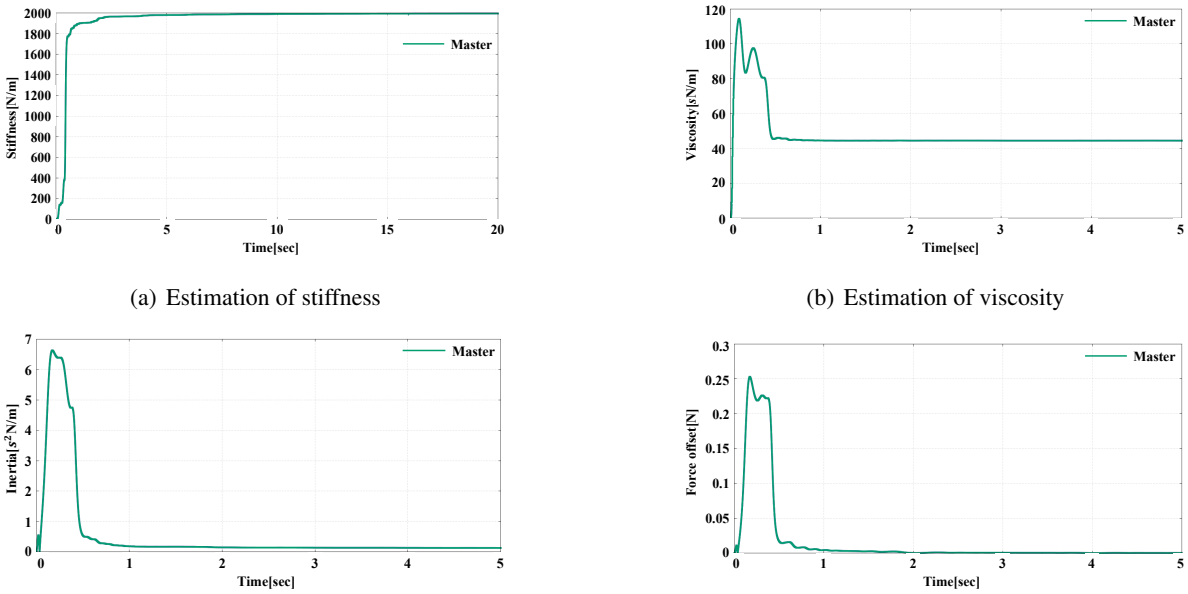

(a) Estimation of stiffness (b) Estimation of viscosity

(c) Estimation of mass (d) Estimation of force offset

Fig. 5-6: The estimation results when the amplitude is set as 1.

The Estimation Performance Evaluation with the Different Amplitude of the Extra Signal

The amplitude of the extra signal was set as different values, and the estimation performance was evaluated with three indexes. Its amplitude was set as 1, 2, 5, and 10. The stiffness and viscosity of operator robot were set as 2000 $\mathrm{N/m}$ and 50 $s\mathrm{N/m}$, while the stiffness and viscosity of environmental objects were set as 500 $\mathrm{N/m}$ and 50 $s\mathrm{N/m}$. In addition, the bandwidth of the extra signal was set as $1-5$ Hz. These simulation parameters were arbitrarily decided.

The responses and estimation results when the amplitude was set as 1 are shown in Figs. 5-5 and 5-6 as an example of the estimation performance. The impedance estimation results of viscosity and

Table 5.2: The estimation results of viscosity with the different amplitude.

Amplitude	Settling time [s]	Absolute error [sN/m]	$(\frac{\text{True value} - \text{Final value}}{\text{True value}}) \times 100$ [%]
1	0.459	5.559	11.119
2	0.442	5.559	11.119
5	0.418	5.559	11.119
10	0.353	5.559	11.119

Table 5.3: The estimation results of stiffness with the different amplitude.

Amplitude	Settling time [s]	Absolute error [N/m]	$(\frac{\text{True value} - \text{Final value}}{\text{True value}}) \times 100$ [%]
1	1.047	2.877	0.144
2	0.466	0.328	0.016
5	0.42	0.392	-0.020
10	0.339	0.498	-0.025

stiffness are summarized in Tables 5.2 and 5.3. The settling time, the absolute error, and the error ratio were almost the same with the different amplitude for the viscosity estimation. The settling time, the absolute error, and the error ratio were also the same except the amplitude is 1 for the stiffness estimation. The stiffness could be estimated almost properly, while some errors were remaining in the viscosity estimation. Many reasons for the poor viscosity estimation comparing with the stiffness estimation can be considered including the design of extra signal, the method for velocity obtainment, the calculation order of RLS, the estimation method, and so forth, and it is tough to identify what is the dominant factor for the viscosity estimation error as well as conventional researches have encountered. In addition, the initial values of estimation parameters affected to the settling time. Since this dissertation assumed that the information with regard to the estimated impedance was not known in advance, the initial values of estimation parameters were set to zero. This is why some shapes of impedance estimation became sharp, and the appropriate design of initial values may improve the settling time. From these results, the amplitude should be set higher than some extent, in this case higher than 1. It is also noted that the time resolution of impedance estimation can be set 0.5 s when the amplitude is higher than 2, and its information is valuable for designing the extra signal.

The mass and the force offsets estimation results with the different amplitude are summarized in Tables 5.4 and 5.5. Since the true value of the force offsets was zero, their error ratios were not computed. The settling time of both the mass and the force offsets estimation were shorter as the amplitude became larger. The absolute error and the error ratio of mass and force offsets estimations became almost the same for the different amplitude. Due to the extra signal design, the mass estimation performance was

Table 5.4: The estimation results of mass with the different amplitude.

Amplitude	Settling time [s]	Absolute error [kgm^2]	$(\frac{\text{True value} - \text{Final value}}{\text{True value}}) \times 100$ [%]
1	8.147	0.384	76.8
2	2.356	0.385	77.0
5	0.79	0.384	76.8
10	0.471	0.384	76.8

Table 5.5: The estimation results of force offsets with the different amplitude.

Amplitude	Settling time [s]	Absolute error [N]	$(\frac{\text{True value} - \text{Final value}}{\text{True value}}) \times 100$ [%]
1	21.948	0.000	-
2	3.929	0.000	-
5	1.848	0.000	-
10	0.8	0.000	-

worse than the viscosity estimation performance.

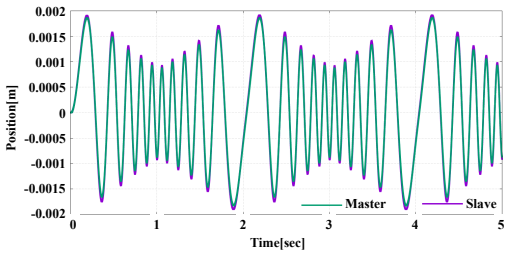

(a) Position response

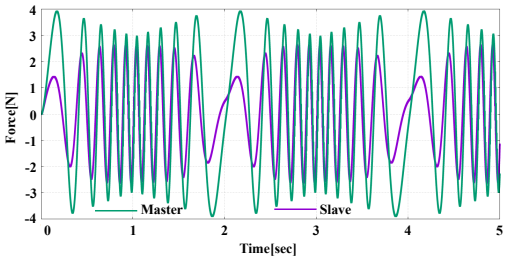

(b) Force response

Fig. 5-7: The responses when the bandwidth is set as $1-5$ Hz.

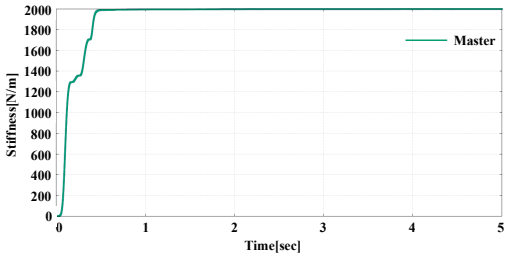

(a) Estimation of stiffness

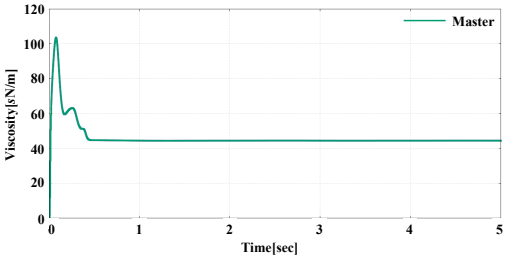

(b) Estimation of viscosity

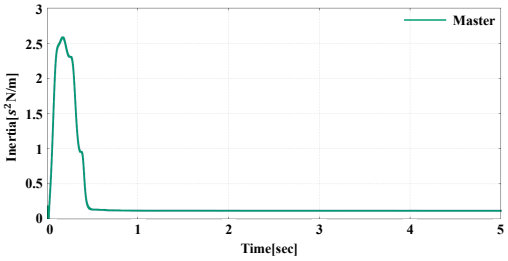

(c) Estimation of mass

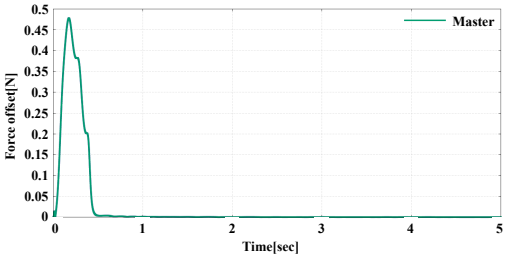

(d) Estimation of force offset

Fig. 5-8: The estimation results when the bandwidth is set as $1-5$ Hz.

The Estimation Performance Evaluation with the Different Bandwidth of the Extra Signal

The bandwidth of the extra signal was set as different values, and the estimation performance was evaluated with three indexes. Its bandwidth was set as $1-5$ Hz, $1-50$ Hz, $1-100$ Hz, and $1-400$ Hz. The stiffness and viscosity of operator robot were set as $2000\ \mathrm{N/m}$ and $50\ s\mathrm{N/m}$, while the stiffness and viscosity of environmental objects were set as $500\ \mathrm{N/m}$ and $50\ s\mathrm{N/m}$. In addition, the amplitude of the extra signal was set as 5. These simulation parameters were also arbitrarily decided.

The responses and the estimation results when the bandwidth was set as $1-5$ Hz are shown in Figs. 5-7 and 5-8 as the example of the estimation performance. The impedance estimation results of

Table 5.6: The estimation results of viscosity.

Bandwidth [Hz]	Settling time [s]	Absolute error [sN/m]	$(\frac{\text{True value} - \text{Final value}}{\text{True value}}) \times 100$ [%]
$1-5$	0.418	5.559	11.119
$1-50$	0.484	10.472	20.945
$1-100$	0.402	12.100	24.200
$1-400$	0.170	14.197	28.394

Table 5.7: The estimation results of stiffness.

Bandwidth [Hz]	Settling time [s]	Absolute error [N/m]	$(\frac{\text{True value} - \text{Final value}}{\text{True value}}) \times 100$ [%]
$1-5$	0.42	0.392	-0.020
$1-50$	0.432	101.797	-5.090
$1-100$	0.852	205.690	-10.284
$1-400$	4.041	460.780	-23.039

viscosity and stiffness are summarized in Tables 5.6 and 5.7. The settling time of the viscosity estimation was almost the same except the bandwidth was $1-400$ Hz. The absolute error and the error ratio became larger as the bandwidth becomes wider. The settling time of the stiffness estimation was shorter when the bandwidth is $1-5$ Hz and $1-50$ Hz. The absolute error and the error ratio of the stiffness estimation became larger as the bandwidth becomes wider. From these results, the bandwidth should be set $1-5$ Hz among other bandwidth from the perspective of error. The time resolution of impedance estimation can be set 0.5 s when the bandwidth is $1-5$ Hz.

The mass and the force offsets estimation results with the different bandwidth are summarized in Table 5.8 and Table 5.9. The error ratio of force offsets was not computed because of the same reason in Section 5.2.1. The settling time of mass estimation was shorter when the bandwidth was $1-5$ Hz. At the same time, the absolute errors when the bandwidth was $1-5$ Hz were better than others, but errors were large overall conditions. The settling time of force offsets was longer when the bandwidth was $1-5$ Hz.

Table 5.8: The estimation results of mass.

Bandwidth [Hz]	Settling time [s]	Absolute error [kgm^2]	$(\frac{\text{True value} - \text{Final value}}{\text{True value}}) \times 100$ [%]
$1-5$	0.018	0.384	76.8
$1-50$	0.922	0.424	84.8
$1-100$	0.947	0.446	89.2
$1-400$	0.96	0.469	89.8

Table 5.9: The estimation results of force offsets.

Bandwidth [Hz]	Settling time [s]	Absolute error [N]	$(\frac{\text{True value} - \text{Final value}}{\text{True value}}) \times 100$ [%]
$1-5$	1.848	0.000	-
$1-50$	0.384	0.000	-
$1-100$	0.308	0.000	-
$1-400$	0.891	0.000	-

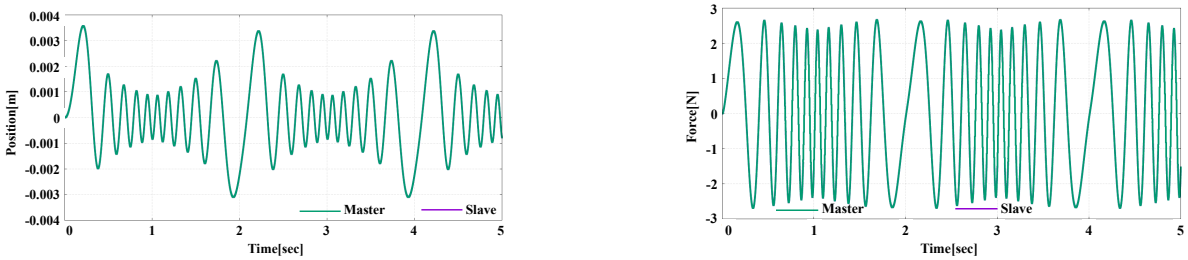

(a) Position response

(b) Force response

Fig. 5-9: The responses when the operator and environmental stiffness and viscosity are $500\ \mathrm{N/m}$ and $50\ s\mathrm{N/m}$.

The Estimation Performance Evaluation with the Different Impedance of Operator Robot and Environmental Objects

The impedance of operator robot and environmental objects were set as different values, and the estimation performance was evaluated with three indexes. The stiffness of the operator robot and the environmental object were set as $500\ \mathrm{N/m}$, $2000\ \mathrm{N/m}$, $5000\ \mathrm{N/m}$, and $10000\ \mathrm{N/m}$, while on the other hand, their viscosity were set as $50\ s\mathrm{N/m}$, $100\ s\mathrm{N/m}$, $200\ s\mathrm{N/m}$, and $500\ s\mathrm{N/m}$. The amplitude of the extra signal was set as 5, while its bandwidth was set as $1 - 5\ \mathrm{Hz}$. These simulation parameters were also arbitrarily decided.

The responses and the estimation results when the stiffness and viscosity of operator robot and environmental objects were $500\ \mathrm{N/m}$ and $50\ s\mathrm{N/m}$ are shown in Figs. 5-9 and 5-10 as the example of the estimation performance. The impedance estimation results of viscosity and stiffness with the different environmental impedance are summarized in Tables 5.10 and 5.11. It is noted that the stiffness and the viscosity of operator robot were fixed as $2000\ \mathrm{N/m}$ and $50\ s\mathrm{N/m}$, respectively. The settling time of the viscosity estimation was shorter with the larger stiffness. The absolute error and the error ratio of the viscosity estimation became almost the same with the different impedance although some errors were remaining in the viscosity estimation as similar as other cases. The settling time of the stiffness estimation was longer as the larger stiffness. It can be improved by designing the initial values of RLS properly. The absolute error and the error ratio of stiffness estimation were smaller when the viscosity was set as $100\ s\mathrm{N/m}$ and $200\ s\mathrm{N/m}$. From these results, the proposed method can be applicable to all environmental impedance set-up when the virtual stiffness and the virtual viscosity of the operator robot is set as $2000\ \mathrm{N/m}$ and $50\ s\mathrm{N/m}$. The time resolution of impedance estimation can be set as 0.5 s if the

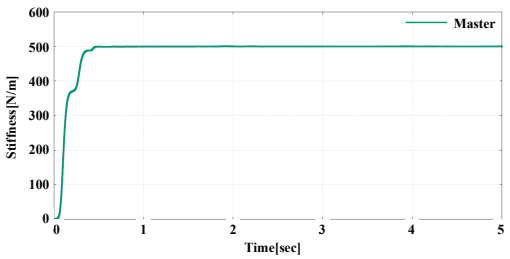

(a) Estimation of stiffness

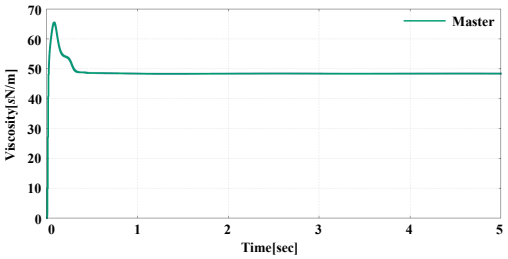

(b) Estimation of viscosity

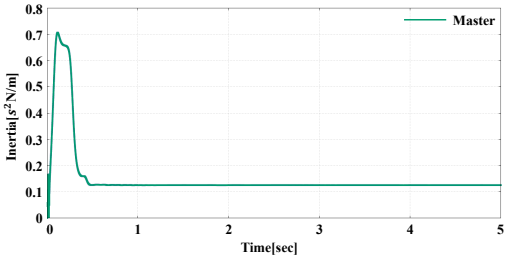

(c) Estimation of mass

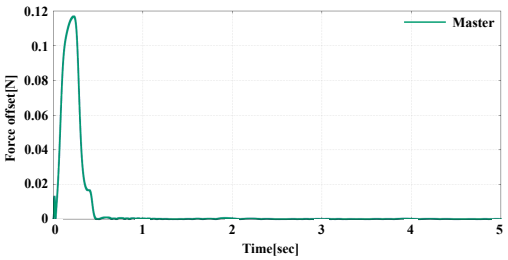

(d) Estimation of force offset

Fig. 5-10: The estimation results when the operator and environmental stiffness and viscosity are $500\ \mathrm{N/m}$ and $50\ s\mathrm{N/m}$.

slave stiffness is not extremely high ($k_{\mathrm{e}} = 10000$ N/m).

The mass and the force offsets estimation results with the different environmental impedance are summarized in Tables 5.12 and 5.13. The error ratio of force offsets was not computed because of the same reason in Section 5.2.1. The settling time of mass estimation was longer when the impedance became larger. The absolute error and the error ratio of mass estimation became almost the same for the different environmental impedance. The settling time of force offsets estimation was longer when the viscosity became large.

Table 5.10: The estimation results of viscosity.

Env. stiffness [N/m]	Env. viscosity [sN/m]	Settling time [s]	Absolute error [sN/m]	$(\frac{\text{True value} - \text{Final value}}{\text{True value}}) \times 100$ [%]
500	50	0.418	5.559	11.119
500	100	0.425	5.538	11.075
500	200	0.431	5.533	11.067
500	500	0.355	5.582	11.163
2000	50	0.419	5.607	11.215
2000	100	0.426	5.578	11.155
2000	200	0.434	5.558	11.117
2000	500	0.437	5.586	11.171
5000	50	0.116	5.64	11.295
5000	100	0.119	5.623	11.245
5000	200	0.125	5.596	11.192
5000	500	0.137	5.596	11.192
10000	50	0.103	5.661	11.321
10000	100	0.101	5.649	11.298
10000	200	0.103	5.629	11.259
10000	500	0.112	5.612	11.225

Table 5.11: The estimation results of stiffness.

Env. stiffness [N/m]	Env. viscosity [sN/m]	Settling time [s]	Absolute error [N/m]	$(\frac{\text{True value} - \text{Final value}}{\text{True value}}) \times 100$ [%]
500	50	0.420	0.392	-0.020
500	100	0.430	0.286	-0.014
500	200	0.446	0.121	-0.006
500	500	0.504	0.538	0.027
2000	50	0.425	0.446	-0.022
2000	100	0.434	0.294	-0.015
2000	200	0.449	0.078	-0.004
2000	500	0.513	0.646	0.032
5000	50	0.441	0.329	-0.016
5000	100	0.450	0.183	-0.009
5000	200	0.465	0.084	0.004
5000	500	0.652	0.881	0.044
10000	50	0.628	0.089	0.004
10000	100	0.636	0.241	0.012
10000	200	0.654	0.508	0.025
10000	500	0.876	1.342	0.067

Table 5.12: The estimation results of mass.

Env. stiffness [N/m]	Env. viscosity [sN/m]	Settling time [s]	Absolute error [kgm^2]	$(\frac{\text{True value} - \text{Final value}}{\text{True value}}) \times 100$ [%]
500	50	0.018	0.384	76.8
500	100	0.017	0.384	76.8
500	200	0.017	0.384	76.8
500	500	3.887	0.384	76.8
2000	50	0.925	0.384	76.8
2000	100	1.042	0.384	76.8
2000	200	1.909	0.384	76.8
2000	500	4.170	0.384	76.8
5000	50	1.832	0.384	76.8
5000	100	2.061	0.384	76.8
5000	200	2.921	0.384	76.8
5000	500	5.877	0.384	76.8
10000	50	3.785	0.384	76.8
10000	100	3.867	0.384	76.8
10000	200	4.353	0.384	76.8
10000	500	7.088	0.383	76.6

Table 5.13: The estimation results of force offsets.

Env. stiffness [N/m]	Env. viscosity [sN/m]	Settling time [s]	Absolute error [N]	$(\frac{\text{True value} - \text{Final value}}{\text{True value}}) \times 100$ [%]
500	50	1.848	0.000	-
500	100	1.904	0.000	-
500	200	3.922	0.000	-
500	500	22.001	0.000	-
2000	50	1.863	0.000	-
2000	100	1.913	0.000	-
2000	200	3.927	0.000	-
2000	500	11.967	0.000	-
5000	50	1.913	0.000	-
5000	100	1.941	0.000	-
5000	200	3.929	0.000	-
5000	500	7.978	0.000	-
10000	50	1.929	0.000	-
10000	100	1.940	0.000	-
10000	200	1.956	0.000	-
10000	500	5.953	0.000	-

Table 5.14: The estimation results of viscosity.

Ope. stiffness [N/m]	Ope. viscosity [sN/m]	Settling time [s]	Absolute error [sN/m]	$(\frac{\text{True value} - \text{Final value}}{\text{True value}}) \times 100$ [%]
500	50	0.286	1.625	3.250
500	100	0.277	2.001	2.006
500	200	0.271	2.757	1.378
500	500	0.238	5.010	1.002
2000	50	0.418	5.559	11.119
2000	100	0.411	5.978	5.978
2000	200	0.332	6.746	3.373
2000	500	0.311	8.977	1.795
5000	50	0.129	13.343	26.686
5000	100	0.434	13.845	13.845
5000	200	0.433	14.711	7.355
5000	500	0.429	16.990	3.398
10000	50	0.112	26.221	52.441
10000	100	0.111	26.794	26.794
10000	200	0.117	27.805	13.902
10000	500	0.446	30.328	6.066

The impedance estimation results of viscosity and stiffness with the different operator impedance are summarized in Tables 5.14 and 5.15. It is noted that the stiffness and the viscosity of environmental object were set as $500\ \mathrm{N/m}$ and $50\ s\mathrm{N/m}$, respectively.

The settling time of the viscosity estimation was almost the same although some impedance set-up, i.e., $5000\ \mathrm{N/m}$ and $50\ s\mathrm{N/m}$, showed the different values. The absolute error of viscosity estimation became larger when the impedance became larger, while the error ratio became larger with the larger stiffness and the smaller viscosity. The settling time of the stiffness estimation was longer with the larger impedance. The absolute error and the error ratio of the stiffness estimation were larger as the impedance became larger when the stiffness was set as $500\ \mathrm{N/m}$ and $2000\ \mathrm{N/m}$, while they became smaller when the viscosity became smaller with the stiffness $10000\ \mathrm{N/m}$. From these results, the proposed method can be applicable to all environmental impedance set-up when the stiffness and the viscosity of the operator robot is set as $500\ \mathrm{N/m}$ and $50\ s\mathrm{N/m}$. The time resolution of impedance estimation can be set as 1 s in the range that the environmental stiffness is smaller than $10000\ \mathrm{N/m}$. The time resolution of impedance estimation can be shortened for designing the initial values of estimation process.

The mass and the force offsets estimation results with the different operator impedance are summarized in Tables 5.16 and 5.17. The error ratio of force offsets was not computed because of the same reason in Section 5.2.1. The settling time of mass estimation was longer when the stiffness/viscosity became larger/shorter. The absolute error and the error ratio of mass estimation became almost the same for the different environmental impedance. The settling time of force offsets estimation was longer when

Table 5.15: The estimation results of stiffness.

Ope. stiffness [N/m]	Ope. viscosity [sN/m]	Settling time [s]	Absolute error [N/m]	$(\frac{\text{True value} - \text{Final value}}{\text{True value}}) \times 100$ [%]
500	50	0.323	0.377	-0.075
500	100	0.336	0.805	-0.161
500	200	0.361	1.696	-0.339
500	500	0.507	5.079	-1.016
2000	50	0.420	0.392	-0.020
2000	100	0.431	0.907	-0.045
2000	200	0.447	1.837	-0.092
2000	500	0.494	5.069	-0.253
5000	50	0.435	0.519	0.010
5000	100	0.444	0.175	-0.0035
5000	200	0.460	1.141	-0.023
5000	500	0.586	3.566	-0.071
10000	50	0.636	7.195	0.072
10000	100	0.645	6.137	0.061
10000	200	0.668	5.372	0.054
10000	500	0.949	4.957	0.050

Table 5.16: The estimation results of mass.

Ope. stiffness [N/m]	Ope. viscosity [sN/m]	Settling time [s]	Absolute error [kgm^2]	$(\frac{\text{True value} - \text{Final value}}{\text{True value}}) \times 100$ [%]
500	50	0.456	0.385	77.0
500	100	0.458	0.385	77.0
500	200	0.467	0.387	77.4
500	500	0.038	0.390	78.0
2000	50	0.790	0.385	77.0
2000	100	0.660	0.386	77.2
2000	200	0.656	0.387	77.4
2000	500	0.690	0.390	78.0
5000	50	3.821	0.386	77.2
5000	100	2.107	0.386	77.2
5000	200	1.860	0.387	77.4
5000	500	1.877	0.391	78.2
10000	50	16.315	0.388	77.6
10000	100	9.940	0.388	77.6
10000	200	6.311	0.386	77.2
10000	500	4.996	0.391	78.2

the operator stiffness became larger.

Table 5.17: The estimation results of force offsets.

Ope. stiffness [N/m]	Ope.viscosity [sN/m]	Settling time [s]	Absolute error [N]	$(\frac{\text{True value} - \text{Final value}}{\text{True value}}) \times 100$ [%]
500	50	0.480	0.000	-
500	100	0.482	0.000	-
500	200	0.662	0.000	-
500	500	0.061	0.000	-
2000	50	1.848	0.000	-
2000	100	1.842	0.000	-
2000	200	1.856	0.000	-
2000	500	1.899	0.000	-
5000	50	3.932	0.000	-
5000	100	1.951	0.000	-
5000	200	1.947	0.000	-
5000	500	3.917	0.000	-
10000	50	20.001	0.000	-
10000	100	5.985	0.000	-
10000	200	5.975	0.000	-
10000	500	5.979	0.000	-

Table 5.18: The trajectory of the operator robot.

Time [s]	Type of motion
0-1	Keeping position
1-4	Moving 1 cm forward
4-6	Keeping position
6-9	Moving 1 cm backward
9-10	Keeping position

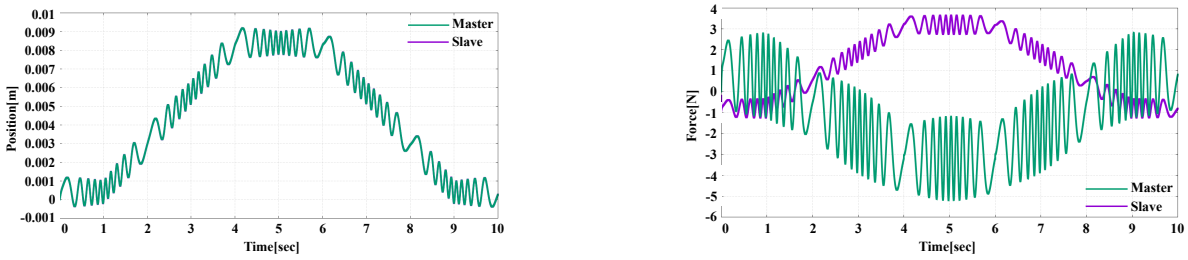

(a) Position response

(b) Force response

Fig. 5-11: The responses with the moving operator robot.

5.2.2 Bilateral Control with the Moving and the Variable Impedance Operator Robot

This section considers the moving and the variable impedance operator robot. The amplitude and the bandwidth of the extra signal were fixed as 2 and $1-5$ Hz, respectively.

Bilateral Control with the Moving Operator Robot

The operator robot was operating the master robot while executing interactive motions. This case took the movement of operator robot into consideration. The trajectory of the operator robot is shown in Table 5.18.

The position and force responses are shown in Fig. 5-11. The estimation results of impedance are shown in Fig. 5-12. The red lines show the expected values of viscosity and stiffness, which is designed in the operator robot. The estimated viscosity between the with compensation and the without compensation showed the similar behaviour. On the other hand, the estimated stiffness of master side with the compensation almost converged at their expected values, while the estimated stiffness without the compensation converged at one of the environmental values. Since the effect of movement is much larger than the effect of extra signal, the estimation results without compensation were highly affected by the effect of bilateral controller. The appropriate estimation of the original movement is one of the issues to tackle with.

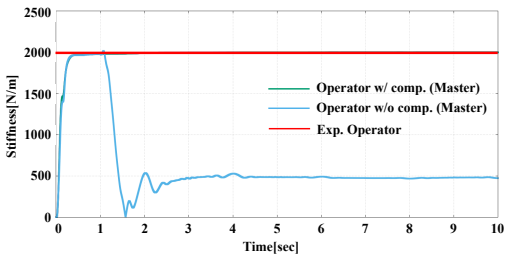

(a) Estimation of stiffness

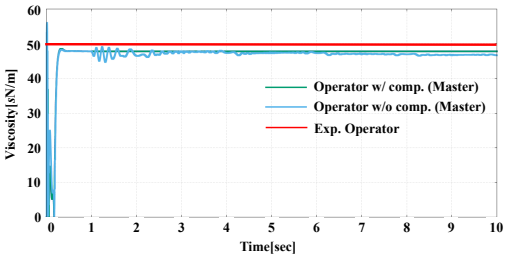

(b) Estimation of viscosity

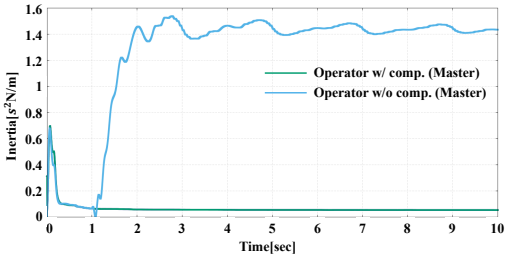

(c) Estimation of mass

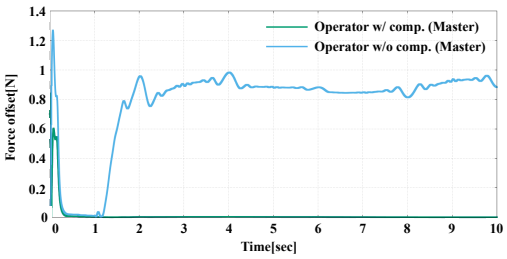

(d) Estimation of force offset

Fig. 5-12: The estimation results with the moving operator robot.

Table 5.19: The stiffness and the viscosity variations of the operator robot.

Time [s]	Stiffness [N/m]	Viscosity [sN/m]
0-1	500	50
1-4	2000	100
4-6	2000	50
6-9	500	100
9-10	500	50

Bilateral Control with the Variable Impedance Operator Robot

The impedance of human operator is known to be constantly changing for adapting the surrounded environment and realizing tasks. Although it is better to update the impedance estimation process at every sampling time, this dissertation updated its process in each 1 s from the perspective of convergence speed of RLS, which is obtained in Section 5.2, and the signal design. The stiffness and the viscosity variations of operator robot is summarized in Table 5.19.

The position and force responses are shown in Fig. 5-13. The impedance estimation results are shown in Fig. 5-14. Both the stiffness and viscosity were almost properly estimated in each 1 s. The time resolution of impedance estimation should be variable based on the type of motion since the impedance estimation is constrained by the setting of extra signal, which is related to the estimation accuracy of the

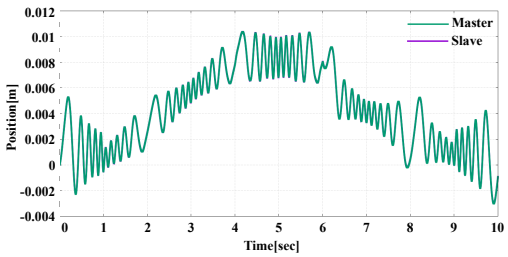

(a) Position response

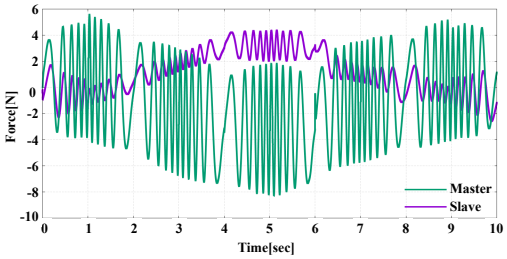

(b) Force response

Fig. 5-13: The responses with the variable virtual impedance operator robot.

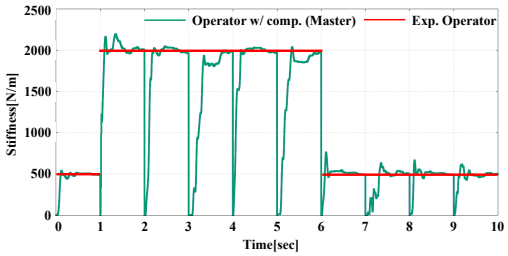

(a) Estimation of stiffness

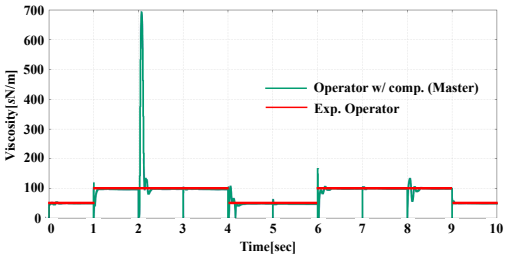

(b) Estimation of viscosity

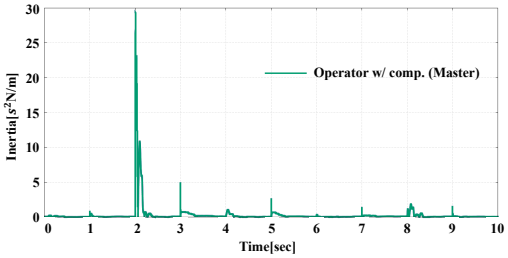

(c) Estimation of mass

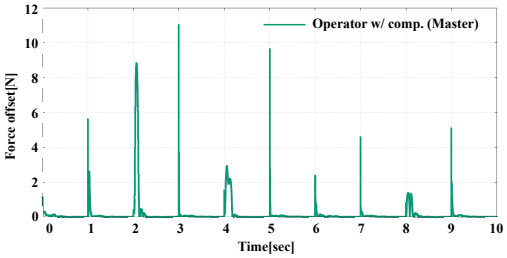

(d) Estimation of force offset

Fig. 5-14: The estimation results with the variable virtual impedance operator robot.

original motion.

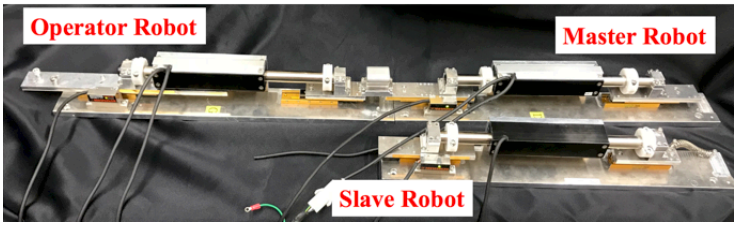

Fig. 5-15: Experimental set-up.

5.3 Experiment

The purpose of this experiment was confirming the effectiveness of proposed estimation method. The experiment was conducted as a similar condition as Section 5.2.2, and the experimental set-up is shown in Fig. 5-15. Three linear motors were utilized as the operator, the master, and the slave robots. Since the true values of operator's end-point impedance were unknown and the purpose of its experiment was showing the validity of the proposed impedance estimation method, the operator robot that impedance values could be freely set was utilized instead of the motion execution by the operators. Encoders were attached alongside the motors for obtaining the position response. The velocity and acceleration were obtained by the pseudo derivative of position information obtained by the encoders, and the external force was obtained by RFOB. The spring was attached in front of the slave robot as the environment. The experimental parameter was the same as one in the simulations.

The position and force responses are shown in Fig. 5-16. The results of impedance estimation are shown in Fig. 5-17. Although some estimation errors were confirmed, the tendency of impedance variation was properly observed. The estimation value of stiffness followed the expected value in each 1 s. The estimation performance of viscosity was sometimes poor as well as most of other impedance estimation studies show [52]. Some elements of viscosity estimation including the method for velocity obtainment, the design of extra signal, the estimation method, the calculation order of RLS, and the noise should be considered further as one of our future works.

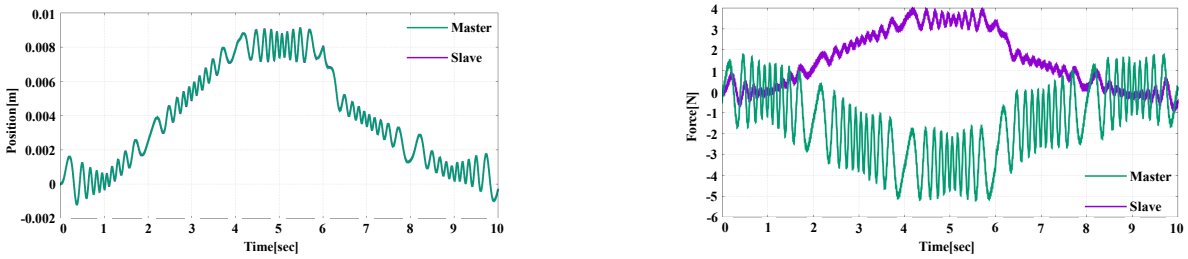

(a) Position response (b) Force response

Fig. 5-16: The responses when the operator and environmental stiffness and viscosity are $500\ \mathrm{N/m}$ and $50\ s\mathrm{N/m}$.

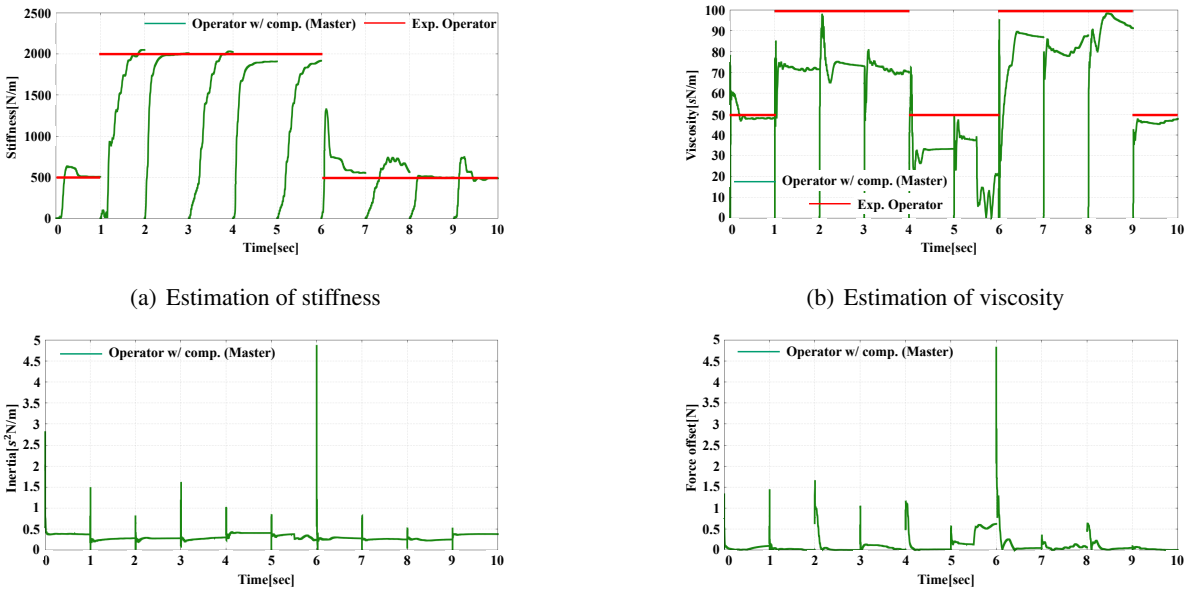

(a) Estimation of stiffness (b) Estimation of viscosity

(c) Estimation of mass (d) Estimation of force offset

Fig. 5-17: The estimation results when the operator and environmental stiffness and viscosity are $500\ \mathrm{N/m}$ and $50\ s\mathrm{N/m}$.

5.4 Summary

This dissertation proposed the end-point impedance estimation method based on bilateral control system. The operators constantly change their impedance in order to adapt to the surrounded uncertain environments and realizing the complicated tasks. Most of conventional studies, however, considered the non-contact impedance or simple tasks such as only holding the vibrated sticks due to the experimental constraint. Because this dissertation uses the bilateral controller, the operators and environmental objects can be treated at the same time. The extra signal is added to the force controller, and the original motion is estimated and removed in order to estimate the end-point impedance. The effectiveness of the proposed method was validated through the simulations and the experiment. The amplitude of extra signal should be set higher in some extent, in this time higher than 1, as simulation results show. The range of bandwidth should not be wider when the target is dynamical as the simulation results of different bandwidth show although it is not appropriate from the perspective of persistently exciting. The proposed method can be applied to various conditions regarding environmental impedance as the simulation results of different environmental impedance show. Both the stiffness and viscosity estimation performances became worse as the impedance of operators became larger from the simulation results of different operator impedance. In the experiment, the estimation performance of stiffness was confirmed even if the operator robot was moving and changing its end-point impedance. The estimation performance of viscosity was not good as the one of stiffness estimation, but the tendency of viscosity variation was observed from the experimental result. Because the extra signal degrades the performance of task execution, the estimation strategy should be designed by taking the content of task, the length of estimation period, and the expected estimation performance into consideration.

This chapter collects real motion data through bilateral control and estimates the impedances of operator and environmental objects simultaneously. The proposal helps to build the database regarding the transition of control impedance. The position or force commands can be easily designed by sensing the actual motions, however, the design policy of control impedance is still not clear. Data-driven design helps to design some parameters in motion control.

Chapter 6

Evaluation Index-based Data-driven Design

This chapter discusses an approach to evaluation index-based gain tuning for bilateral control. In Section 6.1, the transfer function of master or slave is explained. In Section 6.2, the analysis for gain setting is introduced. In Section 6.2.1, the outline of analysis is explained. In Section 6.2.2, the evaluation method of analysis is explained. In Section 6.2.3, the case when the gains between master and slave are the same is discussed. In Section 6.2.4, the case when the gains between master and slave are different is discussed. In Section 6.2.5, the frequency analysis is discussed. In Section 6.2.6, the analysis of other cases different from Sections 6.2.2 is discussed. In Section 6.3, the gain tuning method is introduced. In Section 6.3.1, the outline of gain tuning method is explained. In Section 6.3.2, the gain tuning when the gains between master and slave are the same is discussed. In Section 6.3.3, the gain tuning when the gains between master and slave are different is discussed. In Section 6.4, the experiments are introduced. In Section 6.4.1, the set-ups of experiment are explained. In Section 6.4.2, the set-ups of each approach are explained. In Section 6.4.3, the results of experiment are discussed. This chapter is summarized in Section 6.5.

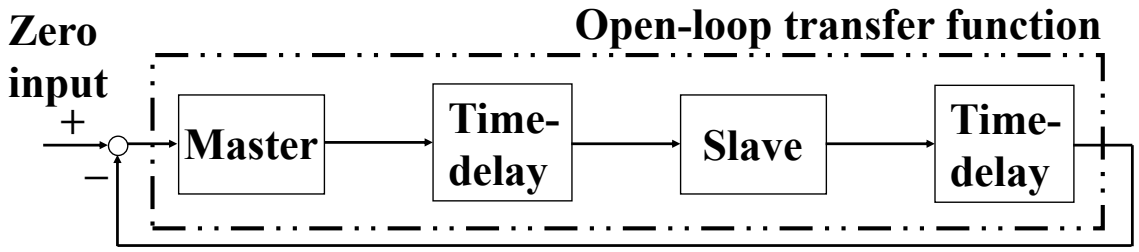

Fig. 6-1: The block diagram of entire system

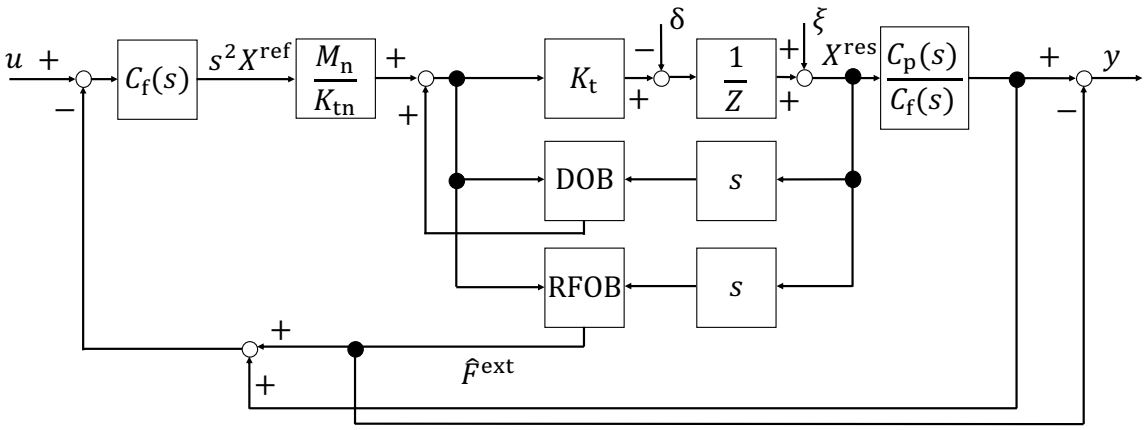

Fig. 6-2: The block diagram of master or slave

6.1 Transfer Function of Master and Slave

The outline of bilateral control was briefly discussed in Chapter 2. This section unifies position and force information [113, 114] in order to consider the master or slave as single input system. The block diagram of entire system is shown in Fig. 6-1 by considering the data flow. Since the control goals of bilateral control are 1) position tracking and 2) achievement of law of action and reaction that are described by the relationship between the master and slave regarding the position and force, the command becomes zero to the system. The open-loop transfer function is computed as the multiplication of master and slave with the time-delays due to the transmission of haptic data. This dissertation postulates that the time-delay is simply one sample.

The block diagram of master or slave described in Fig. 6-1 is shown in Fig. 6-2. A P controller is applied to the force controller and a PD or position-velocity controller is applied to the position controller

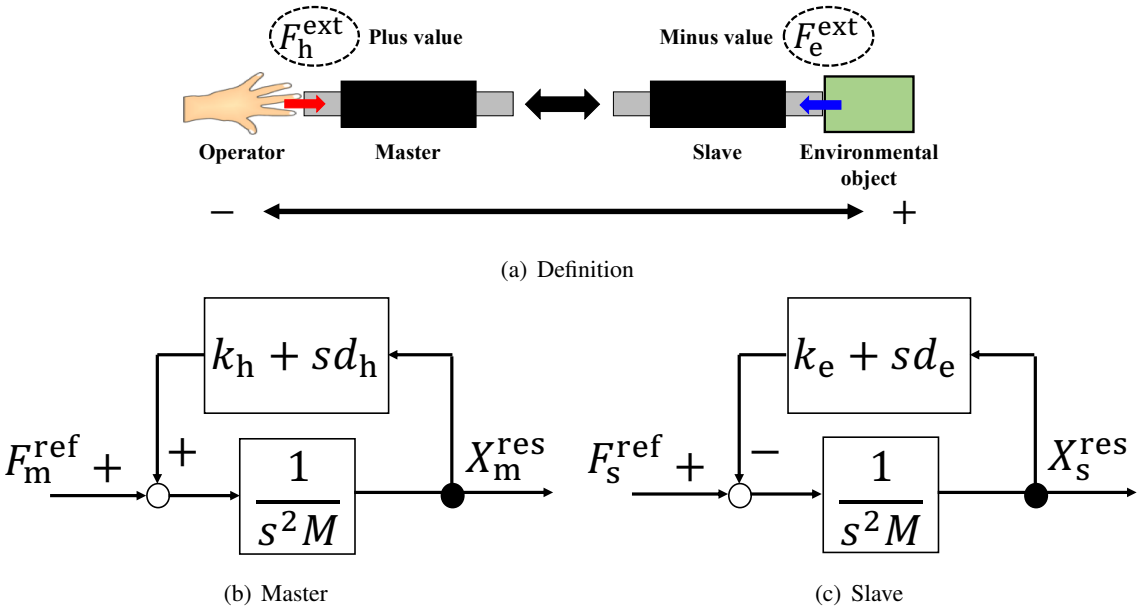

(a) Definition

(b) Master

(c) Slave

Fig. 6-3: Definition of motion direction and the block diagrams

as follows:

$$C_{\mathrm{f}}(s) = K_{\mathrm{f}}, \tag{6.1}$$

$$C_{\mathrm{p}}(s) = K_{\mathrm{p}} + sK_{\mathrm{v}}. \tag{6.2}$$

The derivative term is designed for making the system critical damping and computed as follows:

$$K_{\mathrm{v}} = 2\sqrt{K_{\mathrm{p}}}. \tag{6.3}$$

The only difference between the master and slave is the impedance term and the direction of disturbance from operator and environmental object if all parameter values are set the same between the master and slave. The definition of motion direction and the block diagrams of motors with operator and environmental object are shown in Fig. 6-3. The definition of motion direction in master and slave are the same, and the direction of forces added by the operator and environmental object are opposite. The mechanical impedance of master and slave are computed from Figs. 6-3 (b) and (c) and modeled as follows:

$$Z_{\mathrm{m}}(s) = s^2M - sd_{\mathrm{h}} - k_{\mathrm{h}}, \tag{6.4}$$

$$Z_{\mathrm{s}}(s) = s^2M + sd_{\mathrm{e}} + k_{\mathrm{e}}. \tag{6.5}$$

If DOB and RFOB ideally work by setting the cut-off frequency as infinity and all nominal values are

properly identified, the transfer function from the input to the output of Fig. 6-2 is computed as follows:

$$\begin{aligned} G_{\mathrm{sys1}}(s) &= \frac{C_{\mathrm{p}}(s) - C_{\mathrm{f}}(s)Z_{\mathrm{h/e}}(s)}{C_{\mathrm{p}}(s) + C_{\mathrm{f}}(s)Z_{\mathrm{h/e}}(s)} \\ &= \frac{G_1(s) - 1}{G_1(s) + 1}, \\ G_1(s) &= \frac{C_{\mathrm{p}}(s)}{C_{\mathrm{f}}(s)Z_{\mathrm{h/e}}(s)}, \end{aligned} \tag{6.6}$$

where $\bigcirc_{\mathrm{h/e}}$ specifies that the operator/environmental values are utilized in the master/slave. Eq. (6.6) shows the reflection coefficient of two port-circuit, and it is often utilized for the discussion of passivity-based approach [115].

The transfer function of master/slave system is recomputed as follows if the cut-off frequencies of observers are not infinity and the nominal values are not identified properly:

$$\begin{aligned} G_{\mathrm{sys2}}(s) &= \frac{G_2(s)}{G_3(s)}, \\ G_2(s) &= \frac{K_{\mathrm{t}}}{K_{\mathrm{tn}}}C_{\mathrm{p}}(s)M_{\mathrm{n}} - \frac{K_{\mathrm{t}}}{K_{\mathrm{tn}}}C_{\mathrm{f}}(s)G_{\mathrm{r}}(s)M_{\mathrm{n}}Z(s) \\ &+ \{1 - G_{\mathrm{r}}(s)\}\frac{K_{\mathrm{t}}}{K_{\mathrm{tn}}}C_{\mathrm{f}}(s){M_{\mathrm{n}}}^2 s, \\ G_3(s) &= \{1 - G_{\mathrm{d}}(s)\}\{Z + K_{\mathrm{t}}M_{\mathrm{n}}s\} + \frac{K_{\mathrm{t}}}{K_{\mathrm{tn}}}C_{\mathrm{p}}(s)M_{\mathrm{n}} \\ &+ C_{\mathrm{f}}(s)G_{\mathrm{r}}(s)M_{\mathrm{n}}Z(s) - \{1 - G_{\mathrm{r}}(s)\}\frac{K_{\mathrm{t}}}{K_{\mathrm{tn}}}C_{\mathrm{f}}(s){M_{\mathrm{n}}}^2 s. \end{aligned} \tag{6.7}$$

The transfer function of closed-loop system shown in Fig. 6-1 is computed as follows:

$$\begin{aligned} G_{\mathrm{sys3}}(s) &= \frac{L(s)}{1 + L(s)}, \\ L(s) &= G_{\mathrm{sys2,m}}(s)G_{\mathrm{sys2,s}}(s)e^{-2Ts}. \end{aligned} \tag{6.8}$$

The time-delay for the communication is considered as one sample in this dissertation.

6.2 Analysis for Gain Setting

6.2.1 Outline

This section aims at discussing the strategy of gain setting for bilateral control. Many analytical or numerical gain tuning methods have been studied. However, this dissertation makes clear the gain tuning through the evaluation index-based approach by using the experimental data. It is because the modeling of contact motion and precise identification of some nonlinear terms such as noise, saturation, friction, and so forth are sometimes highly difficult. The gains of position/velocity and force of master and slave are evaluated by the actual experiment in two cases: 1) same gains between master and slave and 2) different gains between master and slave, although the gains of master and slave tend to be set the same. The obtained knowledge of gain tuning is also analyzed through frequency analysis.

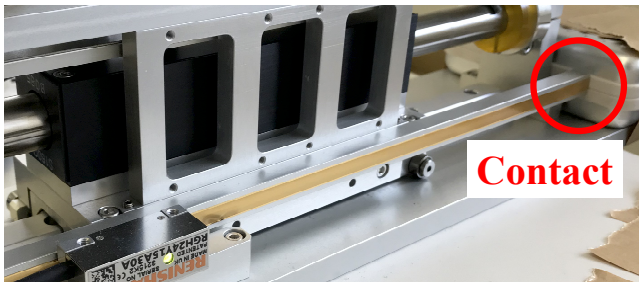

Fig. 6-4: Picture of experimental set-up (slave side)

6.2.2 Evaluation

The control goals of bilateral control include both the position and force components, and both of them are needed to be incremented into the evaluation index in order to reduce both errors.

A cost function is designed based on the equivalent energy as follows:

$$J = \sqrt{\sum_{i=1}^{S} \frac{(X_{\mathrm{m},i}^{\mathrm{res}} - X_{\mathrm{s},i}^{\mathrm{res}})^2}{S}} \sqrt{\sum_{i=1}^{S} \frac{(\hat{F}_{\mathrm{m},i}^{\mathrm{ext}} + \hat{F}_{\mathrm{s},i}^{\mathrm{ext}})^2}{S}}. \tag{6.9}$$

Its objective is to minimize the cost function, which is also used in other haptic research [116].

$\sqrt{\sum_{i=1}^{S} \frac{(X_{\mathrm{m},i}^{\mathrm{res}} - X_{\mathrm{s},i}^{\mathrm{res}})^2}{S}}$ shows a Root Mean Square Error (RMSE) of position tracking, while $\sqrt{\sum_{i=1}^{S} \frac{(\hat{F}_{\mathrm{m},i}^{\mathrm{ext}} + \hat{F}_{\mathrm{s},i}^{\mathrm{ext}})^2}{S}}$ shows a RMSE of force feed-back. The weights of both the position and force components can be treated equivalently in this cost function.

This dissertation considers the contact motion to a screw box, which surface is made by plastic. The slave side of experimental set-up is shown in Fig. 6-4 [117]. A linear motor was utilized in both the master and slave sides. Position responses were obtained by encoders, and the velocity responses were computed by the pseudo derivative of measured position responses. The stick attached to the slave contacted the screw box. Because the linear motor is horizontally set, the effect of gravity and coriolis force are assumed to be negligibly small. Viscous friction is identified in advance and removed from the disturbance in the feed-forward manner. Therefore, the components of disturbance except external force are removed, and only external force can be estimated by RFOB.

The same disturbance is added to the master in each trial for identifying the appropriate combination of gains. The position and force responses of trial motion with one gain setting ($K_{\mathrm{v}} = 100\ s, K_{\mathrm{f}} = 10\ \mathrm{kg}^{-1}$) is shown in Fig. 6-5. This motion is designed from the actual manipulation conducted by the operator, and it contains the slow/quick and free/contact motions. Parameter settings of an actual

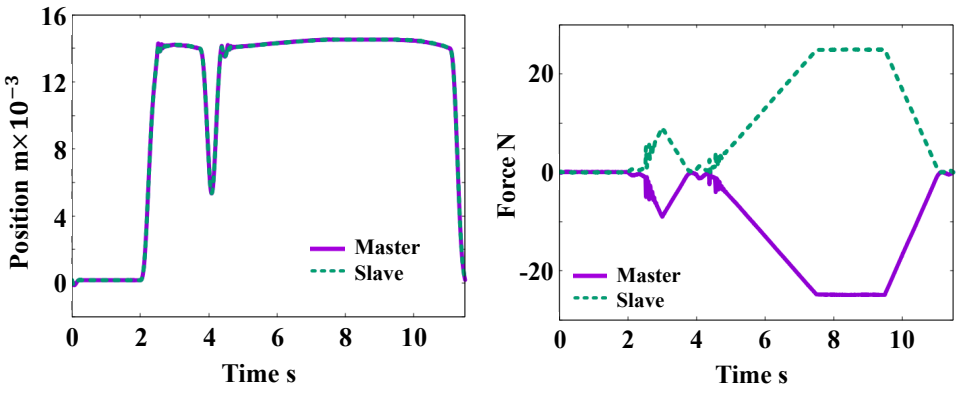

(a) Position (b) Force

Fig. 6-5: Position and force responses of trial motion

Table 6.1: Parameter settings of an actual experimental set-up

Description	Value
Nominal masses of master and slave	2.1 kg
Cut-off frequencies of DOB and RFOB	500 rad/s
Stiffness of operator	2000 N/m
Viscosity of operator	20 sN/m
Stiffness of environmental object	29800 N/m
Viscosity of environmental object	29.8 sN/m
Sampling time	0.1 ms

experimental set-up are summarized in Table 6.1. The stiffness of environmental object was measured in advance, while the stiffness of operator was designed from the literature [80, 118].

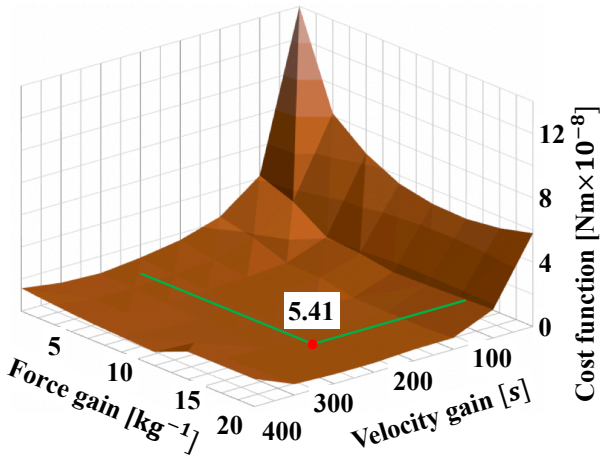

Fig. 6-6: Results of experimental analysis for the same gain case

6.2.3 Same Gains Between Master and Slave

This subsection considers a case when the velocity and force gains between the master and slave are set the same. The grid search was carried out in order to grasp the tendency of cost function versus gain setting. The force gain was changed from 2.5 kg^{-1} to 25 kg^{-1} in each 2.5 kg^{-1} (10 gain cases), while the velocity gain was changed from 50 s to 500 s in each 50 s (10 gain cases). The position gain was designed based on Eq. (6.3). Therefore, 100 different gain settings (10×10) were experimentally analyzed. The result of experimental analysis is shown in Fig. 6-6. As the velocity or force gain became higher, the cost function basically became smaller. The cost function gradually became larger by increasing the velocity and force gains if they were higher than 250 s and 15 kg^{-1}, respectively. The system vibrated due to the effect of noise or quantization error when the velocity and force gains became higher than 400 s and 20 kg^{-1}. These values can be considered as limit sensitivities. The smallest cost function value was 5.41×10^{-8} Nm, and it was achieved when the velocity and force gains were 250 s and 15 kg^{-1}. The shape of cost function in Fig. 6-6 is almost a convex function, but some areas have unevenness shape. The enhancement of velocity control performance and the enhancement of force control performance are often considered to have trade-off relationship from the perspective of velocity and force or reproducibility and operationality [86, 119], but the improvement effect of cost function can be dominant rather than the deterioration effect of cost function. Therefore, the velocity and force gains should be basically increased. Since the shape of cost function is almost convex, the effects of velocity and force gains may not be deeply interfered each other and enable them to increase independently.

Table 6.2: Results of experimental analyses for the different gain case

Velocity gain of master s	Force gain of master kg^{-1}	Velocity gain of slave s	Force gain of slave kg^{-1}	RMSE of position tracking $\mathrm{m} \times 10^{-6}$	RMSE of force feed-back $\mathrm{N} \times 10^{-3}$	Cost function $\mathrm{Nm} \times 10^{-8}$	Remark
250	15	250	15	4.95	10.93	5.41	The best performance in Section 6.2.3
300	5	150 - 300	25 - 30	5.01 - 5.38	8.08 - 8.48	4.27 - 4.47	
250	10 - 15	300	25	4.65 - 4.93	9.19 - 9.38	4.37 - 4.43	
300	10	50 - 250	25	4.94 - 5.35	8.46 - 9.19	4.26 - 4.41	
300	15	150 - 200	25	4.69 - 4.93	9.12 - 9.27	4.34 - 4.50	
300	10	200	25	4.94	8.62	4.26	The best performance among all trials.

6.2.4 Different Gains Between Master and Slave

The impedances of operator and environmental object are not necessarily the same because the operators adjust their motions by changing not only impedance but also the equilibrium point. Hence, the transfer functions of master and slave are better to be set differently, and the velocity and force gains of master and slave should not be the same in some cases. The grid search was also carried out in order to grasp the tendency of cost function versus gain setting. The force gain was changed from 5 kg^{-1} to 30 kg^{-1} in each 5 kg^{-1} (6 gain cases), while the velocity gain was changed from 50 s to 400 s in each 50 s (8 gain cases). Therefore, 2304 different gain settings (6×6×8×8) were experimentally analyzed. Since the visualization of its result is tough because of the high dimensionality, some gain settings, which cost function was smaller than 4.5×10^{-8} Nm, are summarized in Table 6.2. The velocity gain of master should be set as high as possible, while the force gain of master should not be set high as well as the one of slave. Therefore, the enhancement of velocity control performance is necessary for the master. The velocity gain of slave should be set relatively high, while the force gain should be selected as high as possible. Therefore, the enhancement of force control performance is necessary for the slave. There were no combination of gains that overwhelmed both RMSEs of position tracking and force-feedback simultaneously, and the tuning should be carried out by considering the balance of them. The costs based on another functions: Eq. (6.9) with the normalized position and force values, the continuous energy ($\frac{1}{S}\sum\left\{\sqrt{(X_{\mathrm{m}}^{\mathrm{res}}-X_{\mathrm{s}}^{\mathrm{res}})^2}\sqrt{(\hat{F}_{\mathrm{m}}^{\mathrm{ext}}+\hat{F}_{\mathrm{s}}^{\mathrm{ext}})^2}\right\}$), and the continuous energy with the normalized position and force values were also computed. The obtained knowledge: 1) the velocity gain of master should be set as high as possible and 2) the force gain of slave should be set as high as possible, are same with

Eq. (6.9) in this analytical setting although the amount of cost function and the combination of gains when the system achieves the smallest cost function are slightly different. The system vibrated when the velocity or force gain was high enough. In addition to that, the system vibrated when the velocity and force gains in the master were high, while the force gain of slave was comparatively small. This implies that the order of gain tuning has to be deeply considered.

To recapitulate, the obtained knowledge through evaluation index-based gain tuning are 1) the velocity gain of master should be set as high as possible under the condition where the force gain of slave is set high and 2) the force gain of slave should be set high as possible.

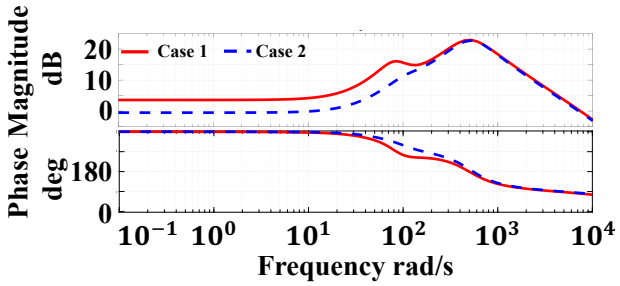

Fig. 6-7: Bode diagram of Cases 1 and 2

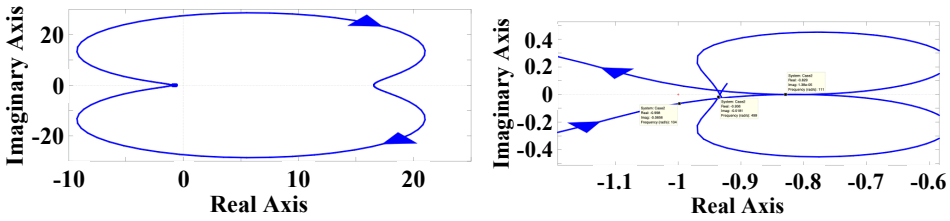

(a) Entire view (b) Enlarged view

Fig. 6-8: Nyquist plot of Case 2

6.2.5 Frequency Analysis

The Bode diagrams are drawn in order to investigate the characteristics of system. Two different gain settings are compared, and they are summarized in Table 6.3. Cases 1 and 2 are obtained results of gain settings from Sections 6.2.3 and 6.2.4. The Bode diagrams of the entire loop G_{sys3} are depicted, and its results are shown in Fig. 6-7. The magnitude of Case 2 does not become completely 0 dB but closer to 0 dB than the one of Case 1 in the low frequency, which explains that the control goals are achieved more precisely. The balance between the velocity and force gains affects its performance, and the gains of master and slave should be set differently.

The stability of Case 2 was investigated by drawing nyquist plot as shown in Fig. 6-8. The line passes through (Re, Im)=(-0.998, -0.0656) at 104 rad/s, (Re, Im)=(-0.829, 1.38e-05) at 111 rad/s, and (Re, Im)=(-0.938, -0.0181) at 499 rad/s. Therefore, the gain could be set approximately 1.2 times larger till the system reached at the stability limit. The reciprocal from nyquist plot at 499 rad/s to (Re, Im)=(-1, 0) in real axis was approximately 1.07. The system can be said stable although the amount of stability margin was not large.

The stability of system is guaranteed by checking the stability after updating gains in the flowchart.

The flowchart can be flexibly designed if there exists a required stability margin.

Table 6.3: Ideal gain setting for the contact to screw box

	$K_{\mathrm{v,m}}\ s$	$K_{\mathrm{f,m}}\ \mathrm{kg}^{-1}$	$K_{\mathrm{v,s}}\ s$	$K_{\mathrm{f,s}}\ \mathrm{kg}^{-1}$
Case 1	250	15	250	15
Case 2	300	10	200	25

Table 6.4: Ideal gain setting for the contact to sponge

	$K_{\mathrm{v,m}}\ s$	$K_{\mathrm{f,m}}\ \mathrm{kg}^{-1}$	$K_{\mathrm{v,s}}\ s$	$K_{\mathrm{f,s}}\ \mathrm{kg}^{-1}$
Case 3	200	15	200	15
Case 4	300	10	150	15

6.2.6 Other Cases

This subsection discusses two other cases: 1) different environmental object and 2) different manipulated motion. The grid search was also carried out in order to analyze the effects of the different impedance of environmental object and manipulated motion.

Different environmental object

This dissertation considers the case when the impedance of environmental object is smaller than the one in Table 6.1. The sponge was placed in front of the slave motor instead of the screw box. Its stiffness is measured as $1630\ \mathrm{N/m}$, and the viscosity is set as $16.3\ s\mathrm{N/m}$. The grid search was carried out for both the same gain and different gain cases as well as Sections 6.2.3 and 6.2.4. The obtained ideal gain settings are summarized in Table 6.4. Case 3 shows the ideal gain setting for the case of same gain, while Case 4 shows the ideal gain setting for the case with different gain.

The velocity gain of slave should be set smaller when the impedance of environmental object is smaller from the results of Cases 1 and 3. The amounts of velocity and force gains in the slave side should be set smaller as the impedance of environmental object becomes smaller from the results of Cases 2 and 4. At the same time, the amounts of velocity and force gains in the slave side should be set smaller as the impedance of environmental object becomes smaller. The Bode diagrams are drawn in order to investigate the characteristics of system and shown in Fig. 6-9. The magnitude of Case 4 does not become completely 0 dB but closer to 0 dB than the one in Case 3. Moreover, the resonance and anti-resonance are observed at around 10–30 rad/s in Case 3. The velocity and force gains should be finely adjusted when considering the contact motion to soft objects.

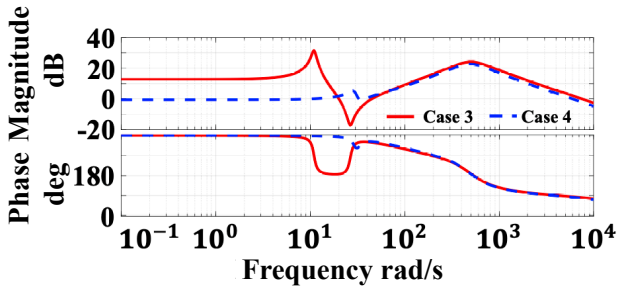

Fig. 6-9: Bode diagram of Cases 3 and 4

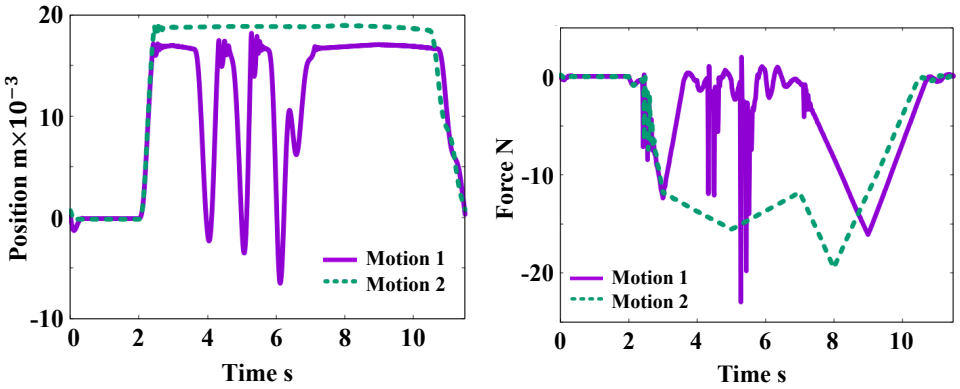

(a) Position (b) Force

Fig. 6-10: Position and force responses of other manipulated motions

Different manipulated motion

This dissertation considers the case of two different manipulated motion as shown in Fig. 6-10. Motion 1 is composed more for the transient contacts rather than the original motion discussed in Section 6.2.2. The motor quickly contacted the screw box, and it soon left from the box. Motion 2 is composed more for stable contacts. The motor changed the applied force while keeping the contact state. The results of ideal gain setting are summarized in Table 6.5. The force gain in the slave side can be slightly smaller in Motion 1. This might be because of avoiding the overshoot of force response. The velocity gain in the slave side should be set larger as the length of contact state became longer from the result of Motion 2. It is noted that the gain tuning is the same as one of original motion. The velocity gain in the master side should be set as large as possible, and the force gain in the slave side should also be set relatively large. Therefore, the ideal gain setting is affected by the manipulated motion, but the basic gain tuning

Table 6.5: Ideal gain setting for different manipulated motions

	$K_{\mathrm{v,m}}\ s$	$K_{\mathrm{f,m}}\ \mathrm{kg}^{-1}$	$K_{\mathrm{v,s}}\ s$	$K_{\mathrm{f,s}}\ \mathrm{kg}^{-1}$
Motion 1	300	10	200	20
Motion 2	300	10	250	20

do not change much. The fine tuning can be made if the outline of target manipulated motion is known in advance.

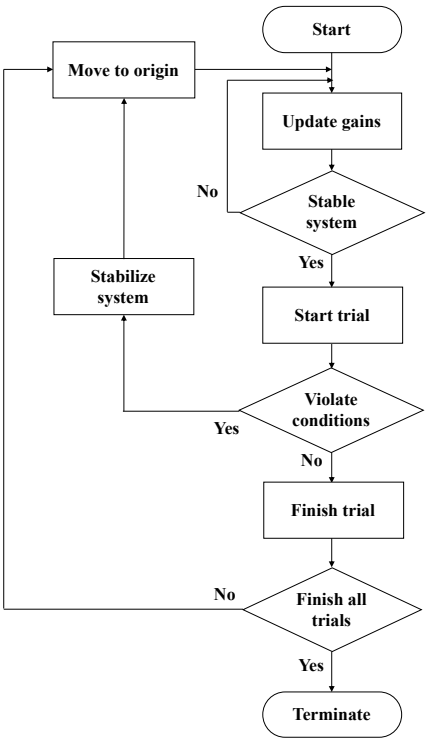

Fig. 6-11: Flowchart of gain tuning through experiments

6.3 Gain Tuning Based on Gradient Descent

6.3.1 Outline

The evaluation index-based gain tuning for bilateral control has been experimentally and analytically discussed in Section 6.2. However, the gain tuning is necessarily for each experimental set-ups or task with the limited number of trials in practice. Therefore, the gradient-descent based gain tuning of bilateral control through the experiments is discussed by taking the obtained knowledge of gain tuning into consideration. Two cases: 1) same gains and 2) different gains between the master and slave are considered differently.

The flowchart of gain tuning through the experiments is shown in Fig. 6-11. The gains are updated before starting each trial. Once the gains are updated, the stability of system with updated gains is analyzed. If the system is analyzed as stable, the trial is started. Otherwise, the algorithm updates the gains. The flowchart can be flexibly designed if there exists a required stability margin. If the motion violates the predetermined conditions during the trial, the motors are shifted to the stabilizing mode and move to the original position. Otherwise, the motion is performed till the end of trial. The motors move

to the original position after each trial, and then the gain is updated. This cycle is continuously conducted until all trials are completed. Due to the predetermined conditions, it enables to avoid a risk of breaking down the experimental set-up and automatically carry out all trials. Since the cost is not the convex function, in particular the case when the gains of master and slave are different, the order of gain tuning has to be taken into consideration. At the same time, the number of gain update is limited because it is experiment-based and takes long time, unlike the simulation. Therefore, the number of each experiment has to be also considered.

Algorithm 2 Velocity-force approach

1: **while** $c < N$ **do**
2: **if** $c < n$ **then**
3: $K_{\mathrm{v}} \leftarrow K_{\mathrm{v}} - (1 - \frac{c}{n})\alpha \frac{\partial J}{\partial K_{\mathrm{v}}}$
4: **end if**
5: **if** $c >= n$ **then**
6: $K_{\mathrm{f}} \leftarrow K_{\mathrm{f}} - (1 - \frac{c-n}{N-n})\beta \frac{\partial J}{\partial K_{\mathrm{f}}}$
7: **end if**
8: Perform trial
9: **if** Condition==False **then**
10: Stabilize System
11: **if** $c < n$ **then**
12: $K_{\mathrm{v}} \leftarrow \omega K_{\mathrm{v,min}} + (1 - \omega) K_{\mathrm{v,min}} \frac{c}{n}$
13: **end if**
14: **if** $c >= n$ **then**
15: $K_{\mathrm{f}} \leftarrow \omega K_{\mathrm{f,min}} + (1 - \omega) K_{\mathrm{f,min}} \frac{c-n}{N-n}$
16: **end if**
17: **end if**
18: Store the smallest cost function and its gain combinations as J_{min}, $K_{\mathrm{v,min}}$, and $K_{\mathrm{f,min}}$
19: $c \leftarrow c + 1$
20: **end while**

6.3.2 Same Gains Between Master and Slave

The velocity and force gains between master and slave are set the same and tuned. Although the gains of master and slave should be different based on the results of grid search in Section 6.2.4, the tuning for same gains is simple and sometimes practical because of fewer designing parameters rather than the case of different gains.

Three approaches are considered from the perspective of tuning order: 1) velocity-force, 2) force-velocity, and 3) mixed. In velocity-force approach, the velocity gain is tuned at first, and then the force gain is tuned. In the force-velocity approach, the force gain is tuned at first, and then the velocity gain is tuned. In the mixed approach, both the velocity and force gains are tuned simultaneously.

The algorithm of velocity-force approach is shown in Alg. 2. The algorithm is based on gradient descent [120]. Other gradient-based approaches such as Newton's method, quasi-Newton method, or Levenberg-Marquardt method can be implemented into Lines 3 and 6 in Alg. 2, but the main focus is not the selection of approach but the composition of algorithm. The amount of gain update is gradually

decreased as the number of trials is increased as Lines 3 and 6 of Alg. 2 show. The velocity or force gain is designed based on its best value in the history when the system violates conditions, but its amount is reduced by the learning rate as Lines 12 and 15 of Alg. 2 show. The process of Line 9 is considered when the system is judged as unstable at the decision block in flowchart or violates the predetermined condition.

Its algorithm can be utilized for force-velocity approach if the signs of inequality and the variables: $\frac{c}{n}$ and $\frac{c-n}{N-n}$ are opposite. In addition, its algorithm can be utilized for mixed approach if all inequalities are removed and the variable becomes $\frac{c}{N}$ instead of $\frac{c}{n}$ and $\frac{c-n}{N-n}$.

6.3.3 Different Gains Between Master and Slave

The velocity and force gains between master and slave are set different and tuned in this case. Alg. 2 is mainly applicable for case where the number of tuning parameters is few because both the order and number of tuning are needed to be designed. Hence, it becomes much more troublesome to utilize the algorithm as the number of tuning parameters is increased. Therefore, Alg. 3 is applied for the case of different gains as follows. $K_{\mathrm{v,m}}$, $K_{\mathrm{f,m}}$, $K_{\mathrm{v,s}}$, and $K_{\mathrm{f,s}}$ are substituted into $K_{\bigcirc}$ in Lines 3, 11, and 25 of Alg. 2 if $r \bmod 4$ is 0, 1, 2, and 3, respectively. The velocity and force gains of master and slave are tuned several times in turn, and it is managed by the coefficient r. Once one gain tuning is completed, r is increased by 1 as shown in Lines 14 or 20 of Alg. 3 show. The tuning gain is selected by the division remainder of r. Each gain is updated as long as the cost function J becomes smaller than the smallest cost function so far. However, each gain is updated at least 2 times as conditional sentences in Lines 9 or 19 of Alg. 3 show because the gains should be updated to both positive and negative directions. The number of each gain tuning is not needed to be designed, but the order of gain tuning may affect the result. The process of Line 7 is considered when the system is judged as unstable at the decision block in flowchart or violates the predetermined condition.

The algorithms are based on gradient descent and may encounter local optimum because the evaluation index is not a convex function obtained from limited trials of experiments. The guarantee for global optimum is not necessarily essential since the number of trials is limited. If the global optimum value must be obtained at any cost, other algorithms such as Bayesian optimization should be applied with a larger number of trials [121].

Algorithm 3 Approach for different gains

while $c < N$ **do**
  if $r \bmod 4 == 0, 1, 2, 3$ **then**
    $K_{\bigcirc} \leftarrow K_{\bigcirc} - (1 - \frac{c}{N})\alpha \frac{\partial J}{\partial K_{\bigcirc}}$
  end if
  Perform trial
  Compute J
  if Condition==False **then**
    Stabilize System
    if $t <= 2$ **then**
      if $r \bmod 4 == 0, 1, 2, 3$ **then**
        $K_{\bigcirc} \leftarrow K_{\bigcirc,\min}\{\omega + (1 - \omega)\frac{c}{N}\}$
      end if
    else
      $r \leftarrow r + 1$
      $t \leftarrow 0$
      $J_{\min} \leftarrow \infty$
    end if
  end if
  if $(t > 2) \cdot (J_{\min} < J)$ **then**
    $r \leftarrow r + 1$
    $t \leftarrow 0$
    $J_{\min} \leftarrow \infty$
  end if
  if $J_{\mathrm{str}} > J$ **then**
    $K_{\bigcirc,\min} \leftarrow K_{\bigcirc}$
  end if
  $t \leftarrow t + 1$
  $J_{\min} \leftarrow J$
  $c \leftarrow c + 1$
end while

6.4 Experiments

6.4.1 Experimental Set-Ups

The purpose of experiments is to investigate the effectiveness of each gain tuning approach and to see the transition of cost function. The gains were updated fifty times in each method. Since each trial took approximately 12 seconds as shown in Fig. 6-5, it took 10 minutes per each approach in total. Some conditions are needed in order to avoid a risk of breaking down the experimental set-up, and the predetermined conditions are designed as follows:

- The absolute value of estimated external force should be smaller than 0.1 N between 0 to 2 seconds (stay at the origin).
- The absolute value of velocity should be smaller than 0.05 m/s all the time.
- The absolute value of estimated external force should be smaller than 30 N all the time.

Each value was roughly designed based on Fig. 6-5.

Table 6.6: Parameters for algorithms

Description	Value
Initial K_{v}	100 s
Initial K_{f}	10 kg^{-1}
Initial $\frac{\partial J}{\partial K_{\mathrm{v}}}$	- $\frac{N-c}{N}$
Initial $\frac{\partial J}{\partial K_{\mathrm{f}}}$	- $\frac{N-c}{N}$
α	100 s
β	10 kg^{-1}
ω	0.95

6.4.2 Set-Ups of Each Approach

Operator-based approach

The velocity and force gains of master and slave were tuned by an operator. The operator has experience of haptics research over 10 years and has no prior experience to perform gain tuning studies. The operator tuned the gains, and the evaluation was carried out in each trial. After each trial, the calculation result of cost function was provided to the operator and recorded at a result sheet, which the operator was able to check during experiment. The operator updated the gains after checking the result of cost function without having any time limitations.

Same gains between master and slave

The number of trials in velocity-force and force-velocity were designed. The number of velocity gain updates n in Alg. 2 was gradually increased from 3 to 48 in each 3. The velocity and force gains were updated n and $N - n$ times, respectively. The parameters utilized in Alg. 2 is summarized in Table 6.6. The relatively smaller values were arbitrarily chosen for the initial gains and amounts of gain updating. These values can be properly chosen if the operator knows the range of ideal gain values: however, this dissertation assumes that there is no prior knowledge.

The result of designing n is shown in Fig. 6-12. vel-for and for-vel stand for velocity-force and force-velocity. The horizontal axis represents the trial number when the switching of gain tuning occurred. For instance, the velocity gain was updated 20 times when the horizontal axis was 20 and vel-for was considered. The force gain was updated 30 times in this example. The cost function was gradually decreased as the number of velocity gain updates was increased in both vel-for and for-vel. Moreover, the velocity gain should be tuned before tuning the force gain since the cost function of vel-for was smaller than for-vel even if the number of velocity or force gain updates were the same. The velocity

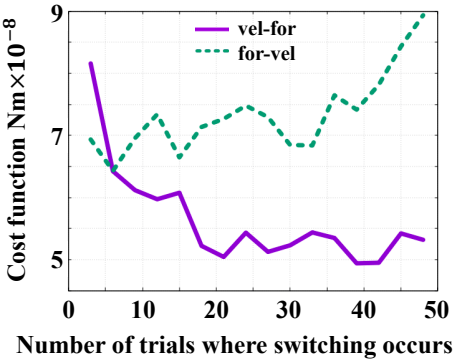

Fig. 6-12: The result of designing n

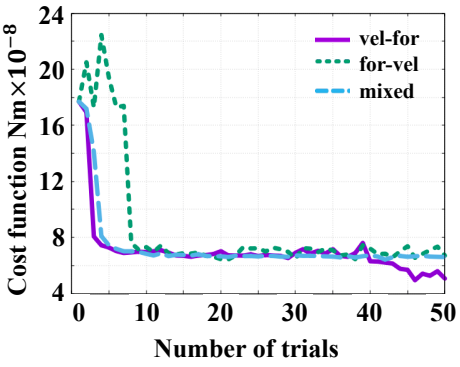

Fig. 6-13: The transition result of cost function in the same gain approaches

gains can be increased even if the force gains are not set the high, while on the other hand, the force gains cannot be increased if the velocity gains are not sufficiently high. The transition results of cost function in the same gain approaches: vel-for, for-vel, and mixed, are shown in Fig. 6-13. $n = 39$ and $n = 6$ in Fig. 6-12 are utilized as the results of vel-for and for-vel, which were the best results of them. vel-for and mixed approaches showed similar behaviors from one to eight trials. This implies that mixed approach updated the gains mainly based on velocity component in these trials. The cost function of for-vel also decreased at the sixth trial when the switching occurred. Both for-vel and mixed approaches oscillated at the similar cost function value after ten trials due to the learning rate although there was partial vibration in the system. The cost function of vel-for approach was decreased after forty trials when the switching occurred. Since the shape of cost in Fig. 6-6 is not convex function, the order of gain tuning affects the performance. The smallest cost function of vel-for was 4.84×10^{-8} Nm, which is smaller than the one in Fig. 6-6. The fine tuning may improve performance and can achieve smaller cost function.

Table 6.7: Patterns

Pattern	Gains
A	$K_{\mathrm{v,m}} \rightarrow K_{\mathrm{f,m}} \rightarrow K_{\mathrm{f,s}} \rightarrow K_{\mathrm{v,s}}$
B	$K_{\mathrm{v,m}} \rightarrow K_{\mathrm{f,m}} \rightarrow K_{\mathrm{v,s}} \rightarrow K_{\mathrm{f,s}}$
C	$K_{\mathrm{v,m}} \rightarrow K_{\mathrm{f,s}} \rightarrow K_{\mathrm{f,m}} \rightarrow K_{\mathrm{v,s}}$
D	$K_{\mathrm{v,m}} \rightarrow K_{\mathrm{f,s}} \rightarrow K_{\mathrm{v,s}} \rightarrow K_{\mathrm{f,m}}$
E	$K_{\mathrm{v,m}} \rightarrow K_{\mathrm{v,s}} \rightarrow K_{\mathrm{f,m}} \rightarrow K_{\mathrm{f,s}}$
F	$K_{\mathrm{v,m}} \rightarrow K_{\mathrm{v,s}} \rightarrow K_{\mathrm{f,s}} \rightarrow K_{\mathrm{f,m}}$

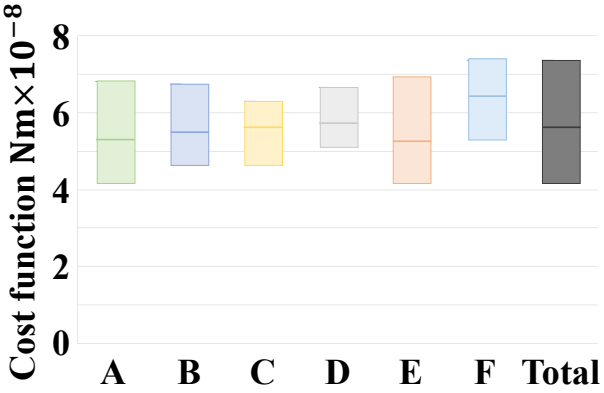

Fig. 6-14: Results of pattern comparison

Different gains between master and slave

There are 24 (=4!) combinations regarding the order of gain tuning, and its order is designed for Alg. 3. These combinations were classified into six patterns as shown in Table 6.7, and each pattern has four orders. The results of pattern comparison are shown in Fig. 6-14. The colored box whiskers show the minimum, the mean, and the maximum values in each pattern. The rightmost box shows the total result of patterns A–F. Patterns A and E achieved the smaller cost function when $K_{\mathrm{v,m}} \rightarrow K_{\mathrm{f,m}} \rightarrow K_{\mathrm{f,s}} \rightarrow K_{\mathrm{v,s}}$ and $K_{\mathrm{v,m}} \rightarrow K_{\mathrm{v,s}} \rightarrow K_{\mathrm{f,m}} \rightarrow K_{\mathrm{f,s}}$ were applied, and each cost function was 4.19×10^{-8} Nm and 4.18×10^{-8} Nm. Moreover, the average values of these two patterns were smaller than other patterns. Pattern F of $K_{\mathrm{v,s}} \rightarrow K_{\mathrm{f,s}} \rightarrow K_{\mathrm{f,m}} \rightarrow K_{\mathrm{v,m}}$ achieved the largest cost function among others, and its value was 7.37×10^{-8} Nm. Even in the worst case, the algorithm enables to reduce the cost function properly. It was inferred to tune the velocity gain of master as many times as possible rather than other gains. The final result is changed based on the order of gain tuning, but Alg. 3 enables to tune gains even if the number of trials was only fifty.

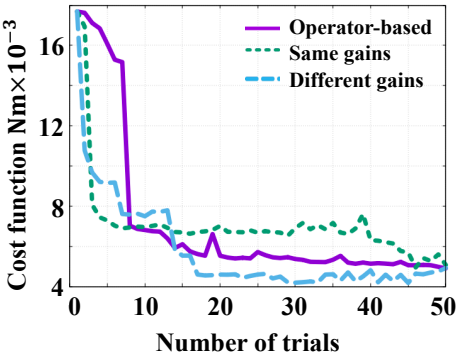

Fig. 6-15: Transition results of three approaches

6.4.3 Results

The transition results of cost function in three approaches: operator-based approach, vel-for for the same gains (one in Fig. 6-13), and $K_{\mathrm{v,m}} \rightarrow K_{\mathrm{v,s}} \rightarrow K_{\mathrm{f,m}} \rightarrow K_{\mathrm{f,s}}$ for the different gains, are summarized in Fig. 6-15. The cost functions of same gain and different gain approaches decreased in the first five trials, and the cost function of operator-based approach was also dramatically decreased once the velocity gain was highly increased. The cost function of operator-based approach kept on decreasing, but the operator has struggled for tuning gains. The cost function of different gains achieved the smallest value among others. It took approximately ten minutes to complete the tuning in the case the same gain and different gain approaches were applied, while on the other hand, it took about an hour to complete the fifty trials in the case of operator-based approach.

The transitions of velocity and force gains in each approach is shown in Fig. 6-16. The operator carefully tuned the velocity gain at first, and the other two approaches also tuned the velocity gain at first. The operator started tuning the force gains from the tenth trial, and the operator started separately tuning the gains of master and slave from twenty-eighth trials. The gains of same gain approach seem not converging at the ideal values. The inclinations of gain update highly depend on the parameter setting of α or β, and they should be higher for achieving the ideal value by the fewer trials in this case. However, the ideal values are not known in most of cases, and α and β should be set small.

The ideal gain setting in each approach is summarized in Table 6.8. The final results of operator-based approach were close to the one of same gain approach. The gain setting for different gain approach was closer to the gain setting for Case 2 in Table 6.4. The velocity gain of master and force gain of slave should be set relatively high in this dissertation.

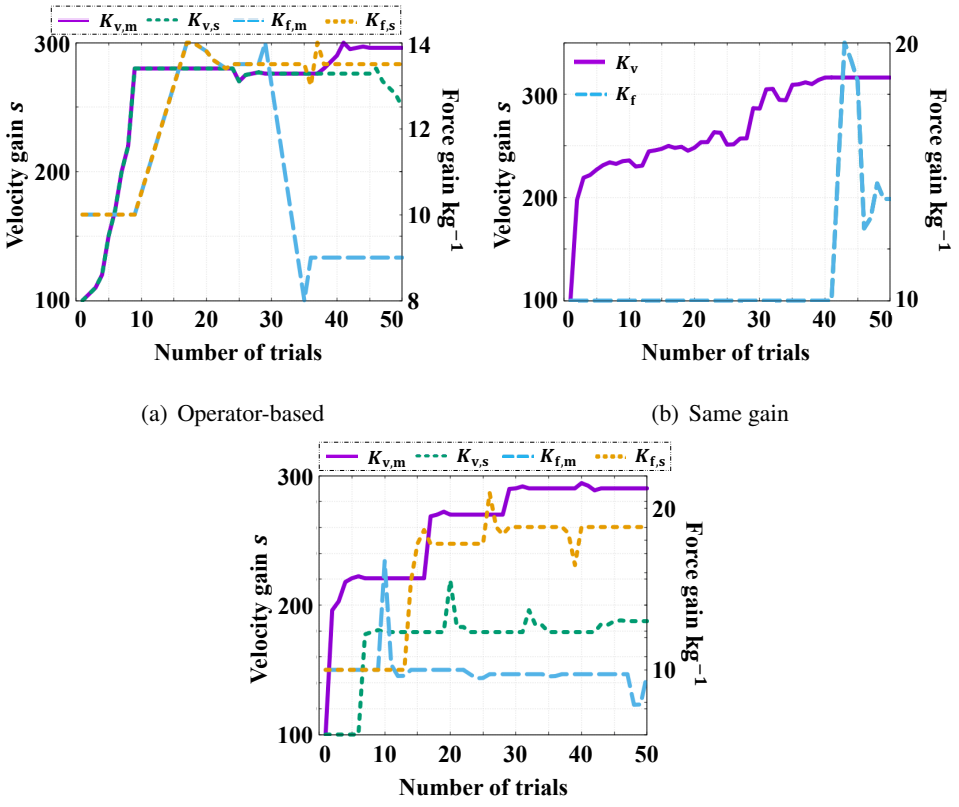

(a) Operator-based

(b) Same gain

(c) Different gain

Fig. 6-16: Transitions of each gain

Table 6.8: Ideal gain setting in each approach

	$K_{v,m}$ s	$K_{f,m}$ kg^{-1}	$K_{v,s}$ s	$K_{f,s}$ kg^{-1}	J_{min} Nm
Operator-based	296	9.00	250	13.5	$4.95^{\S}$
Same gain	316	12.8	316	12.8	$4.84^{\S}$
Different gain	290	9.73	188	18.8	$4.18^{\S}$

$^{\S}\times 10^{-8}$

The force gain of slave should be set as high as possible if the manipulated motion and the impedance of environmental object are not known in advance. As this dissertation has already stated in Section 6.2.3, the system vibrates if the velocity and force gains in the master side are set high due to the noise or quantization error. Although this dissertation only focuses on the design of velocity and force gains, the improvement of velocity controller in the master and force controller in the slave may improve the performance of bilateral control further.

The values of the smallest cost function in Fig. 6-6 and same gain tuning were 4.84×10^{-8} Nm and

Table 6.9: RMSE of position tracking and force feed-back in each approach

	RMSE of position tracking	$\mathrm{m} \times 10^{-6}$	RMSE of force feed-back	$\mathrm{N} \times 10^{-3}$
Operator-based	5.49		9.02	
Same gain	5.47		8.86	
Different gain	4.95		8.45	

5.41×10^{-8} Nm, and the amount of improvement was approximately 10 % ($\approx \frac{5.41\times10^{-8}-4.84\times10^{-8}}{5.41\times10^{-8}}$). Just Noticeable Differences (JNDs) of force is 5–15% depending on the part of the human body, posture of measurement, range of measurement, and so forth [35]. These statistics imply that the operator notices the performance improvement although the cost function shows the difference between the master and slave and not able to directly discuss with JNDs. RMSEs of position tracking and force feed-back in each approach is shown in Table 6.9.

6.5 Summary

This dissertation proposed the evaluation index-based gain tuning for bilateral control by using the experimental data. Moreover, this dissertation discusses the gain tuning based on gradient-descent for two cases: the same and different gains between the master and slave. From the experimental and numerical analyses, the obtained knowledge of gain tuning are that 1) the velocity gain of master should be set high under the condition where the force gain of slave is set high, 2) the force gain of slave should be set high, 3) the amounts of velocity and force gains in the slave side should be set smaller as the impedance of environmental object becomes smaller, and 4) the velocity gain in the slave side should be set larger as the continuous contact time becomes longer, for realizing much more precise impedance transmission. The experiments were also carried out for confirming the effectiveness of proposed gain tuning and gradient-descent based gain tuning.

This chapter collects real motion data of bilateral control and investigates the relationship between the evaluation index and control gains. These control gains can be designed based on some mathematical analyses or simulations, however, it is sometimes hard to prepare the perfect model. Therefore, the real experimental data was collected and utilized for solving optimization problem as the data-driven control design.

Chapter 7

Task Implementation-based Data-driven Design

This chapter discusses a selection of required controller for position and force-based task in motion copying system.

In Section 7.1, the task statement is introduced. In Section 7.1.1, the content of task is explained. In Section 7.1.2, the set-ups of experiments is explained. In Section 7.2, the task and motion analyses for MCS is introduced. In Section 7.2.1, the learning from demonstration is explained. In Section 7.2.2, the motion decomposition is explained. In Section 7.2.3, the labeling and phase connection is explained. In Section 7.2.4, the compensation of environmental variations is explained. In Section 7.3, the experiments are introduced. In Section 7.3.1, the set-ups of experiment are explained. In Section 7.3.2, the task realization based on the required controller is discussed. In Section 7.3.3, the task realization with the environmental variations is discussed. In Section 7.3.4, the task realization based on the conditions for success is discussed. This chapter is summarized in Section 7.4.

7.1 Task Statement

7.1.1 Content of Task

This dissertation considers the allen screw driving of M3-size allen screw that is a position and force based task. Since the allen screw driving needs both position and force components, this task is suitable for discussing the environmental variations in MCS and the selection strategy of position and/or force controllers. The allen screw is inserted into the allen screw hole but loosened in some extent in advance, and the task is to properly tightened it. The realization of the task is evaluated whether the allen screw is properly tightened or not where the criteria of proper tightening is whether the applied torque can become more than 0.23 Nm, which is the result of LfD.

Some tasks cannot be realized by the balance between the position and force controllers. Moreover, the coordinate transformation regarding work space or environmental object should be considered for the task realization. However, this dissertation only focuses on the simple task, which can be considered by the balance between position and force controllers.

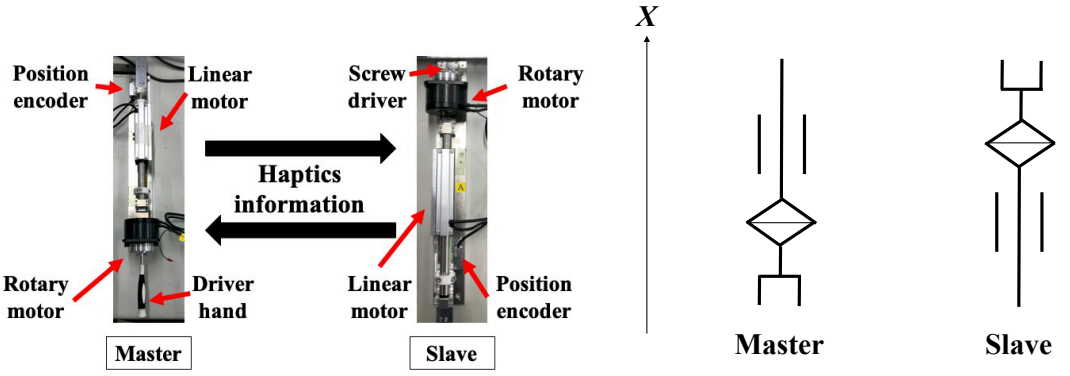

(a) Picture of experimental set-ups

(b) Illustration of mechanism in master and slave motors

Fig. 7-1: Structure of master and slave.

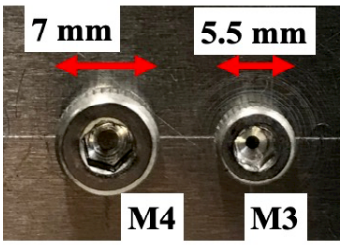

Fig. 7-2: Picture of allen screw hole.

7.1.2 Set-ups of Experiments

Both the master and slave have 2 DOF: the translation of x axis and the roll axis, and the master and slave have the same structures as shown in Fig. 7-1. The picture of allen screw hole is shown in Fig. 7-2. The allen screwdriver is attached in front of the rotary motor, and the commands are given not to the workspace but to the joint space. The basement of linear motor is fixed to the ground. The motor utilized for the translational motion is GHC, S160Q, and its position response is measured by Renishaw, RGH24Y. The motor utilized for the rotational motion is MTL, MDH-7018 with its micro encoder. ELMO, Gold-Twitter is utilized as the motor driver, and the system is connected to a computer running Real Time Application Interface (RTAI) of Linux.

This dissertation assumes that the allen screw driver is already attached to the motors. The allen screw hole was placed 0.02 m ahead from the allen screw driver, and the angle of hole was randomly shifted from the one of driver at the initial state of demonstration. The demonstrator was asked to operate the

master for approaching the slave to the allen screw hole and adjust the angle for inserting the allen screw by rotating the allen screw driver mainly in clockwise because the allen screw was loosened or dropped if it rotates counter clockwise excessively at the initial state. The operator felt the haptic information and adjusted the axis of allen screw driver and its hole. Then, the demonstrator was asked to tighten the allen screw as much as possible and retract the master. The skilled motion includes all approaching, adjusting, and screwing motions. This study was approved by the ethics committee of Keio university (31-79).

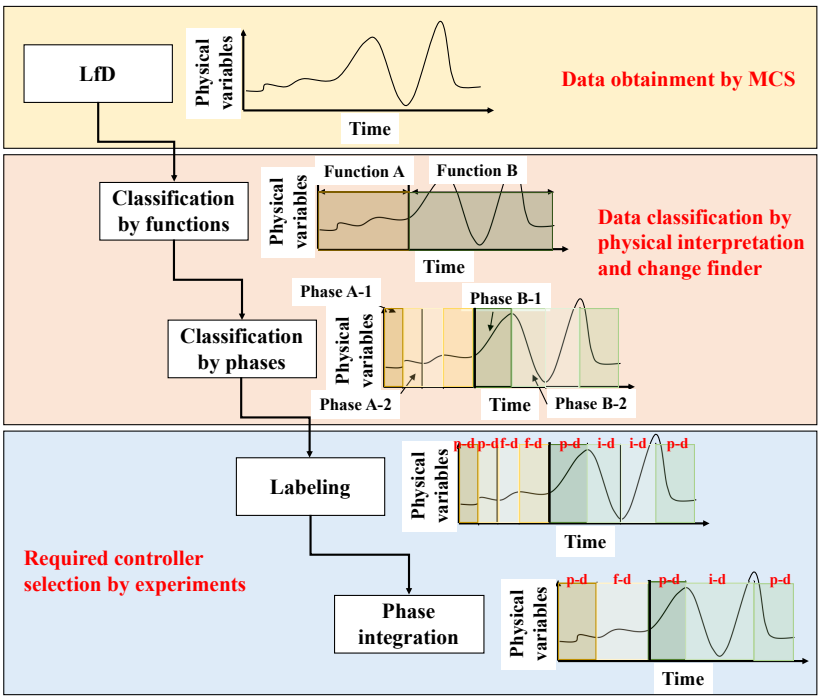

Fig. 7-3: The illustration of task and motion analyses process for MCS.

7.2 Task and Motion Analyses for MCS

The illustration of task and motion analyses process for MCS is summarized in Fig. 7-3. Each process is explained in the following sections.

Table 7.1: Parameters used in this dissertation.

Description	Value
Nominal mass of linear motor	$1.5\ \mathrm{kg}$
Nominal mass of rotary motor	$0.8\ \mathrm{kg}$
Nominal inertia of rotary motor	$8.6 \times 10^{-5}\ \mathrm{kgm}^2$
Position gain for linear or rotational motion	$1600\ s^{-2}$
Force gain for linear motion	$\frac{1}{M_\mathrm{n}}\ 1/\mathrm{kg}$
Force gain for rotational motion	$\frac{1}{J_\mathrm{n}}\ 1/\mathrm{kgm}^2$
Cut-off frequency of DOB	$300\ \mathrm{rad/s}$
Cut-off frequency of RFOB	$300\ \mathrm{rad/s}$
Cut-off frequency of pseudo derivative	$300\ \mathrm{rad/s}$
Sampling time	$0.1\ \mathrm{ms}$

7.2.1 Learning from Demonstration

Outline of Learning from Demonstration

This section explains the method for obtaining the motion data demonstrated by the operator as the skilled motion data, which is corresponding with the motion saving phase of MCS. Some approaches for LfD have been known [28, 29], but this dissertation utilizes MCS in order to obtain not only the position response from the position encoder but also the external force from the observer in the same axis simultaneously. Especially, the external force information is highly useful when the interactive motion with the environmental objects is considered. The controller utilized in MCS is the 4ch bilateral control. This chapter considers not only linear but also rotation motions, and the angle θ, the torque τ, and the inertia J are utilized instead of position, force, and mass when the rotational motion is considered. The responses of position and external force in the master side are stored in the motion database as the skilled motion data.

Parameters used in this dissertation are summarized in Table 7.1.

Results of Learning from Demonstration

The tightening of allen screw was performed, and the transition of skilled motion data is shown in Fig. 7-4. The motion was mainly composed of approaching, pushing while adjusting the rotation, pushing while screwing, and retracting.

The responses of allen screw driving is shown in Figs. 7-5 and 7-6. In addition to position, velocity,

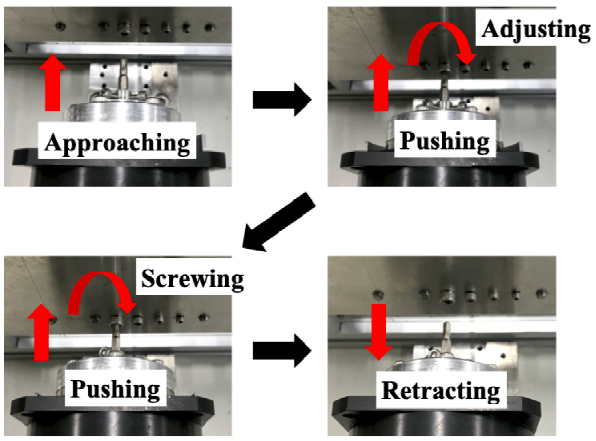

Fig. 7-4: Transition of skilled motion data.

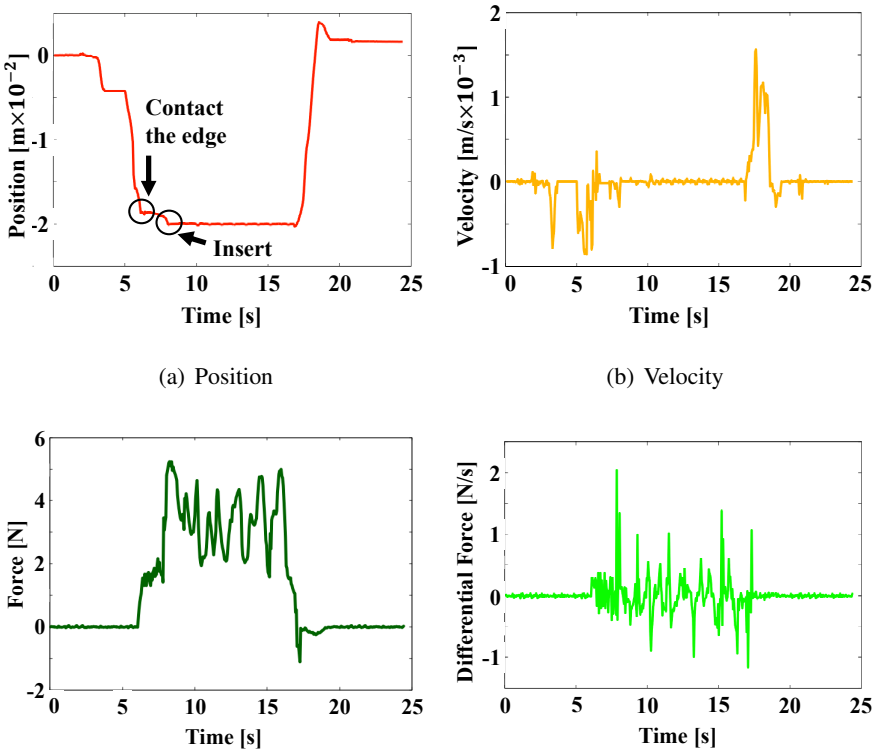

(a) Position

(b) Velocity

(c) Force

(d) Differential force

Fig. 7-5: The demonstrated motion in x axis.

and external force information, the differential force, which shows the force difference from the previous sample, were also obtained for utilizing the motion analysis. The motors approached to the hole and

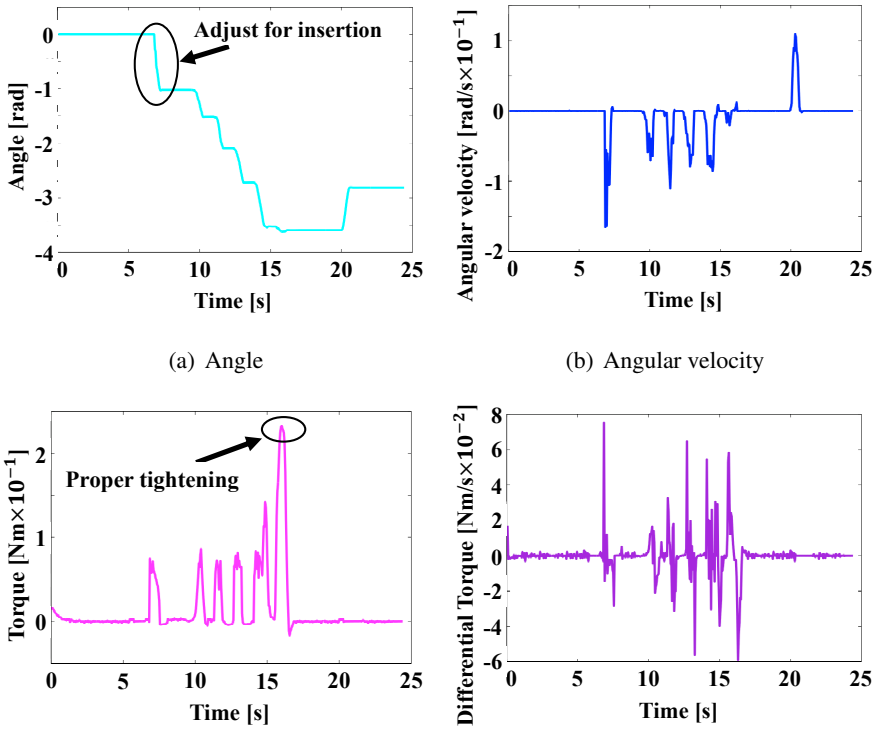

(a) Angle

(b) Angular velocity

(c) Torque

(d) Differential torque

Fig. 7-6: The demonstrated motion in the roll axis.

contacted the edge at approximately 6 s. Since the allen screwdriver is hexagonal shape, the angle of it has to be adjusted by considering the allen screw hole. It can be considered to adjust its rotation by cameras, but the allen screw hole is sometimes overlapped with the allen screwdriver and the visual field is restricted. Therefore, the allen screwdriver was gradually rotated in the clockwise, and the motion data intentionally includes its rotational motion of search by fumble more than 60 degrees, which is approximately 1 radian. The angle of screw driver was adjusted for about 1 s, and the screw driver was inserted into the hole. The allen screw was gradually tightened from approximately 6 s to 15 s, and the proper tightening was confirmed at around 16 s. The proper tightening specifies whether the applied torque can become more than 0.23 Nm or not from the result of LfD. Although it seems the simple motion, the purpose of motion in each time and axis seems different, and the control strategy should be varied in each time and axis.

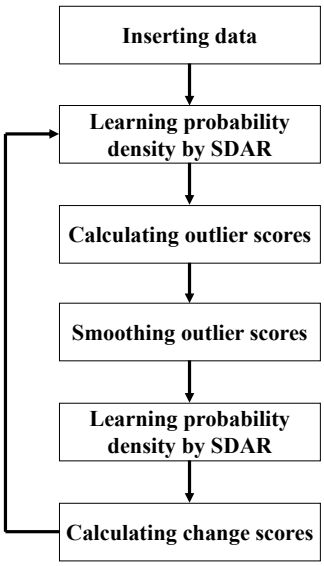

Fig. 7-7: Algorithm of change finder.

7.2.2 Motion Decomposition

Outline of motion decomposition

This dissertation decomposes the obtained motion by LfD into the function and phase, and the meanings of these words in this dissertation are as follows.

- Function: Components of motion and classified by the operator in a qualitative manner
- Phase: Precise description of each function and classified by the mathematical analysis in a quantitative manner

The motion is classified by the operator in the function level, which means the function is intuitively understandable for the operator. It is somehow able to decompose the obtained motion as shown in Fig. 7-4 by the operator, and the motion classification based on the function is necessary from the perspective of physical interpretation. The motion in this time was decomposed into three functions: contacting, screwing, and retracting.

The divided functions were classified into phases by the motion segmentation method in each function. This dissertation utilized change finder to classify the functions [122,123]. The algorithm of change finder is summarized in Fig. 7-7. This algorithm discriminates the outlier and change points. The outlier point increases/decreases instantaneously and comes back to the steady state in the next step, while the

change point represents that the characteristic of time-series data varies dramatically. First, the time-series data is given to the algorithm. Second, the probability density is learned based on Sequentially Discounting Auto Regressive (SDAR). Third, the outlier scores are computed based on the learned probability density in each time. Forth, the outlier scores are smoothed. Fifth, the probability density is relearned based on SDAR. Sixth, the change scores are calculated. Change finder assumes SDAR model and computes the logarithm of the likelihood ratio, which is the change score, between the predicted data and raw data of all eight variables all at once. The smoothing helps to focus on the change instead of noise. The motion was decomposed in the descending order of change score. The parameter design of motion segmentation is often the big concerns, but the stricter decomposition or parameterization in some extent would be preferable because the segmented motion would be connected after this process. This dissertation gradually changes the maximum number of change point till the shortest phase became 50 ms, which is the time resolution of operator against the weak stimulus [32]. The forgetting parameter was set as 0.01.

Results of motion decomposition

The results of motion decomposition in the function and phase levels are shown in Fig. 7-8. The bold black lines are for the division of function level, while the light black lines are for the division of phase level. The motion was decomposed to three functions and approximately fifty phases.

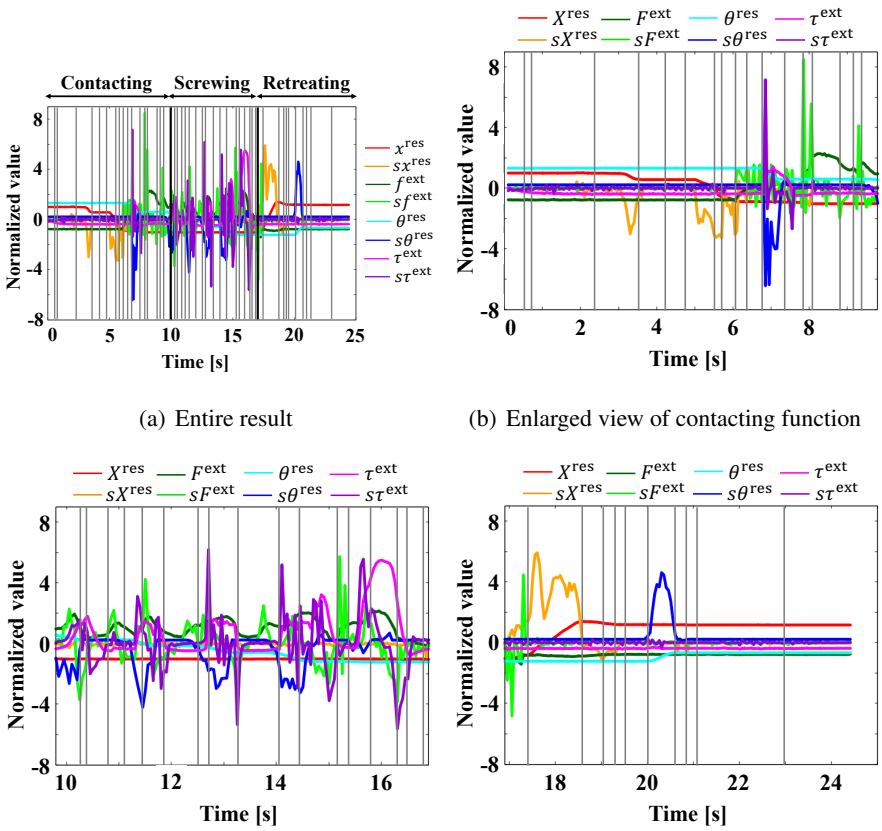

(a) Entire result

(b) Enlarged view of contacting function

(c) Enlarged view of screwing function

(d) Enlarged view of retracting function

Fig. 7-8: Result of motion decomposition in the phase level.

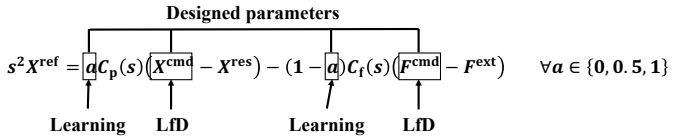

Fig. 7-9: The outline of designed parameters of HPFC.

7.2.3 Labeling and Phase Connection

Labeling

The purpose of this process is to determine the required controller in each axis and phase in order to change the motion flexibility of robot as well as the operator does. The labeling is conducted by the experiments, and this procedure makes clear the required controller of each divided phase for the task realization.

The controller in the motion loading phase in MCS is equivalent with HPFC. The position command, the force command, and the required controller a are three parameters to design for HPFC as shown in Fig. 7-9. The position and force responses of LfD can be utilized as the position and force commands of HPFC in the motion loading phase. Unlike the position and force commands, the motion flexibility, which is corresponding with a, of operator is hard to be obtained since the active and passive force generated by operators are tough to distinguish. Due to the difficulty of directly utilizing the human parameter regarding the motion flexibility, this dissertation learns the required controller from not only the operator but also in the task implementation. The coefficient a can be the continuous value, but it takes the discrete value in this dissertation. The operator adjusts its motion in order to adapt to the environmental variations, and the understanding of required controller in each phase and axis is highly helpful to design control parameters and realize the tasks.

The label of each phase: position-dominant (p-d), impedance-dominant (i-d), and force-dominant (f-d) is corresponding with the required controller: $a = 1$, $a = 0.5$, and $a = 0$. When the label of i–th phase is investigated, its controller is changed to $a = 1$ and $a = 0$ while the controllers in other phases are $a = 0.5$. This dissertation labels each phase as position-dominant (p-d) if the task is success by $a = 1$ in i–th phase, impedance-dominant (i-d) if the task is success only by $a = 0.5$ in i–th phase, and force-dominant (f-d) if the task is success by $a = 0$ in i–th phase from the perspective of simple controller design. For instance, if the results of task completion are the success for $a = 1$ and not success

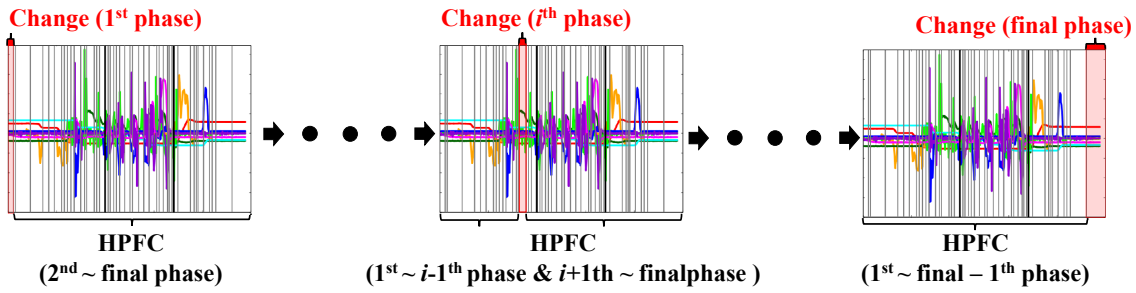

Fig. 7-10: The illustration of investigation process.

Table 7.2: The combinatorial patterns of control strategy of investigated phase.

	x axis	Roll axis
1	Position	HPFC
2	HPFC	Position
3	HPFC	HPFC
4	HPFC	Force
5	Force	HPFC

for $a = 0$, its phase is labeled as p-d and the position component can be said essential to realize the task.

The illustration of investigation process is shown in Fig. 7-10. In this figure, the controller of 1st phase is changed according to the combinatorial patterns of control strategy summarized in Table 7.2. The remaining of phases are manipulated by HPFC. This investigation process is repeated by moving the investigated phase. The algorithm of labeling is summarized in Alg. 4.

When the environmental condition is the same as one in LfD, the task can be realized by utilizing the position and force responses as the commands as they are. Therefore, the environmental variations were made on purpose for the labeling. The position variation related with each phase was considered, and the relative location of environment from the initial position of driver's tip was changed in some small extents. Two position variations: the translational x axis and roll axis were considered in this case, and both of them were changed approximately 2 mm and 10 degrees. The amount of position variations was determined considering the task realization by HPFC. The environmental location of translational x axis was varied if the phase at contacting function was investigated. The amount of position variation was compensated in the screwing and retracting functions. The environmental location of roll axis was varied if the phase at contacting and screwing functions were investigated.

Algorithm 4 The process of labeling

$c \leftarrow$ The changed phase
$i \leftarrow$ The identified number of phases
$n \leftarrow$ The total number of divided phases
while $c \leq n$ **do**
  while $i \leq n$ **do**
    if $c = i$ **then**
      The controller of i–th phase is set as the combinatorial patterns as shown in Table 7.2
    end if
    if $c \neq i$ **then**
      The controller of i–th phase is set as HPFC in both y and roll axes
    end if
    $i = i + 1$
  end while
  The task is reproduced, and the success of task is evaluated
  if Task is success **then**
    The set controller of c–th phase such as $a = 0, a = 0.5$, and $a = 1$ is stored
  end if
  $i = 1$
  $c = c + 1$
end while

The transition of controllers for labeling

In order to realize the variation of the control strategy based on the labeling, the strategy for the controller variation is needed. Four variations could occur: HPFC $\rightarrow$ Position control, HPFC $\rightarrow$ Force control, Position control $\rightarrow$ HPFC, and Force control $\rightarrow$ HPFC. The first two variations need to continuously decrease the force or position gain, while the latter two variations need to continuously increase the force or position gain. The weight function, which is shown in Fig. 7-11, is designed, and its amount is linearly changed between 0 and 1 in 10 ms. w_1, w_2, and t in Fig. 7-11 denote the weight function of decreasing, the weight function of increasing, and the time when the controller is changed. The amount change is completed in $t + 10$, which means 10 ms later. The weight function of decreasing is multiplied to the force or position gain in the case of HPFC $\rightarrow$ Position control or HPFC $\rightarrow$ Force control, respectively.

The control gain needs to be continuously increased in the case of Position control $\rightarrow$ HPFC or Force control $\rightarrow$ HPFC: however, the sudden change of force or position command should be avoided. There-

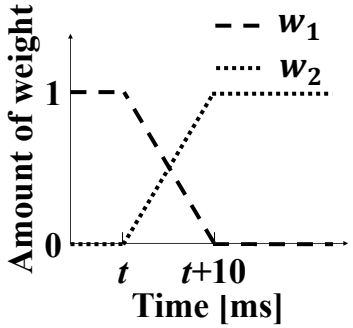

Fig. 7-11: The variation of weight function.

fore, the compensation value is designed as well as the weight functions. The acceleration references of Position control → HPFC and Force control → HPFC in the linear motion are designed as follows:

$$
\begin{aligned}
s^2 X^{\mathrm{ref}} &= C_{\mathrm{p}}(s)(X^{\mathrm{cmd}} - X^{\mathrm{res}}) - w_2 C_{\mathrm{f}}(s)(F^{\mathrm{cmd}} - F^{\mathrm{ext}} + F^{\mathrm{comp}}), && (7.1)\\
F^{\mathrm{comp}} &= w_1(F^{\mathrm{ext}'} - F^{\mathrm{cmd}'}),\\
s^2 X^{\mathrm{ref}} &= w_2 C_{\mathrm{p}}(s)(X^{\mathrm{cmd}} - X^{\mathrm{res}} + X^{\mathrm{comp}}) - C_{\mathrm{f}}(s)(F^{\mathrm{cmd}} - F^{\mathrm{ext}}), && (7.2)\\
X^{\mathrm{comp}} &= X^{\mathrm{res}'} - X^{\mathrm{cmd}'}.
\end{aligned}
$$

The superscript $\bigcirc'$ denotes the fixed value, and $F^{\mathrm{ext}'} - F^{\mathrm{cmd}'}$ is the constant value and shows the error between the external force at the end of position control and the force command at the beginning of HPFC. $X^{\mathrm{res}'} - X^{\mathrm{cmd}'}$ shows the error between the position response at the end of force control and the position command at the beginning of HPFC. Therefore, the force or position compensation mitigates the dramatic change of command and makes the smooth command value. Unlike the force command, the error between the position response at the end of force control and the position command at the beginning of HPFC is substituted until the end of trial.

Phase connection

Once the labeling process was completed, the phase connection was carried out. If the label of $i-1$–th phase was the same as one of i–th phase, these phases were connected. Otherwise, these phases were remained separated. The results of labeling are summarized in Table 7.3 where "-" denotes no constraints regarding the required controller. The phase was connected based on the results of labeling as shown in Fig. 7-12. The contacting function, the screwing function, and retracting function are composed of four,

Table 7.3: Summary of labeling.

Motion	x axis	Roll axis
Contacting 1	-	-
Contacting 2	i-d, f-d	-
Contacting 3	i-d, f-d	p-d, i-d
Contacting 4	-	-
Screwing 1	-	-
Screwing 2	i-d, f-d	i-d, f-d
Retracting	-	-
p-d: a=1	i-d: a=0.5	f-d: a=0

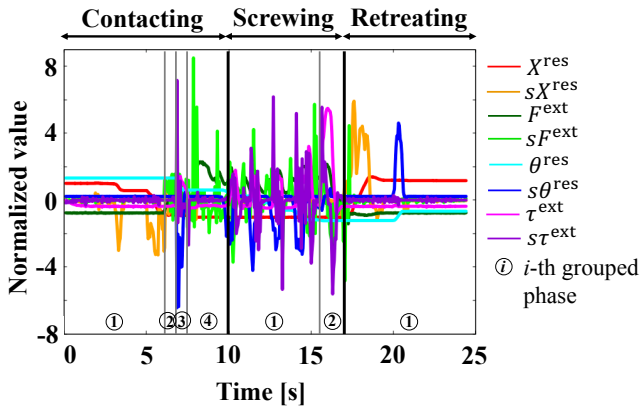

Fig. 7-12: Result of phase connection.

two, and one grouped phases that is depicted by the circle in Fig. 7-12, and this dissertation writes the first grouped phase of contacting function as the phase of contacting 1. Other grouped phases are also accordingly. The phase of contacting 1 aims at approaching to the allen screw hole from the initial position. Both the translational x axis and roll axis have no requirements regarding the selection of controller. The phase of contacting 2 aims at contacting to the edge of allen screw hole. The translational x axis is labeled as i-d or f-d, which means the robot moves till it feels the reaction force and the force component is essential. The roll axis has no requirements. The phase of contacting 3 aims at inserting the allen screwdriver into the allen screw hole. The translational x axis is labeled as i-d or f-d, and it can be considered that some extents of force have to be applied for inserting the allen screwdriver into the allen screw hole. At the same time, the roll axis is labeled as p-d or i-d for rotating the driver properly.

The phase of contacting 4 is the phase for transiting to the screwing function, and both translational x axis and roll axis have no requirements regarding the selection of controller. The phase of screwing 1 aims at tightening the allen screw. However, both translational x axis and roll angle have no requirements regarding the selection of controller, and it means this phase is not highly related with the task realization. The phase of screwing 2 aims at tightening the screw properly. The force component is dominant for both translational x axis and roll axis in order to apply the sufficient force and torque for realizing the proper tightening. The phase of retracting aims at retracting from the allen screw hole, and both the translational x axis and roll axis have no requirements.

To recapitulate, the motion is classified into seven phases based on the transition of required controller. The requirements about controller exist at the phase of contacting 2, 3 and screwing 2 phases, and each physical interpretation should be respected for designing the parameters. The required controller explicitly specifies the conditions for success or the physical variable of control goals in each divided motion. Here, the conditions for success means the type of controller that needs for the position/force-based task realization. For instance, when the required controller is f-d, the conditions for success of that phase can be said to be described by the force element and only force control goal should be satisfied. Although the sequence of required controller has possibility to change once other position and force command values are considered, the obtained conditions for success is highly useful to design not only the type of controller but also the position/force command values. Therefore, the proposed motion analysis method can be said that it tries to make clear the conditions for success.

7.2.4 Compensation of Environmental Variations

Outline of compensation

This dissertation compensates the environmental variations by substituting the compensation values. The acceleration reference in the task execution in the linear motion is computed as follows:

$$s^2 X^{\mathrm{ref}} = aC_{\mathrm{p}}(s)(X^{\mathrm{cmd}} - X^{\mathrm{res}} + X^{\mathrm{comp}}) - (1-a)C_{\mathrm{f}}(s)(F^{\mathrm{cmd}} + F^{\mathrm{ext}} + F^{\mathrm{comp}}). \quad (7.3)$$

When its phase is labeled as p-d or i-d and some environmental variations occurred, the position compensation value is substituted. Otherwise, the position compensation value is set as 0. When the phase is labeled as i-d or f-d and some environmental variations occurred, the force compensation value is substituted. Otherwise, the force compensation value is set as 0. The design of position compensation value is simple since the compensation value should basically be the same as the amount of position variation. On the other hand, the design of force compensation value is complicated since it does not necessarily vary the linear manner. For instance, it might not be appropriate to add the double times larger force even if the impedance of environmental objects becomes double times larger for holding up some objects. Therefore, the construction of compensation logic for the impedance variation is needed unlike the most of position variation cases.

Learning for the impedance variation

This dissertation considers the situation where another size of allen screw is inserted as a considerable situation of impedance variation. Since the force compensation value does not tend to generate in the linear manner, the compensation logic for the impedance variation has to be constructed. This dissertation obtained the skilled motion data against M3-size and M4-size allen screws ten times in each. The applied average force of x axis in the screwing function is learned. At the same time, the maximum rotating torque of roll axis is obtained because its information is useful for proper tightening. This two information are summarized in Fig. 7-13. The written values show the maximum, average, and minimum values of each column. The applied average force in the screwing function of M4-size is slightly larger than one of M3-size although some trials are overlapped between two sizes. The maximum rotating torque of M4-size is completely larger than one of M3-size, and the substitution of compensation value is definitely needed.

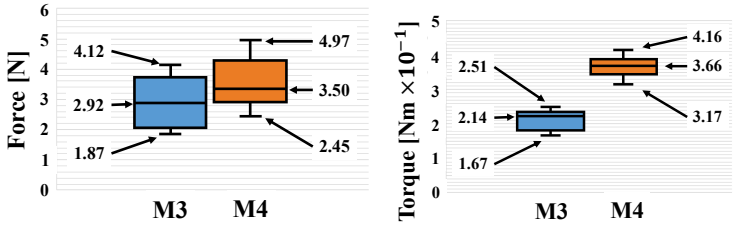

(a) x axis (b) Roll axis

Fig. 7-13: Required force and torque between M3-size and M4-size screwing.

Table 7.4: Transition of control strategy.

Motion	x axis	Roll axis
Contacting 1	HPFC	HPFC
Contacting 2	Force	HPFC
Contacting 3	Force	Position
Contacting 4	HPFC	HPFC
Screwing 1	HPFC	HPFC
Screwing 2	Force	Force
Retracting	HPFC	HPFC

7.3 Experiments

7.3.1 Experimental Set-ups

Three types of experiment were conducted for confirming three things, 1. the effectiveness of labeling as Experiment 1 (Exp. 1), 2. the adaptability to the environmental variations as Experiment 2 (Exp. 2), 3. The effectiveness of command and controller designs based on the conditions for success as Experiment 3 (Exp. 3).

In Exp. 1, the motion was conducted by the command obtained by LfD and the transition of control strategy as shown in Table 7.4 is utilized under the same environmental condition with the one in LfD.

In Exp. 2, the motion was conducted by the same condition in Exp. 1, but both the position and impedance variations occurred. The allen screw hole was placed farther than the one in LfD, and the M4-size allen screw was inserted instead of M3-size as the impedance variation. The average force and maximum torque of LfD were 3.26 N and 0.23 Nm: therefore, only the force compensator of roll axis is designed for making the maximum torque 0.366 Nm. The designed control strategy was compared with the position-based MCS, the force-based MCS, and the original MCS (HPFC).

In Exp. 3, the position and force commands were generated based on the conditions for success, and only required controller was utilized for designing the control strategy. The generated motion was composed of three components: the contacting to the edge of allen screw hole by the force control at x axis, the inserting the allen screwdriver into the allen screw hole by the force control at x axis and position control at the roll axis, and the screwing by the force control of both x axis and roll axis. The designed control strategy was compared with the position-velocity and force controls, and the control strategies are shown in Table 7.5. The commands in each control strategy were designed by the trial and

Table 7.5: Control strategies in Exp. 3.

(a) Proposal

Time [s]	x (Command)	Roll (Command)
0 - 1	Force (2 N)	Ang.Vel.(0 rad/s)
1 - 3	Force (2 N)	Ang.Vel.(0.5 rad/s)
3 - 4	Force (3 N)	Torque (0.23 Nm)
4 - 5	Velocity (Retracting)	Angle(Fixing)

(b) Only position control

Time [s]	x (Command)	Roll (Command)
0 - 1	Velocity (0.019 m/s)	Ang.Vel.(0 rad/s)
1 - 3	Velocity(0.01 m/s)	Ang.Vel.(0.5 rad/s)
3 - 4	Velocity(0.015 m/s)	Ang.Vel.(10.0 rad/s)
4 - 5	Velocity (-0.01 m/s)	Ang.Vel.(0 rad/s)

(c) Only force control

Time [s]	x (Command)	Roll (Command)
0 - 1	Force (2 N)	Torque (0 Nm)
1 - 3	Force (2 N)	Torque (0.072 Nm)
3 - 4	Force (3 N)	Torque (0.23 Nm)
4 - 5	Force (-0.3 N)	Torque (0 Nm)

Table 7.6: Summary of experimental set-ups.

	Exp. 1	Exp. 2	Exp. 3
Environmental position	Same	Farther	Same
Environmental impedance	M3-size	M4-size	M3-size
Command	LfD	LfD	Table 7.5
Controller	Table 7.4	Table 7.4	Table 7.4

error with the best effort.

The summary of experimental set-ups is shown in Table 7.6.

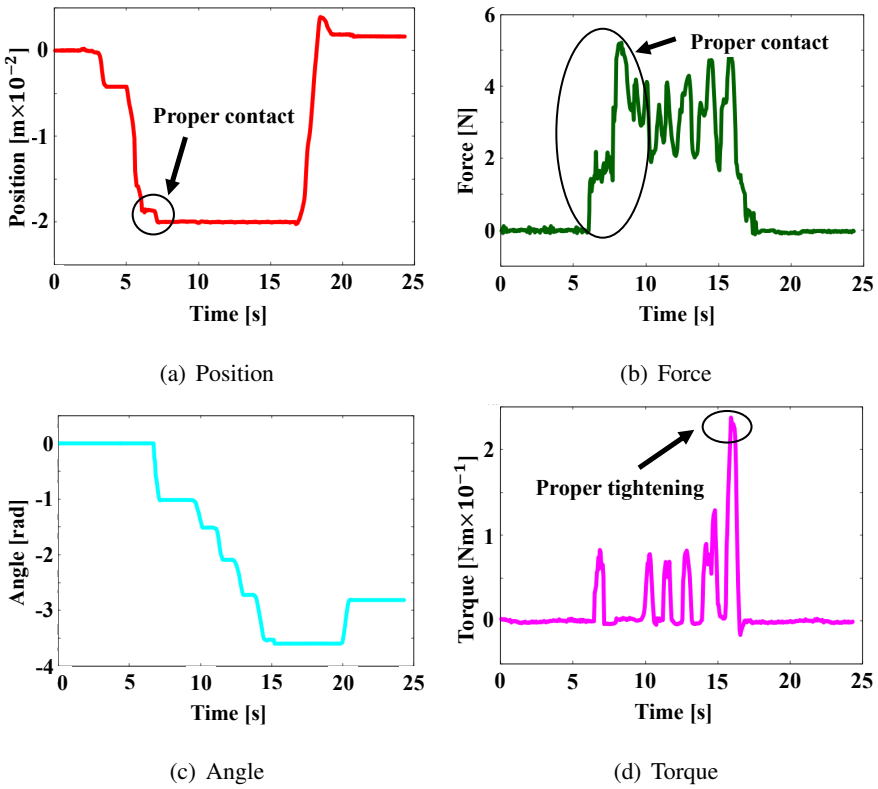

(a) Position (b) Force

(c) Angle (d) Torque

Fig. 7-14: Experimental results in x axis based on the required control stiffness.

7.3.2 Task Realization Based on the Required Controller (Exp. 1)

This experiment considered to perform the motion based only on the required controller. The results of Exp. 1 are shown in Fig. 7-14. The experimental results show that the motion performed only by the required controller moved as the similar manner with the one of LfD. The tip of the allen screwdriver properly contacted the edge of screw hole and inserted into its hole. The maximum external torque of roll axis became almost 0.23 Nm, and the proper tightening was confirmed. Therefore, the motion performed only by the required controller achieved the task realization as similar as the original motion when the environmental conditions are the same.

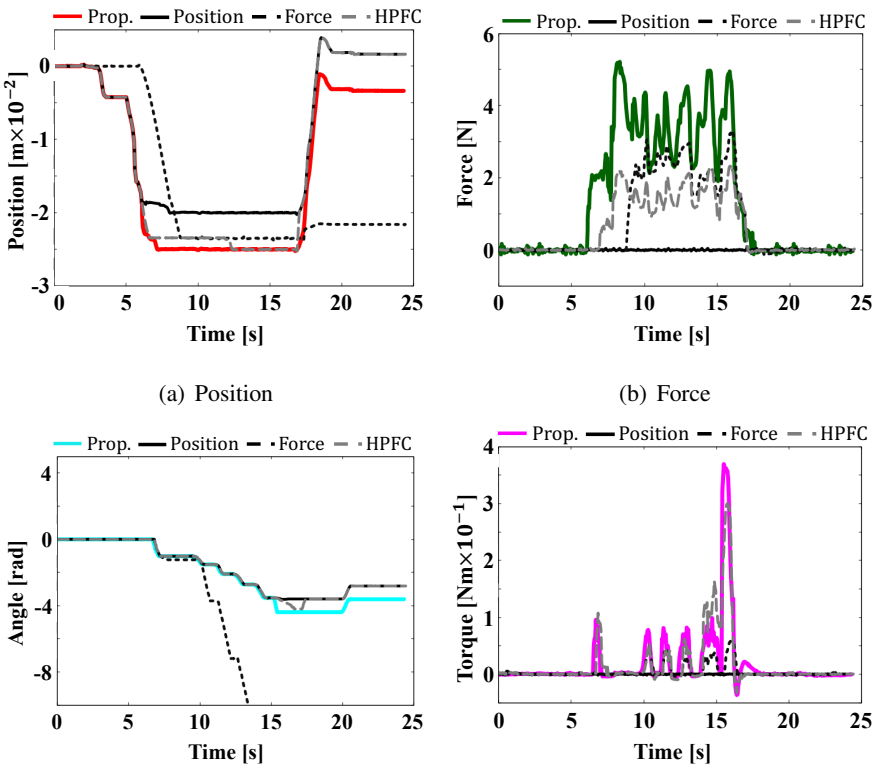

(a) Position (b) Force

(c) Angle (d) Torque

Fig. 7-15: Experimental results with the environmental variations in x axis

7.3.3 Task Realization with the Environmental Variations (Exp. 2)

This experiment considered the adaptability to the environmental variations. The force compensation value was referred from the one learning in Section 7.2.4. The results of Exp. 2 are shown in Fig. 7-15. The legend "Prop.", "Position", "Force", and "HPFC" denote the proposed controller selection, the position-based MCS, the force-based MCS, and the original MCS (HPFC).

The tip of allen screwdriver was properly contacted the edge of screw hole since the external force was observed although the screw hole was located approximately 0.005 m away in the case of proposal. At the same time, the sufficient torque was generated for realizing the proper tightening of M4-size screw. It eventually adapted to the position variation of roll axis. Therefore, the experimental results show that the motion performed by the required controller compensated the environmental variations and made realized the task. The proposal successfully compensates the environmental variations by incorporating the pros of both the position and force controllers. This dissertation only considers M3-size and M4-size,

but it can be extended to other sizes if the compensation values of force and torque can be designed.

The tip of allen screwdriver was not able to contact the edge of screw hole in the case of position-based MCS. Therefore, the values of external force and torque became constantly 0 although the rotary motor moved according to the angle command.

The tip of allen screwdriver contacted the edge of screw hole in the case of force-based MCS, but it took much more time than the proposal because the force command was almost 0 from 0 s to around 7 s. Since the angular velocity was not regulated by the position control, the allen screwdriver could not be inserted into the allen screw hole. Therefore, it kept on rotating and its rotated angle reached more than -10 rad and went out the range of figure.

The tip of allen screwdriver contacted the edge of screw hole in the case of HPFC. However, the pushing force was not sufficient and could not insert the screwdriver because of the position controller. The sign of reference values generated by position and force controllers were opposite. The position controller tried to retract and follow the trajectory as the same one as position-based MCS, while the force controller tried to move forward for generating the larger reaction force. The allen screwdriver was inserted at around 12 s, and it started to tight the allen screw. However, the amount of tightening was not sufficient again because the sign of reference values generated by the position and force controls were opposite.

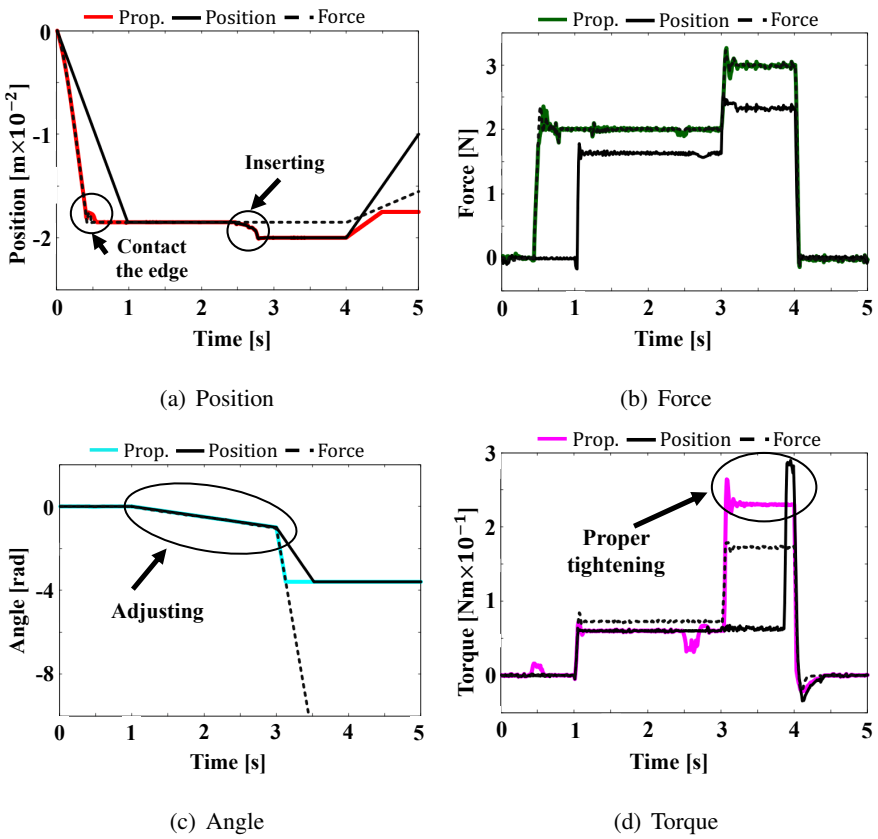

(a) Position (b) Force

(c) Angle (d) Torque

Fig. 7-16: Experimental results of task reproduction in x axis

7.3.4 Task Realization Based on the Conditions for Success (Exp. 3)

This experiment considered the effectiveness of command and controller designs based on the conditions for success for realizing the task. The results of Exp. 3 are shown in Fig. 7-16. In the proposed strategy, the tip of the allen screwdriver properly contacted the edge of allen screw hole thanks to the force control of linear motor from 0–1 s, and it was inserted into the hole by the combination of force and position control of linear and rotary motors from 1–3 s. The torque control of rotary motor generated approximately 0.23 Nm external torque and realized the proper tightening from 3–4 s. Therefore, the experimental results show that the designed motion successfully reproduced the task thanks to the satisfaction of conditions for success. The proposal enables to design the control strategy according to the required motion in each axis and time.

The tip of the allen screwdriver also properly contacted the edge of allen screw hole at 1 s in the case of position control because the command was given by the velocity. The allen screwdriver was successfully

inserted into the hole because the velocity of rotation was regulated and properly tightened the allen screw. Since the screw tightening is not extremely difficult task, the command can be alternatively designed by the position-velocity instead of force. However, some motions such as tightening should be designed by the force because the command design based on position-velocity sometimes outputs the excessive force in interactive task and the sensitive command design is expected more than the case of force control.

The tip of the allen screwdriver also properly contacted the edge of allen screw hole at 1 s when the force control is considered, but the allen screwdriver could not be inserted into the hole although the torque command of rotational motion was tuned several times. As a consequent, the rotary motor moved more than -10 rad. The trajectory can be similar even if the force control is considered, but the realization of precise motion such as the insertion, is sometimes difficult to achieve.

7.4 Summary

This dissertation considered the method for selecting the required controller in each phase and axis for the MCS. The motion flexibility of the MCS is conventionally fixed, and this study aimed to select the required controller by considering the task realization. The results of Exp. 1 showed that the task was realized by the motion based only on the required controller, and it was confirmed that the required controller was properly extracted. At the same time, the adaptability to the environmental variations and the effectiveness of command design considering the conditions for success and type of controller design were confirmed through Exps. 2 and 3.

This chapter collects real motion data through bilateral control, and these data are analyzed. Moreover, the analyses are also carried out in the actual experiments further. The required controller was made clear in each time and axis through these analyses. Data-driven approach helps us to understand the task and design the position/force controller.

Chapter 8

Conclusion

The design of position/force controller is sometimes hard in the theoretical or systematic manner. This dissertation tackles with its issue by considering the concept of data-driven approach, and three types of data-driven control design were introduced: experimental data, database, and cerebellar calculation model. Force control is designed based on the concept of cerebellar calculation model of data-driven control design in Chapter 3. Operator's sensation and motion data are collected for constructing database in Chapters 4 and 5. Position/force control is also designed from the perspective of evaluation-index and task implementation in Chapters 6 and 7.

In Chapter 3, a development method of force control with DOB and neural network is discussed based on the concept of cerebellar calculation model in data-driven control design of force control. This chapter tries to improve the performance of force control by owning the feed-back and feed-forward characteristics to the NN. As the humans adapt to surrounded uncertain environment and change motions, the motion controller can be considered to dynamically change its characteristics. Therefore, this dissertation aims at implementing the dynamical controller by learning the elements of feed-back and feed-forward in the NN from the real data. The NNs have been implemented for modeling the specific physical variables in the related studies, however, this dissertation combines the NNs with DOB and expects NNs working as similar to DOB. The combination of NNs with DOB was investigated, and this dissertation considers that NNs should be utilized for avoiding the interference with DOB in the frequency range. Although the situations such as environmental impedance are partially limited, the proposal works in the normal use. This dissertation shows the effectiveness of combination between the conventional approaches such as DOB and the concept of cerebellar calculation model in data-driven control design. Some studies replace

all controllers by NN, but NN should be combined with the classical methods such as PI controller and DOB for taking advantages of both approaches.

In Chapter 4, a JNDs-based design policy of haptics system is discussed as an approach of operator's sensation-based data-driven design. Database was constructed based on operator's sensation and utilized for determining the parameter of control system. Some teleoperation products or methods have already known, and some of them insists to have tactile sensation. However, there is no clear standard for what reason they insists to have tactile sensation. In particular, the quantitative discussion is hard in the case of human support robots that works to the operators' sensation. Therefore, the data-driven product or design based on the real data regarding the operators' sensation can become much more important and essential. This chapter considers the traffic data reduction as an example and proposed to build the look-up table based on the real data. The effectiveness of data-driven approach is shown for tackling with the problem concerning the coexistence of performance and resource in the position/force controller.

In Chapter 5, an estimation method of end-point impedance based on bilateral control system is discussed as an approach of operator's motion-based data-driven design. Database can be designed based on the operator's impedance estimated by the proposal and apply the parameter of control system. As the humans adapt to surrounded uncertain environment and change motions, the motion controller can be considered to dynamically change its characteristics. Especially, the abstraction and understanding of skilled motion are helpful to design the controller. Many impedance estimation researches have been carried out, however, the behaviours at the moment of interaction are still not clear. This dissertation proposed the abstraction method of operators' impedance at the moment of interaction. Data-driven design of control impedance in position/force controller is available based on the proposal in this chapter.

In Chapter 6, an approach to evaluation index-based gain tuning for bilateral control is discussed as an index-based data-driven design. Experimental data was collected and utilized for solving the optimization problem. The gains of position/force controller in master/slave system is sometimes hard to decide uniquely. This dissertation tackles with its issue by considering the evaluation index as the part of design policy. Because the transfer functions of master and slave are not the same, this dissertation considers that the gains of master and slave should not necessarily the same. In addition, this dissertation shows the order of gain tuning at least similar situation with this dissertation. Position/velocity gains of master should be tuned finely, and then the force controller of slave should be tuned. The effectiveness of data-driven approach to position/force controller design is shown, which is sometimes difficult to obtain the clear solution based on the formula expansion.

In Chapter 7, a selection of required controller for position and force-based task in motion copying system is discussed as a task implementation-based data-driven design. Experimental data was collected and analyzed in order to make clear the required controller in each axis and time. Because HPFC treats multiple contradicted physical variables simultaneously, it is sometimes difficult to design. This dissertation considers the necessarily elements for the task success at first and concludes that the understanding of tasks before the controller design is important and essential. Therefore, the abstraction of necessarily control impedance in each task is proposed. As the humans adapt to surrounded uncertain environment and change motions, the controller should also change in each time and axis. This dissertation shows a study of controller design from the perspective of control impedance by considering the simple task. However, the human-like flexible motion can be realized by collecting real data regarding the required controller in each task as the data-driven approach.

From these discussions, the effectiveness of data-driven design in position/force control is shown for overcoming the problems that the motion control is hard to tackle with. Robots in Society 5.0 will be realized by motion control, which combines modeling-analysis-synthesis approach and data-driven approach.

References

[1] ソフトバンクロボティクス: “Pepper for Biz”, https://www.softbank.jp/biz/robot/pepper/

[2] 文部科学省: “2050 年までに、AI とロボットの共進化により、自ら学習・行動し人と共生するロボットを実現”, https://www8.cao.go.jp/cstp/moonshot/concept3.pdf

[3] S. Katsura and K. Ohnishi: “Modal system design of multirobot systems by interaction mode control”, *IEEE Transactions on Industrial Electronics*, Vol. 54, No. 3, pp. 1537–1546, Jun. 2007.

[4] T. Nozaki, T. Mizoguchi, and K. Ohnishi: “Motion expression by elemental separation of haptic information”, *IEEE Transactions on Industrial Electronics*, Vol. 61, No. 11, pp. 6192–6201, Nov. 2014.

[5] T. Nozaki, T. Mizoguchi, and K. Ohnishi: “A controller design method for multirobot systems based on task projection matrix”, *Proc. of 2013 IEEE International Conference on Mechatronics*, pp. 213–218, Feb. 2013.

[6] 熊本水頼: “二関節筋　その意味とはたらき”, *Sportsmedicine*, 2008 年 11 月.

[7] K. Ohnishi, M. Shibata, and T. Murakami: “Motion control for advanced mechatronics”, *IEEE/ASME Transactions On Mechatronics*, Vol. 1, No. 1, pp. 56–67, Mar. 1996.

[8] Cabinet office of Japan: “Basic Outlook and Key Strategies”, $https://www.kantei.go.jp/jp/singi/keizaisaisei/pdf/miraitousi2018_en.pdf$

[9] 金子修: “データから直接コントローラをつくる”, $https://www.uec.ac.jp/research/information/opal-ring/pdf/0007003.pdf$

[10] M. C Campi, A. Lecchini, and S. M Savaresi: “Virtual reference feedback tuning: a direct method for the design of feedback controllers”, *Automatica*, Vol. 38, No. 8, pp. 1337–1346, Jan. 2002.

[11] S. Soma, O. Kaneko, and T. Fujii: “A new method of controller parameter tuning based on input-output data–Fictitious Reference Iterative Tuning (FRIT)–”, *IFAC Proceedings Volumes*, Vol. 37, No. 12, pp. 789–794, Jan. 2004.

[12] 山本透: “データ指向型 PID 制御”, 森本出版株式会社, 2020 年 6 月.

[13] T. Murakami, F. Yu, and K. Ohnishi: “Torque sensorless control in multidegree-of-freedom manipulator”, *IEEE Transactions on Industrial Electronics*, Vol. 40, No. 2, pp. 259–265, Apr. 1993.

[14] Y. Nagatsu and S. Katsura: ”High-order disturbance estimation using Kalman filter for precise reaction-torque control”, *Advanced Motion Control, 2004. 8th IEEE International Workshop On*, pp. 79–84, Jun. 2016.

[15] S. Sakaiano, T. Sato, and K. Ohnishi: “Force-based disturbance observer for dynamic force control and a position/force hybrid controller”, *IEEJ Transactions on Electrical and Electronic Engineering*, Vol.8, No.5, pp.505–514, Jul. 2013.

[16] L. G. Garcia-Valdovinos, V. Parra-Vega, and M. A. Arteaga: ”Higher-order sliding mode impedance bilateral teleoperation with robust state estimation under constant unknown time delay”, *Proceedings, 2005 IEEE/ASME International Conference on Advanced Intelligent Mechatronics*, pp.1293–1298, Sep. 2005.

[17] H. Gomi and M. Kawato: “Neural network control for a closed-loop system using feedback-error-learning”, *Neural Networks*, Vol.6, No.7, pp.933–946, Jan. 1993.

[18] M. Teshnehlab and K. Watanabe: “Neural network controller with flexible structure based on feedback-error-learning approach”, *Journal of Intelligent and Robotic Systems*, Vol.15, No.4, pp.367–387, Apr. 1996.

[19] E. Kayacan: “Sliding mode control for systems with mismatched time-varying uncertainties via a self-learning disturbance observer”, *Transactions of the Institute of Measurement and Control*, Vol.41, No.7, pp.2039–2052, Apr. 2019.

[20] J. Nakanishi and S. Schaal: “Feedback error learning and nonlinear adaptive control”, *Neural Networks*, Vol.17, No.10, pp.1453–1465, May 2004.

[21] T. Fukuda and T. Shibata: “Theory and applications of neural networks for industrial control systems”, *IEEE Transactions on Industrial Electronics*, Vol.39, No.6, pp.472–489, Dec. 1992.

[22] Z. Su and K. Khorasani: “A neural-network-based controller for a single-link flexible manipulator using the inverse dynamics approach”, *IEEE Transactions on Industrial Electronics*, Vol.48, No.6, pp.1074–1086, Dec. 2001.

[23] H. Gao, W. He, C. Zhou, and C. Sun: “Neural network control of a two-link flexible robotic manipulator using assumed mode method”, *IEEE Transactions on Industrial Informatics*, Vol.15, No.2, pp.755–765, Mar. 2018.

[24] M. Kawato: “Feedback-error-learning neural network for supervised motor learning”, *Advanced neural computers*, pp.365–372, 1990.

[25] T. Tsuji, K. Ito, and P. G. Morasso: “Neural network learning of robot arm impedance in operational space”, *IEEE Transactions on Systems, Man, and Cybernetics, Part B (Cybernetics)*, Vol.26, No.2, pp.290–298, Apr. 1996.

[26] X. Yao, Y. Zhang, B. Li, Z. Zhang, and X. Shen ”Machining force control with intelligent compensation”, *The International Journal of Advanced Manufacturing Technology*, Vol.69, No.5–8, pp.1701–1715, Jul. 2013

[27] S. Bhasin, K. Dupree, P. M. Patre, and W. E Dixon ”Neural network control of a robot interacting with an uncertain viscoelastic environment”, *IEEE Transactions on Control Systems Technology*, Vol.19, No.4, pp.947–955, Jul. 2010.

[28] B. Hannaford: “A design framework for teleoperators with kinesthetic feedback”, *IEEE Transactions on Robotics and Automation*, Vol. 5, No. 4, pp. 426 – 434, Aug. 1989.

[29] D. A. Lawrence: “Stability and transparency in bilateral teleoperation”, *IEEE Transactions on robotics and automation*, Vol. 9, No. 5, pp. 624 – 637, Oct. 1993.

[30] H. Zhang, C. Reardon, and L. E. Parker: ”Bilateral control of teleoperators with time delay”, *IEEE Transactions on Cybernetics*, Vol. 43, No. 5, pp. 1429 – 1441, Oct. 2013.

[31] G. R. Wallace: ”The JPEG still picture compression standards”, *Communications of the ACM*, Vol. 34, No. 4, pp. 30 – 44, Apr. 1991.

[32] S. J. Lederman and R. L. Klatzky: “Haptic perception: A tutorial”, *Attention, Perception, & Psychophysics*, Vol. 71, No. 7, pp. 1439 – 1459, Oct. 2009.

[33] S. Allin, Y. Matsuoka, and R. Klatzky: “Measuring just noticeable differences for haptic force feedback: implications for rehabilitation”, *Haptic Interfaces for Virtual Environment and Teleoperator Systems, 2002. HAPTICS 2002. Proceedings. 10th Symposium on*, pp. 299 – 302, Mar. 2002.

[34] M. A, Srinivasan and JS Chen: “Human performance in controlling normal forces of contact with rigid objects”, *American Society of Mechanical Engineers, Dynamic Systems and Control Division (Publication) DSC*, Vol. 49, pp. 119 – 125, Dec. 1993.

[35] S. Feyzabadi, S. Straube, M. Folgheraiter, E. A. Kirchner, S. K. Kim, and J. C. Albiez: “Human force discrimination during active arm motion for force feedback design”, *IEEE transactions on haptics*, Vol. 6, No. 3, pp. 309 – 319, Jul. 2013.

[36] S. Okamoto and Y. Yamada: ”Lossy data compression of vibrotactile material-like textures”, *IEEE transactions on haptics*, Vol. 6, No. 1, pp. 69 – 80, Mar. 2013.

[37] H. Tanaka and K. Ohnishi: ”Haptic data compression/decompression using DCT for motion copy system”, *2009 IEEE International Conference on Mechatronics*, pp. 1 – 6, Apr. 2009.

[38] T. Kaneko, S. Ito, S. Sakaino, and T. Tsuji: ”Haptic data compression for rehabilitation databases”, *2014 IEEE International Workshop on Advanced Motion Control*, pp. 657 – 662, Mar. 2014.

[39] C. Shahabi, A. Ortega, and M. R Kolahdouzan: ”A comparison of different haptic compression techniques”, *Proceedings. IEEE International Conference on Multimedia and Expo*, Vol. 1, pp. 657 – 662, Aug. 2002.

[40] Hangai, Satoshi and Nozaki, Takahiro: ”Haptic Data Prediction and Extrapolation for Communication Traffic Reduction of 4-channel Bilateral Control System”, *IEEE Transactions on Industrial Informatics*, 2020.

[41] Y. You and M. Y. Sung: ”Haptic data transmission based on the prediction and compression”, *Communications, 2008. ICC'08. IEEE International Conference on*, pp. 1824 – 1828, May 2008.

[42] D. Botturi, M. Vicentini, M. Righele, and C. Secchi: ”Perception-centric force scaling in bilateral teleoperation”, *Mechatronics*, Vol. 20, No. 7, pp. 802 – 811, Oct. 2010.

[43] H. Son, T. Bhattacharjee, and H. Hashimoto: ”Effect of impedance-shaping on perception of soft tissues in macro-micro teleoperation”, *IEEE Transactions on Industrial Electronics*, Vol. 59, No. 8, pp. 3273 – 3285, May 2012.

[44] P. Hinterseer, S. Hirche, S. Chaudhuri, E. Steinbach, and L. M. Buss: ”Perception-based data reduction and transmission of haptic data in telepresence and teleaction systems”, *IEEE Transactions on Signal Processing*, Vol. 56, No. 2, pp. 588 – 597, Feb. 2008.

[45] E. Steinbach, S. Hirche, J. Kammerl, I. Vittorias, and R. Chaudhari: ”Haptic data compression and communication”, *IEEE Signal Processing Magazine*, Vol. 28, No. 1, pp. 87 – 96, Jan. 2011.

[46] X. Xu, C. Schuwerk, B. Cizmeci, and E. Steinbach: ”Energy prediction for teleoperation systems that combine the time domain passivity approach with perceptual deadband-based haptic data reduction”, *IEEE transactions on haptics*, Vol. 9, No. 4, pp. 560 – 573, Oct. 2016.

[47] N. Sakr, J. Zhou, N. D Georganas, and J. Zhao: ”Prediction-based haptic data reduction and transmission in telementoring systems”, *IEEE Transactions on Instrumentation and Measurement*, Vol. 58, No. 5, pp. 1727 – 1736, May 2009.

[48] N. Sakr, N. D Georganas, and J. Zhao: ”Human perception-based data reduction for haptic communication in six-dof telepresence systems”, *IEEE Transactions on Instrumentation and Measurement*, Vol. 60, No. 11, pp. 3534 – 3546, Nov. 2011.

[49] P. Rahimian and K. K. Joseph: “Optimal Camera Placement for Motion Capture Systems”, *IEEE Transactions on Visualization and Computer Graphics*, Vol. 23, No. 3, pp. 1209 – 1221, Dec. 2016.

[50] J. Deutscher, A. Blake, and I. Reid: “Articulated body motion capture by annealed particle filtering”, *Proc. of 2000 IEEE Conference on Computer Vision and Pattern Recognition*, Vol. 2, pp. 126 – 133, Jun. 2000.

[51] J. Friedman and T. Flash: “Task-dependent selection of grasp kinematics and stiffness in human object manipulation”, *Cortex*, Vol. 43, No. 3, pp. 444 – 460, Jan. 2007.

[52] T. Yoshikawa and Y. Ichinoo: “Impedance identification of human fingers using virtual task environment”, *Proc. of 2003 IEEE/RSJ International Conference on Intelligent Robots and Systems*, pp. 3094 – 3099, Oct. 2003.

[53] A. Z. Hajian and R. D. Howe: “Identification of the mechanical impedance at the human finger tip”, *Journal of biomechanical engineering*, Vol. 119, No. 1, pp. 109 – 114, Feb. 1997.

[54] Z. L. Htoon, S. Na’im, S. Fatai, and M. M. Rashid: “Estimation of Upper Limb Impedance Parameters Using Recursive Least Square Estimator”, *Proc. of 2016 International Conference on Computer and Communication Engineering*, pp. 144 – 148, Jul. 2016.

[55] R. Dong, J. Wu, T. McDowell, D. Welcome, and A. Schopper: “Distribution of mechanical impedance at the fingers and the palm of the human hand”, *Journal of biomechanics*, Vol. 38, No. 5, pp. 1165 – 1175, May 2005.

[56] D. L. Jindrich, A. D. Balakrishman, and J. T. Dennerlein: “Finger joint impedance during tapping on a computer keyswitch”, *Journal of Biomechanics*, Vol. 37, No. 10, pp. 1589 – 1596, Oct. 2004.

[57] C. Fu and M. Oliver: “Direct measurement of index finger mechanical impedance at low force”, *Proc. of 2005 and Symposium on Haptic Interfaces for Virtual Environment and Teleoperator Systems, Eurohaptics Conference*, pp. 657 – 659, Mar. 2005.

[58] A. Israr, S. Choi, and H. Z. Tan: “Detection threshold and mechanical impedance of the hand in a pen-hold posture”, *Proc. 2006 IEEE/RSJ International Conference on Intelligent Robots and Systems*, pp. 472 – 477, Oct. 2006.

[59] A. E. Fiorilla, N. G. Tsagarakis, F. Nori, and G. Sandini: "Design of a 2-finger hand exoskeleton for finger stiffness measurements", *Applied Bionics and Biomechanics*, Vol. 6, No. 2, pp. 217 – 228, Jul. 2009.

[60] T. E. Milner and D. W. Franklin: "Characterization of multijoint finger stiffness: dependence on finger posture and force direction", *IEEE Transactions on Biomedical Engineering*, Vol. 45, No. 2, pp. 217 – 228, Jul. 2009.

[61] H. Lee and N. Hogan: "Time-varying ankle mechanical impedance during human locomotion", *IEEE Transactions on Neural Systems and Rehabilitation Engineering*, Vol. 23, No. 5, pp. 755 – 764, Sep. 2015.

[62] M. H. Raibert and J. J. Craig: "Hybrid position/force control of manipulators", *Journal of Dynamic Systems, Measurement, and Control*, Vol. 103, No. 2, pp. 126 – 133, Jun. 1981.

[63] M. T. Mason: "Compliance and force control for computer controlled manipulators", *IEEE Transactions on Systems, Man, and Cybernetics*, Vol. 11, No. 6, pp. 418 – 432, Jun. 1981.

[64] N. Hogan: "Impedance control: An approach to manipulation", *American Control Conference, 1984*, pp. 304 – 313, Mar. 1985.

[65] S. Misra and A. M. Okamura: "Environment parameter estimation during bilateral telemanipulation", *Haptic Interfaces for Virtual Environment and Teleoperator Systems, 2006. 14th Symposium On*, pp. 301 – 307, Mar. 2006.

[66] X. Wang, P. X. Liu, D. Wang, B. Chebbi, and M. Meng: "Environment parameter estimation during bilateral telemanipulation", *Robotics and Automation, 2005. ICRA 2005. Proceedings of the 2005 IEEE International Conference on*, pp. 1127 – 1132, Apr. 2005.

[67] H. Kuwahara, T. Shimono, H. Tanaka, D. Yashiro, and K. Ohnishi: "Abstraction of action components unconstrained by alignment of haptic sensing points", *IEEE Transactions on Industrial Electronics*, Vol. 58, No. 8, pp. 3196 – 3204, Aug. 2011.

[68] T. Shimono, S. Katsura, and K. Ohnishi: "Abstraction and reproduction of force sensation from real environment by bilateral control", *IEEE Transactions on Industrial Electronics*, Vol. 54, No. 2, pp. 907 – 918, Apr. 2007.

[69] C. C Hang, K. J. Åström, and W. K. Ho: "Refinements of the Ziegler–Nichols tuning formula", *IEE Proceedings D (Control Theory and Applications)*, Vol. 138, No. 2, pp. 111 – 118, Mar. 1991.

[70] M. Zhuang and DP Atherton: "Automatic tuning of optimum PID controllers", *IEE Proceedings D (Control Theory and Applications*, Vol. 140, No. 3, pp. 216 – 224, May 1993.

[71] T. S. Schei: "Automatic tuning of PID controllers based on transfer function estimation", *Automatica*, Vol. 30, No. 12, pp. 1983 – 1989, Dec. 1994.

[72] T. Sugiyama and K. Uchida: "Gain scheduled velocity and force controllers for electro-hydraulic servosystem", *IEEJ Transactions on Industry Applications*, Vol. 122, No. 11, pp. 1051 – 1058, Nov.. 2002.

[73] O. Khatib: "A unified approach for motion and force control of robot manipulators: The operational space formulation", *IEEE Journal on Robotics and Automation*, Vol. 3, No. 1, pp. 43 – 53, Feb. 1987.

[74] A. Sano, H. Fujimoto, and M. Tanaka: "Gain-scheduled compensation for time delay of bilateral teleoperation systems", *Proceedings. 1998 IEEE International Conference on Robotics and Automation*, Vol. 3, No. 1, pp. 1916 – 1923, May 1998.

[75] J. H. Cho, H. I. Son, G. Dong, T. Bhattacharjee, and D. Y. Lee: "Gain-scheduling control of teleoperation systems interacting with soft tissues", *IEEE Transactions on Industrial Electronics*, Vol. 60, No. 3, pp. 946 – 957, Feb. 2012.

[76] G J. Raju, G. C Verghese, and T. B Sheridan: "Design issues in 2-port network models of bilateral remote manipulation", *Proceedings, 1989 International Conference on Robotics and Automation*, pp. 1316 – 1317, 1989.

[77] L. Ni and D. WL Wang: "A gain-switching control scheme for position-error-based bilateral teleoperation: Contact stability analysis and controller design", *The International Journal of Robotics Research*, Vol. 23, No. 3, pp. 255 – 274, Mar. 2004.

[78] K. Hashtrudi-Zaad and S. E. Salcudean: "Transparency in time-delayed systems and the effect of local force feedback for transparent teleoperation", *IEEE Transactions on Robotics and Automation*, Vol. 18, No. 1, pp. 108 – 114, Feb. 2002.

[79] M. C. Çavusoglu, A. Sherman, and F. Tendick: "Design of bilateral teleoperation controllers for haptic exploration and telemanipulation of soft environments", *IEEE transactions on robotics and automation*, Vol. 18, No. 4, pp. 641 – 647, Aug. 2002.

[80] J. Kim, P. H. Chang, and H. Park: "Two-channel transparency-optimized control architectures in bilateral teleoperation with time delay", *IEEE Transactions on Control Systems Technology*, Vol. 21, No. 1, pp. 40 – 51, Jan. 2011.

[81] P. Kormushev, S. Calinon, and D. G. Caldwell: "Imitation learning of positional and force skills demonstrated via kinesthetic teaching and haptic input", *Advanced Robotics*, Vol. 25, No. 5, pp. 581 – 603, 2011.

[82] K. Kronander and A. Billard: ”Learning compliant manipulation through kinesthetic and tactile human-robot interaction”, *IEEE transactions on haptics*, Vol. 7, No. 3, pp. 367 – 380, Oct. 2013.

[83] J. D. F. Heredia, J. I. U Rubrico, S. Shirafuji, and J. Ota: ”Teaching tasks to multiple small robots by classifying and splitting a human example”, *Journal of Robotics and Mechatronics*, Vol. 29, No. 2, pp. 419 – 433, Apr. 2017.

[84] Z. Zhu and H. Hu: ”Robot Learning from Demonstration in Robotic Assembly: A Survey”, *Robotics*, Vol. 7, No. 2, pp. 17, Apr. 2018.

[85] Y. Yokokura, S. Katsura, and K. Ohishi: “Stability analysis and experimental validation of a motion-copying system”, *IEEE Transactions on Industrial Electronics*, Vol. 56, No. 10, pp. 3906 – 3913, Oct. 2009.

[86] W. Iida and K. Ohnishi: “Reproducibility and operationality in bilateral teleoperation”, *Proc. of the 8th IEEE International Workshop On Advanced Motion Control*, pp. 217 – 222, Mar. 2004.

[87] K. Miura, A. Matsui, and S. Katsura: “Synthesis of motion-reproduction systems based on motion-copying system considering control stiffness”, *IEEJ Journal of Industry Applications*, Vol. 21, No. 2, pp. 1015 –1023, Apr. 2016.

[88] Y. Nagatsu and S. Katsura: “Decoupling and Performance Enhancement of Hybrid Control for Motion-Copying System”, *IEEE Transactions on Industrial Electronics*, Vol. 64, No. 1, pp. 420 – 431, Nov. 2017.

[89] Y. Hirai, T. Mizukami, Y. Suzuki, T. Tsuji, and T. Watanabe: “Hierarchical Proximity Sensor for High-Speed and Intelligent Control of Robotic Hand”, *J. Robot. Mechatron.*, Vol. 31, No. 3, pp. 453–463, Jun. 2019.

[90] T. Morizono, K. Tahara, and H. Kino: “Choice of Muscular Forces for Motion Control of a Robot Arm with Biarticular Muscles”, *J. Robot. Mechatron.*, Vol. 31, No. 1, pp. 143–155, Feb. 2019.

[91] D. M. Wolpert, R. C. Miall, and M. Kawato: “Internal models in the cerebellum”, *Trends in cognitive sciences*, Vol. 2, No. 9, pp. 338–347, Sep. 1998.

[92] L. Rozo, S. Calinon, D. G. Caldwell, P. Jimenez, and C. Torras: ”Learning physical collaborative robot behaviors from human demonstrations”, *IEEE Transactions on Robotics*, Vol. 32, No. 3, pp. 513 – 527, Apr. 2016.

[93] N. Saito and T. Satoh: “Posture control considering joint stiffness of a robotic arm driven by rubberless artificial muscle”, *International Journal of Automation Technology*, Vol. 10, No. 4, pp. 503–510, Jul. 2016.

[94] F. J Abu-dakka, L. Rozo, amd D. G. Caldwell: "Force-based Learning of Variable Impedance Skills for Robotic Manipulation" *Robotics and Autonomous Systems*, 109: pp. 156 – 167, Nov. 2018.

[95] C. Li, Z. Zhang, G. Xia, X. Xie, and Q. Zhu: "Efficient Force Control Learning System for Industrial Robots Based on Variable Impedance Control", *Sensors*, Vol. 18, No. 8, pp. 2539, Aug. 2018.

[96] R. Wu, H. Zhang, T. Peng, L. Fu, and J. Zhao: "Human-Robot Interaction and Demonstration Learning Mode Based on Electromyogram Signal and Variable Impedance Control", *Mathematical Problems in Engineering*, Vol. 2018, Sep. 2018.

[97] K. Hongo, Y. Nakanishi, M. Yoshida, I. Mizuuchi, and M. Inaba: "Development of bilateral wearable device kento for control robots using muscle-actuator modules", *J. Robot. Mechatron.*, Vol. 22, No. 3, pp. 308, 2010.

[98] M. T. Mason: "Compliance and force control for computer controlled manipulators", *IEEE Transactions on Systems, Man, and Cybernetics*, Vol. 11, No. 6, pp. 418 – 432, Jun. 1981.

[99] E. Sariyildiz and K. Ohnishi: "Stability and robustness of disturbance-observer-based motion control systems", *IEEE Transactions on Industrial Electronics*, Vol. 62, No. 1, pp. 414 – 422, May 2014.

[100] C. J. Kempf and S. Kobayashi: "Disturbance observer and feedforward design for a high-speed direct-drive positioning table", *IEEE Transactions on control systems Technology*, Vol. 7, No. 5, pp. 513 – 526, Sep. 1999.

[101] C. Ott, R. Mukherjee, and Y. Nakamura: "Unified impedance and admittance control", *Proc. of 2010 IEEE International Conference On Robotics and Automation (ICRA),*, pp. 554 – 561, May 2010.

[102] S. Katsura, Y. Matsumoto, and K. Ohnishi: "Modeling of force sensing and validation of disturbance observer for force control", *IEEE Transactions on Industrial Electronics*, Vol. 54, No. 1, pp. 530 – 538, Feb. 2007.

[103] M. Morisawa and K. Ohnishi: "Motion control taking environmental information into account", *EPE journal*, Vol. 12, No. 4, pp. 37 – 41, Nov. 2002.

[104] J. Mazumdar and R. G. Harley: "Recurrent neural networks trained with backpropagation through time algorithm to estimate nonlinear load harmonic currents", *IEEE Transactions on Industrial Electronics*, Vol. 55, No. 9, pp.3483–3491, May 2008.

[105] Z. Xu, Q. Song, D. Wang, and H. Fan: “A training algorithm and stability analysis for recurrent neural networks”, *2012 15th International Conference on Information Fusion,*, pp. 2285 – 2292, Jul. 2012.

[106] Z. Allen-Zhu, L. Yuanzhi, and S. Zhao: “On the convergence rate of training recurrent neural networks”, *Advances in neural information processing systems*, 2019.

[107] A. H. Sayed and T. Kailath: “A state-space approach to adaptive RLS filtering”, *IEEE signal processing magazine*, Vol. 11, No. 3, pp. 18 – 60, Jul. 1994.

[108] M. C Berg, N. Amit, and J D. Powell: ”Multirate digital control system design”, *IEEE Transactions on automatic control*, Vol. 33, No. 12, pp. 1139 – 1150, Dec. 1988.

[109] M. Mizuochi, T. Tsuji, and K. Ohnishi: ”Multirate sampling method for acceleration control system”, *IEEE Transactions on Industrial Electronics*, Vol. 54, No. 3, pp. 1462 – 1471, Apr. 2007.

[110] S. Hirche and M. Buss: ”Human-oriented control for haptic teleoperation”, *Proceedings of the IEEE*, Vol. 100, No. 3, pp. 623 – 647, Mar. 2012.

[111] H. Levitt: ”Transformed up-down methods in psychoacoustics”, *The Journal of the Acoustical society of America*, Vol. 49, No. 2B, pp. 467 – 477, 1971.

[112] M. A. Garcıa-Pérez: ”Forced-choice staircases with fixed step sizes: asymptotic and small-sample properties”, *Vision research*, Vol. 38, No. 12, pp. 1861 – 1881, Jun. 1998.

[113] S. Hyodo and K. Ohnishi: ”A two flow expression method of four-channel bilateral control system with time delay and validation of model-free time delay compensator”, *IEEJ Journal of Industry Applications*, Vol. 4, No. 5, pp. 574 – 581, Sep. 2015.

[114] T. Nozaki, S. Shimizu, T. Murakami, and K. Ohnishi: ”Impedance field expression of bilateral control for reducing data traffic in haptic transmission”, *IEEE Transactions on Industrial Electronics*, Vol. 66, No. 2, pp. 1142 – 1150, May 2018.

[115] Y. Yokokohji and T. Yoshikawa: ”Bilateral control of master-slave manipulators for ideal kinesthetic coupling-formulation and experiment”, *IEEE transactions on robotics and automation*, Vol. 10, No. 5, pp. 605 – 620, Oct. 1994.

[116] T. Nozaki, T. Mizoguchi, and K. Ohnishi: ”Motion-copying system with variable impedance based on scaled bilateral control in one-degree-of-freedom robot”, *IEEJ Journal of Industry Applications*, Vol. 3, No. 1, pp. 1 – 9, Jan. 2014.

[117] T. Matsunaga: ”Development of Haptic End-effector for Medicine and Manufacturing”, 2017.

[118] H. Flemmer, B. Eriksson, and J. Wikander: ”Control design for transparent teleoperators with model parameter variation”, *Proceedings 2002 IEEE International Conference on Robotics and Automation*, pp. 2956 – 2961, May 2002.

[119] A. Suzuki and K. Ohnishi: ”Frequency-domain damping design for time-delayed bilateral teleoperation system based on modal space analysis”, *IEEE Transactions on Industrial Electronics*, Vol. 60, No. 1, pp. 177 – 190, Jan. 2012.

[120] S. Ruder: ”An overview of gradient descent optimization algorithms”, arXiv preprint arXiv:1609.04747, (2016).

[121] M. Pelikan, D. E Goldberg, and E. Cantú-Paz: ”BOA: The Bayesian optimization algorithm”, *Proceedings of the 1st Annual Conference on Genetic and Evolutionary Computation*, Vol. 1, pp. 525 – 532, Jan. 1999.

[122] Y. Kawahara and M. Sugiyama: ”Sequential change-point detection based on direct density-ratio estimation”, *Statistical Analysis and Data Mining: The ASA Data Science Journal*, Vol. 5, No. 2, pp. 114–127, Mar. 2012.

[123] S. Liu, M. Yamada, N. Collier, and M. Sugiyama: ”Change-point detection in time-series data by relative density-ratio estimation”, *Neural Networks*, Vol. 43, pp. 72–83, Jan. 2013.

List of Achievements

Journals (First Author)

[1] Toshiaki Okano, Takahiro Nozaki, and Toshiyuki Murakami, "Development of Neural Network-based Explicit Force Control with Disturbance Observer," *IEEJ Journal of Industry Applications*, vol. 10, no. 2, 12pages, 2021.

[2] Toshiaki Okano, Takahiro Nozaki, and Toshiyuki Murakami, "An Approach to Evaluation Index-Based Gain Scheduling for Acceleration-Based Four-Channel Bilateral Control," *Journal of the Japan Society for Precision Engineering*, vol. 86, no. 9, pp. 720–730, 2020.

[3] Toshiaki Okano, Roberto Oboe, Kouhei Ohnishi, and Toshiyuki Murakami, "Selection of Required Controller for Position- and Force-based Task in Motion Copying System," *Journal of Robotics and Mechatronics*, vol. 32, no 1, pp. 113–127, 2020.

[4] Toshiaki Okano, Kouhei Ohnishi, and Toshiyuki Murakami, "An Estimation Method of End-point Impedance Based on Bilateral Control System," *Advanced Robotics*, vol. 32, no 21, pp. 1151–1167, 2018.

Journals (Co-author)

[1] Kazuki Tanida, Toshiaki Okano, Toshiyuki Murakami, and Kouhei Ohnishi, "An Approach to Architecture Design of Bilateral Control System Based on a Layer Structure," *IEEJ Journal of Industry Applications*, vol. 9, no 4, pp. 318–330, 2020.

[2] Kazuki Tanida, Toshiaki Okano, Toshiyuki Murakami, and Kouhei Ohnishi, "Control Structure Determination of Bilateral System Based on Reproducibility and Operationality," *IEEJ Journal of Industry Applications*, vol. 8, no 5, pp. 767–778, 2019.

International Conferences (First Author)

[1] Toshiaki Okano, Takahiro Nozaki and Toshiyuki Murakami, "Development of Neural Network-based Explicit Force Control for Step Command," in *The IEEJ International Workshop on Sensing, Actuation, Motion Control, and Optimization, SAMCON 2020, Tokyo, Japan*, March 14–16, 2020.

[2] Toshiaki Okano and Toshiyuki Murakami, "An approach to success-based data compression considering position/force task," in *Proceedings of the IEEE International Conference on Industrial Technology, ICIT 2020, Buenos Aires, Argentina*, February 26–28, 2020.

[3] Toshiaki Okano, Kouhei Ohnishi, and Toshiyuki Murakami, "Variable Slave Force Gain for Oblique Coordinate Control Under the Presence of Time-Delay," in *Proceedings of the IEEE International Conference on Mechatronics, ICM 2019, Ilmenau, Germany*, March 18–20, 2019.

[4] Toshiaki Okano, Takahiro Ishikawa, and Toshiyuki Murakami, "Scaling Adjustment Method for Motion Copying System with Environmental Variation," in *Proceedings of the IEEE International Conference on Industrial Informatics, INDIN 2018, Porto, Portugal*, July 18–20, 2018.

[5] Toshiaki Okano, Roberto Oboe, Kouhei Ohnishi, and Toshiyuki Murakami, "Comparative study of soft motion for motion copying system with environmental variations," in *Proceedings of the IEEE/ASME International Conference on Advanced Intelligent Mechatronics, AIM 2018, Auckland, New Zealand*, July 9–12, 2018.

[6] Toshiaki Okano, Kouhei Ohnishi, and Toshiyuki Murakami, "Compensation Method for Environmental Variations of Motion Reproduction System Based on the Different Control Impedance," in *Proceedings of the 2018 IEEE International Conference on Industrial Electronics, ISIE 2018, Cairns, Australia*, June 13–15, 2018.

[7] Toshiaki Okano, Kenji Ogawa, and Kouhei Ohnishi, "Motion Loading System Taking into Account the Variable Control Stiffness and Human Reactions," in *Proceedings of the International Conference on Mechatronics and Machine Vision in Practice, M2VIP 2017, Auckland, New Zealand*, November 21–23, 2017.

[8] Toshiaki Okano, Takahiro Ishikawa, Takahiro Nozaki, and Kouhei Ohnishi, "Identification of Human and Environmental Impedances by Using Bilateral Control System with Low-pass Filtered M-sequence Signal," in *Proceedings of the 43rd Annual Conference of the IEEE Industrial Electronics Society, IECON 2017, Beijing, China*, October 29–November 1, 2017.

International Conferences (Co-author)

[1] Akihiro Kawamura, Toshiaki Okano and Toshiyuki Murakami, "A Control Under Actuated AUV by Nonlinear Controller," in *Proceedings of the IEEE/SICE International Symposium on System Integration, SII 2019, Paris, France*, January 14–16, 2019.

[2] Masashi Fukui, Shuhei Akutsu, Toshiaki Okano, Takahiro Nozaki, and Toshiyuki Murakami, "Design of Iterative Learning Control for Force Control Considering Environmental Impedance," in *Proceedings of the 44th Annual Conference of the IEEE Industrial Electronics Society, IECON 2018, Washington D.C., USA*, October 21–23, 2018.

[3] Akihiro Kawamura, Toshiaki Okano and Toshiyuki Murakami, "Robust Control Strategy for AUV with Workspace Observer," in *Proceedings of the IEEE International Conference on Industrial Informatics, INDIN 2018, Porto, Portugal*, July 18–20, 2018.

[4] Yuta Tawaki, Toshiaki Okano,Toshiyuki Murakami, and Kouhei Ohnishi, "Evaluation of Gait Phase Detection Methods for Walking Assist Robot," in *Proceedings of the 2018 IEEE International Conference on Industrial Electronics, ISIE 2018, Cairns, Australia*, June 13–15, 2018.

[5] Takuya Matsunaga, Toshiaki Okano, Xiaobai Sun, Takahiro Mizoguchi, and Kouhei Ohnishi, "Identification of Human and Environmental Impedances by Using Bilateral Control System with Low-pass Filtered M-sequence Signal," in *Motion Reproduction System Using Multi DoF Haptic Forceps Robots for Ligation Task, IECON 2017, Beijing, China*, October 29–November 1, 2017.

Domestic Conferences (First-author)

[1] Toshiaki Okano, Takahiro Ishikawa, Kouhei Ohnishi, and Toshiyuki Murakami, "Online Parameter Estimation Method of Hunt-Crossley Model Based on Acceleration-based Bilateral Control" in *Journal of Japan Society of Computer Aided Surgery*, vol. 20, no 4, pp. 352–353, 2018.

[2] Toshiaki Okano, Wanping Lyu, Takuya Matsunaga, and Kouhei Ohnishi, "Simplified Motion Reproduction by Force Transmittable Surgical Robots" in *Journal of Japan Society of Computer Aided Surgery*, vol. 19, no 4, pp. 228–229, 2017.

[3] Toshiaki Okano, Yoshiyuki Kambara, Akihiko Yamamuro, and Kouhei Ohnishi, "Human-robot Collaboration System Based on the Cluster Classification for Manipulation Task" in *JIASC2015*, September 2–4, 2015.

Domestic Conferences (Co-author)

[1] Takahiro Ishikawa, Toshiaki Okano, and Toshiyuki Murakami, “Human Gait Classification Based on Deep-Learning with IMU and Infrared Sensor” in *Journal of Japan Society of Computer Aided Surgery*, vol. 20, no 4, pp. 331–332, 2018.